A Study on Efficient Methods for Optimal Design and Countermeasures Using Equivalent Circuit Models to Satisfy EMC Performance in Multi-Component Systems

March, 2024

Shohei Kan

Graduate School of
Natural Science and Technology
(Doctoral Course)
OKAYAMA UNIVERSITY

A Study on Efficient Methods for Optimal Design and Countermeasures Using Equivalent Circuit Models to Satisfy EMC Performance in Multi-Component Systems

Printed in Japan

Abstract

In recent years, high power output and high efficiency are required in the automotive and electronic device fields, and electromagnetic interference (EMI) problems due to conducted electromagnetic noise are increasing as the performance of products improves. For example, with the spread of electric vehicles, there are products such as body domain control, which is a single electronic control unit (ECU) to multiple modules connecting by cables. Such multi-functional, multi-component systems are called multi-component systems, and EMI problems are likely to occur and are difficult to solve. This is because in these systems, the connection of individual components forms a ladder-shaped circuit, causing problems such as resonance at unintended frequencies, resulting in difficulties in achieving electromagnetic compatibility. In addition, an efficient design is required that meets a number of requirements, for example, low cost, small size, and conformity to manufacturer's standards.

In general, the design process of multi-component systems proceeds in the order of specification decision, architectural design, actuator design, control system design, prototype, and reliability test. However, this design process is rarely completed in a single cycle, and in many cases, the required performance is not met in the reliability test. In this case, redesigning after prototyping is difficult and expensive countermeasures are not recommended. Therefore, an optimal design with redundancy design for each design parameter is desired so that the required performance can be met even in the case of element variations and changes in product specifications. In addition, there are cases in which requirements are not met in reliability tests after prototyping due to unexpected specification changes or changes in elements. In such cases, if countermeasures can be taken without rework, product development delays can be reduced. To achieve an efficient design that satisfies the EMC performance of multi-component systems, the purpose of this study is to establish an optimal design method before prototyping (A) and to realize rework-free countermeasures when problems occur after prototyping (B).

The realization of (A) and (B) requires iterative calculations on a PC, for which an equivalent circuit model that can quickly and accurately evaluate EMC performance is essential. By using this model, it is possible to represent the complex characteristics of a brush motor drive system (a system in which brush motors and control ECUs are connected by cables), which is an example of a multi-component system discussed in this thesis. In addition, in order to realize (A), by establishing a multi objective design

method to obtain multiple design parameters that simultaneously satisfy multiple performance requirements accurately, quickly, and widely range, using an equivalent circuit model. In the case of a brush motor drive system, the performance requirements include differential mode and common mode noise attenuation, which are filter characteristics, and the design parameters (X capacitor C_x, Y capacitor C_y, coil L, and cable length Λ) that simultaneously satisfy these requirements must be determined. Therefore, we will establish a multi-objective design method by calculating the relationship between these required performance and design parameters using an equivalent circuit model, mathematical modeling, and Artificial Neural Network (ANN) modeling.

In order to achieve (B), a procedure for implementing rework-free countermeasures is established. In brush motor drive systems, the LC resonance between the parasitic inductance of the cable and the capacitor C_x may not satisfy the requirements. Therefore, a procedure is proposed for implementing RL snubber circuits that can be implemented by creating a mathematical model of LC resonance from an equivalent circuit model. The effectiveness of the countermeasure procedure is confirmed by actual measurements. In order to achieve (A) and (B), thus, this thesis propose an optimal design method and countermeasure method using an equivalent circuit model to satisfy the EMC performance of multi-component systems.

This thesis consists of seven chapters. First, Chapter 2 explains the mechanism of brush noise generation in a brush motor drive system as a typical example of a multi-component system, the suppression method using a brush motor built-in filter, and the EMI problem caused by the filter, using actual measurement results. The built-in EMI filters need to suppress not only brush noise but also resonance simultaneously, because resonance occurs between the filter capacitor C_x and the parasitic inductance of the cable. In order to apply the optimal design, the target performance requirements and design parameters of the brush motor drive system are defined. Finally, the optimal design application phase and the countermeasure phase are described as EMI suppression methods in the design process.

Chapter 3 then describes the identification method of the equivalent circuit model of the conducted EMI environment in brushed motors, which is essential for applying optimal design methods and countermeasure techniques. The equivalent circuit model is identified using a 2-D electrostatic field solver and vector network analyzer (VNA). In particular, new measurement method using artificial mains network (AMN) was developed to evaluate the internal impedance of operating brush motors. As a result, the internal impedance of the operating brush motor was identified and verified under a conducted EMI system according to CISPR25 (Comite international Special des Perturbations Radioelectriques).

Chapter 4 describes the set-based design method as one of the multi-objective design methods. Here, the equivalent circuit model identified in Chapter 3 is combined with meta-modeling. In order to apply the design methodology, first, the relationship between the required performance and design parameters is calculated using the equivalent circuit model with three levels of initial data for the design range. Next, in order to create a

meta-modeling equation, the worst-case values in an appropriate frequency range are used and expressed as a second-order function using the response surface method. As a result, it is shown that by applying the set-based design method twice, an interval solution for multiple design parameters satisfying multiple performance requirements can be obtained.

The method given in Chapter 4 gave only one of interval solutions. In order to search for a wider range of interval solutions, therefore, Chapter 5 investigated an optimal design method using ANNs to obtain multiple local solutions. The modeling accuracy was improved by training the ANN model with the frequency spectrum as training data, which could not be used in the set-based design method in Chapter 4 due to the limitations of the solver. As a result, multiple interval solutions including those obtained by the set-based design method were obtained, indicating the effectiveness of this method. In order to further increase the recall rate, the training data were subjected to the cases of real and imaginary values, as well as to the case where the design parameter is set to five levels. The results show that the latter case increases the size of the interval solutions range, which indicates that the effectiveness of the method has been increased.

In Chapter 6, as a method to prevent rework after prototyping, the effectiveness of implementing RL snubbers in a brush motor drive system was evaluated. Similar to the power conversion circuits in the previous studies, the brush motor drive system implemented with RL snubbers can be expressed as an equivalent circuit characterized by a third-order characteristic equation. The experimental results confirmed that the implementation procedure is effective in suppressing EMI as a method of rework-free countermeasures after prototyping.

Finally, Chapter 7 summarizes the results of the research conducted in this PhD thesis to (A) establish an optimal design method before prototyping and (B) realize rework-free countermeasures when problems occur after prototyping, using an equivalent circuit model to satisfy the EMC performance of multi-component systems.

概要

近年, 自動車や電子部品の分野では高出力で高効率が要求されており, 製品の性能向上に伴い, 伝導電磁ノイズによる Electromagnetic interference (EMI) 問題が増加している. 例えば電気自動車の普及に伴い, 一つの ECU から複数のモジュールにケーブルで接続されたボディドメインコントロールなどの製品がある. このような多機能を実現する, 多くの部品で構成されるシステムはマルチコンポーネントシステムと呼ばれ EMI 問題が顕著となる. これらは異なるインピーダンスの部品が接続されており, 共振などの問題が生じ,Electromagnetic compatibility (EMC) 設計を複雑化させるためである. さらに低コスト化, 小型化, メーカ標準規格への適合など多くの要求を満たす効率的な設計が必要とされている.

一般的に, マルチコンポーネントシステムの設計プロセスは, 仕様決定, 構造設計, アクチュエータ設計, 制御設計, 試作, 信頼性試験の順に進められる. しかし, この設計プロセスを一度で終えることは稀で, 信頼性試験で要求性能を満たさない場合が多い. この場合, 試作前に設計プロセスを戻した設計は困難で, 高価な対策が必要となるため避けたい. そのため, 部品のばらつきや製品仕様の変化に対しても要求性能を満たせるように, 各設計パラメータに冗長設計を持たせた最適設計が望まれる. しかし, 想定外の仕様変更や素子の変化が原因で試作後の信頼性試験で要求を満たさない場合がある. その場合でも手戻りなしの対策が可能であれば, 製品開発の遅れを減らせることができる. 本研究では, マルチコンポーネントシステムの EMC 性能を満足する効率的な設計を実現するために, 試作前の最適設計手法の確立 (A) と試作後の問題発生時に手戻り無い対策の実現 (B) を目的とする.

(A) および (B) の実施は PC 上で行われ, 繰り返し計算を行うには EMC 特性を迅速かつ精度良く評価できる等価回路モデルが必要不可欠である. このモデルを用いることで, 本論文で取り上げるマルチコンポーネントシステムの一例であるブラシモータ駆動系 (ブラシモータと制御 ECU をケーブルで繋いだシステム) の複雑な特性を表現することが可能となる. さらに (A) の達成には, その等価回路モデルを用いて, 複数の要求性能を同時に満たす複数の設計パラメータを精度良く, 迅速に, 広い範囲で求める多目的設計手法を確立することで実現する. ブラシモータ駆動系の場合, 要求性能はフィルタ特性であるディファレンシャルモード, コモンモードノイズ減衰量が必要であり, これらを同時に満たす設計パラメータ (X コンデンサ C_{x},Y コンデンサ C_{y}, コイル L, ケーブル長 Λ) を定める必要がある. そこで等価回路モデルを用いてこれらの要求性能と設計パラメータの関係を計算し, 数理モデリング及び人工ニューラルネットワーク (ANN) を用いたモデルを作成することで多目的設計手法を確立する. また (B) の達成には, 手戻りの無い対策手法の実装手順を確立することで実現する. ブラシモータ駆動系ではケーブルの寄生インダクタンスと

コンデンサ C_{x} とのLC共振により要求を満たさない場合がある．そこで,等価回路モデルからLC共振に関する数理モデルを作成し対策可能なRLスナバ回路の実装手順を提案する．そして対策手順の有効性を実測により確認する．以上の取り組みにより,(A)と(B)の実現を目的としたマルチコンポーネントシステムのEMC特性を満足するため等価回路モデルを用いた効率的な最適設計及び対策手法を提案する．

2章ではブラシモータ駆動系で発生するブラシノイズ発生メカニズム,内部フィルタによる抑制方法,および,それによって発生するEMI増加を実測結果を用いて説明した．ブラシモータ駆動系における内部EMIフィルタは,フィルタのコンデンサとケーブルの寄生インダクタンスとの間で共振が発生するため,ブラシノイズだけでなく共振も同時に抑制する必要がある．そこで,この最適設計を適用するためブラシモータ駆動系における目標となる要求性能と設計パラメータを定義する．最後に,設計プロセスにおけるEMI抑制対策手法として,最適設計の適用フェーズ及び対策手法フェーズを説明した．

3章では最適設計手法及び対策手法の適用に必要不可欠なブラシモータ駆動回路における伝導EMI試験環境の等価回路モデルの同定を行う．等価回路モデルは,2次元静電場ソルバとベクトルネットワークアナライザー(VNA)を用いて同定する．特に動作状態におけるブラシモータのインピーダンス評価方法としてArtificial Mains Network (AMN)を使用した手法を考案した．結果としてComite international Special des Perturbations Radioelectriques 25 (CISPR25)準拠した伝導EMI試験システムの同定,ブラシモータの動作状態のインピーダンスの同定,妥当性を示した．

4章では3章で述べた等価回路モデルとメタモデリングを組み合わせた多目的設計法の1つとして,セットベース設計手法の手順とその適用を示した．設計手法の適用のために,まず等価回路モデルを用いて設計範囲を3分割した初期データを用いて要求性能と設計パラメータの関係を計算する．次にメタモデリング式の作成のため,任意の周波数範囲における最悪値を使用して応答曲面法を用いて2次関数で表現した．結果,セットベース設計法を2回適用することで,複数の要求性能を満足する複数の設計パラメータの範囲解を得られたことを示した．

第4章で示した方法では,区間解は1つしか得られなかった.そこで第5章では,より広い範囲の区間解を探索するために,ANNを用いて複数の局所解を得る最適設計法を検討した．セットベース設計手法ではソルバの制約上,用いることができなかった周波数スペクトルを訓練データとしてANNモデルに学習させることで,モデリング精度を向上させた．結果,セットベース設計手法で得られた解を含めた複数の範囲解を得られたため有効性を示した．さらに再現率増加のため,訓練データを実数値と虚数値の場合と設計範囲を5分割した場合で学習させた．結果,後者の場合,範囲解の広さの増加を確認でき,有効性が高くなったことを示した．

6章では試作後の対策手法として,ブラシモータ駆動系にRLスナバ実装手順を導入し,検証した．従来より提案される最適設計を適用するために,RLスナバを搭載したブラシモータ駆動系を3次特性方程式で特徴付けられる等価回路に表現できることを確認した．実験の結果,実用的なEMI抑制に有効であることが確認された．

7章では本研究を通じて得られた知見をまとめた．(A)と(B)の実現を目的とした,提案したマルチコンポーネントシステムのEMC特性を満足するため等価回路モデルを用いた効率的な最適設計及び対策手法に関してまとめた．

Acknowledgments

This thesis summarizes my doctoral study in Electronic and Information Systems Engineering at Okayama University. The work has been enriching, and I am grateful to many who have contributed to this endeavor.

I am profoundly grateful to Professor Yoshitaka Toyota for granting me the opportunity to embark on this research. His invaluable advice and unwavering encouragement have been important in my work. Associate Professor Kengo Iokibe has provided significant comments, advice, and engaging discussions that sparked many ideas forming the core of this thesis. I would like to thank Professor Norikazu Takahashi for his valuable guidance and support in the research of the ANN model. I also greatly appreciate my advisors Professor Satoshi Denno for his helpful comments on my research work conference.

I extend my thanks to the entire team at the Optical and Electromagnetic Waves Laboratory, Okayama University, including both past and present members, for their collaborative spirit and support. Special thanks to Mr. Kanao Sho, Mr. Masaki Himuro, Mr. Akito Mashino, Mr. Ryo Maekawa, Mr. Sojun Maeta, and Mr. Yoshiaki Tanimoto for their technical expertise and assistance in overcoming numerous challenges.

My appreciation also extends to the university for providing the necessary facilities and resources, and to the technical and administrative staff whose behind the scenes efforts have been invaluable. Ms. Masako Okamoto deserves special mention for her secretarial services, ensuring smooth administrative processes throughout my research. To my job members and peers, thank you for your moral support and for the enriching experiences shared. Your encouragement has been a source of strength.

My deepest appreciation goes to my family, especially my mother, Ms. Kaoru Kan, and my wife, Ms. Michiko Kan, for their unwavering support, encouragement, and resources. Their understanding and patience have been the bedrock of my perseverance. Finally, I extend my gratitude to anyone who has contributed, directly or indirectly, to my research and personal growth during this doctoral work.

Contents

List of Figures

List of Tables

List of Variables

Variable	**Meaning**
b	bias at each epoch in ANN
β	correlation coefficient
C_{bp}	input capacitor of low-side switch MOSFET
C_{is}	capacitance between the coil and the coil
C_{m}	parasitic capacitance inside the motor
C_{s}	parasitic capacitance between the motor and the system ground
C_{x}	X capacitance inside brush motor
C_{y}	Y capacitance inside brush motor
F_{all}	F parameter on the motor and AMNs
F_{GND}	AMN side F parameter on the - terminal
F_{motor}	F parameter on the motor side
F_{power}	AMN side F parameter on the + terminal
f	frequency
I_{ns1}, I_{ns2}	motor A noise current source
k	coupling coefficient
L	coil inside brush motor
L_1, L_2	inductance per meter
L_{pn}	inductance due to magnetic losses
L_{snb}	inductance of RL snubber
L_{x}	parasitic inductance of X capacitance
L_{y}	parasitic inductance of Y capacitance
$\mathit{\Lambda}$	cable length inside brush motor
N_{FN}	number of predicted results that are failure and actual result is failure
N_{FP}	number of predicted results that are failure and actual result is pass
N_{TN}	number of predicted results that are pass and actual result is failure
N_{TP}	number of predicted results that are pass and actual result is pass
Q	quality factor at the resonance frequency
R_{H}	resistance per meter
R_{pn}	resistance due to magnetic losses
R_{q}	interval solution range
R_{snb}	resistance of RL snubber

V	size of interval solution range
V_{CM}	common voltage of AMN in conducted emission
$V_{\mathrm{CMnoiseATT}}$	common mode attenuation in conducted emission
V_{DM}	differential voltage of AMN in conducted emission
$V_{\mathrm{DMnoiseATT}}$	differential mode attenuation in conducted emission
V'_{CM}	common voltage of AMN in conducted emission with filter
V'_{DM}	differential voltage of AMN in conducted emission with filter
V_{H}	positive terminal voltage of AMN in conducted emission
V_{Hmeas}	positive terminal measurement voltage of AMN in conducted emission
V_{L}	negative terminal voltage of AMN in conducted emission
V_{Lmeas}	negative terminal measurement voltage of AMN in conducted emission
X_{C}	capacitive reactance
X_{L}	inductive reactance
Z_1,Z_2	differential mode impedance identified impedance
Z_3	common mode impedance identified impedance
Z_{A}	motor A impedance
Z_{B}	motor B impedance
Z_{loop}	impedance of the resonant loop
ω_0	angular resonant frequency at which imaginary part of impedance becomes zero
w	weight at each epoch in ANN
x_{q}	design parameters
y_{q}	required performance

Chapter 1

General Introduction

1.1 Background

In this chapter, we first discuss an overview of Electromagnetic Compatibility (EMC). We will also provide an overview of the subjects associated with ECU design in automotive products and home appliances. We will then discuss the motivation and objectives of this thesis. Lastly, we will outline the contents of this dissertation.

1.1.1 EMC Design Overview and Design Issues

In recent years, the importance of EMC design has been emphasized. EMC ensures, as shown in Fig. 1.1, that electronic devices do not unintentionally cause what is called Electromagnetic Interference (EMI), and that they possess the ability to appropriately respond to external interferences, known as Electromagnetic Susceptibility (EMS). Especialy, due to the increasing electrification, high power, and complexity of automotive and household electronic products, there has been a noticeable increase in EMI. With the technological advancements in autonomous vehicles and electric vehicles, the importance of EMI filter design in electronic products has been growing. Behind one of this trend, there are the multiple requirements for smaller products and higher performance, etc., which is related to the increase in EMI between electronic devices. In addition,

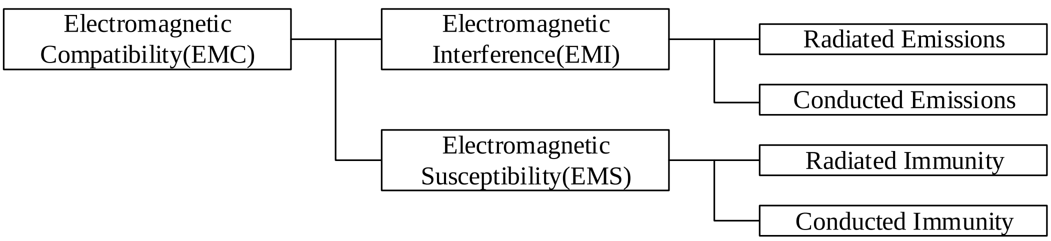

Figure 1.1 A basic illustration of the elements of EMC design.

with the expansion of electronic device products both domestically and internationally, designing products to satisfy the standards set forth in each country has become even more complex. In order to sell a product in the market, it must meet various standards and criteria.However, satisfying these requirements often conflicts with meeting the cost and size constraints of the product. For example, high-quality EMC filters and shielding materials are expensive, and it is difficult to make the best choice within a limited budget. In addtion, even if an EMC filter with simply better characteristics is used, the characteristics may deteriorate due to mutual effects with other components [5–7]. Thus, multiple requirements, especially the technical problems associated with lower cost and smaller size, make it difficult to design and it is difficult to design an EMI filter that satisfies many performance requirements [8–13].

In the current design method, as shown in Fig. 1.2, prototyping and testing are repeated many times to achieve a design that satisfies reliability tests. However, it is difficult and very inefficient to create a design that satisfies all requirements through trial and error.Also, if EMI countermeasures are insufficient in the early stages of design, later stage remedies can be extremely costly. For instance, if EMI issues become apparent during the prototyping stage of the design process, it may become necessary to increase the size of the EMI filter or to redesign before prototyping, often leading to higher costs and extended development process. Therefore, evaluating EMI testing in the early stages of product design is crucial to detect issues in advance and implement efficient solutions. To overcome these subjects, it is necessary to predict problems and investigate solutions quickly from the early design stage by using circuit calculation tools and the mathematic

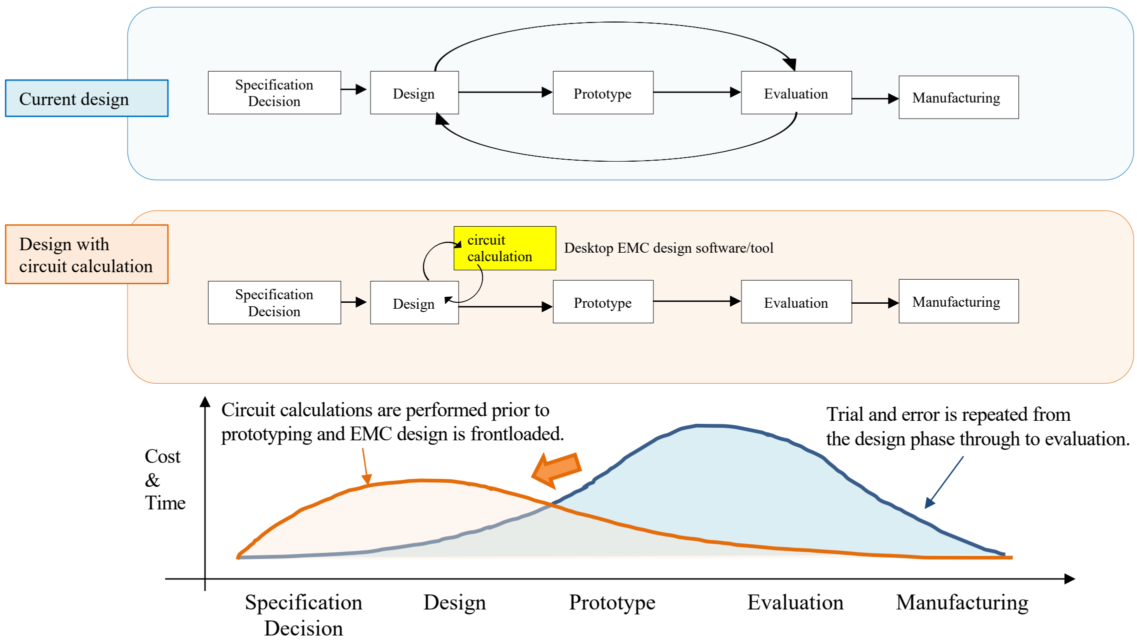

Figure 1.2 Comparison of current EMC design and efficient EMC design using circuit calculations.

modeling of the relationship between the design parameter and the requirement performance that can be calculated on a desktop, as shown in Fig. 1.2 [13–18]. Appropriate approaches to EMC design before prototyping, such as EMC design front loaded, can not only improve product safety and reliability, but also reduce development costs and time to market .

1.1.2 Common Mode and Differential Mode Noise from EMI Testing

This section introduces the configuration of conducted EMI testing environment of the brush motor drive system as one of products of multiple components. Also, differential mode and common mode are described as necessary elements for EMI suppression.

EMI testing is a quantitative evaluation of how a device or system reacts to electromagnetic interference or how much it generates. This testing is essential to verify that a product meets national and international standards and criteria for electromagnetic interference. If the product fails the standard, the EMI test should be redesigned or improved. Fig. 1.3 shows an equivalent circuit for conducted EMI testing system of the brush motor drive system from the equipment under test (EUT). To verify that the regulatory values are met, conducted emissions are measured using artificial mains network (AMN). The AMN is inserted at the measurement point between the EUT and the power supply, and the AMN serves to keep the impedance of the power supply line under test constant during measurement. This stabilization improves the repeatability and reliability of test results [19–23]. Conducted Emission (CE) analysis is important to solve EMI problems. CE can be broadly classified into common mode (CM) noise and differential mode (DM) noise. Since both modes of noise have different propagation paths, effective countermeasures for each are also different. Therefore, it is essential to select effective countermeasures. Common mode noise is that which passes through the system GND and circulates through

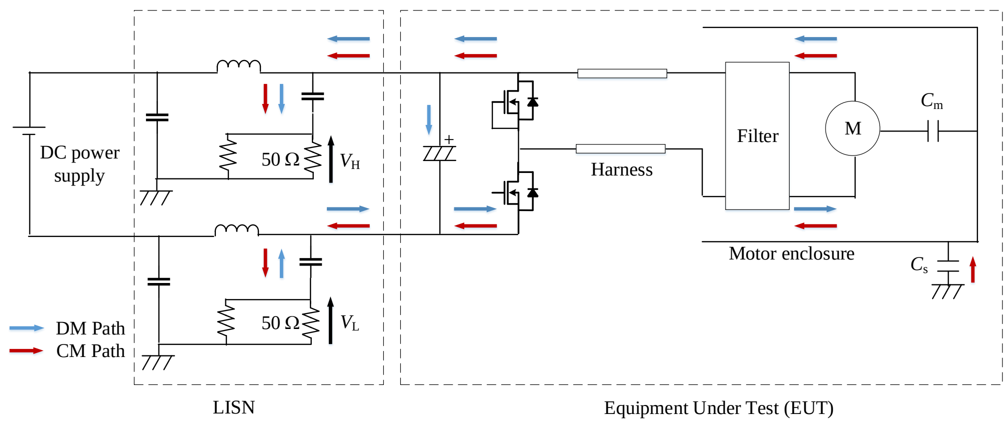

Figure 1.3 Differential mode and common mode noise paths in brush motor drive systems.

the power supply line. This noise often couples to the GND system through parasitic capacitance in the EUT and motor case, and this coupling capacitance can become a CM noise path. In contrast, differential mode noise flows between positive and negative power lines and its return path is compact because it flows in a small loop region. This means that when measured by EMI testing at the AMN terminals, it contains both DM and CM noise components. Therefore, when implementing countermeasures against Conducted Emission, it is necessary to analyze the effectiveness of EMI filters in reducing noise at both DM and CM, and apply countermeasures such as adjusting the appropriate topology and constants of the filters. Thus, based on the V_{H} and V_{L} obtained at the AMN terminals, the following equations can be used to calculate the DM and CM voltages.

$$V_{\mathrm{DM}} = V_{\mathrm{H}} - V_{\mathrm{L}} \tag{1.1}$$

$$V_{\mathrm{CM}} = V_{\mathrm{H}} + V_{\mathrm{L}} \tag{1.2}$$

Especialy, in this study, in order to evaluate the attenuation characteristics $V_{\mathrm{DMnoiseATT}}$ and $V_{\mathrm{CMnoiseATT}}$ by the filter in each mode, the attenuation of DM and CM with and without the filter can be calculated based on the following equations (1.3), (1.4), respectively. Let V'_{DM} and V'_{CM} denote the state where the filter is in use, and V_{DM} and V_{CM} represent the state without the filter. Thus, at the stage of EMI filter design, it is necessary to design the filter to ensure the amount of DM attenuation $V_{\mathrm{DMnoiseATT}}$ and CM attenuation $V_{\mathrm{CMnoiseATT}}$, in each frequency band required [8–13].

$$V_{\mathrm{DMnoiseATT}} = V_{\mathrm{DM}} - V'_{\mathrm{DM}} \tag{1.3}$$

$$V_{\mathrm{CMnoiseATT}} = V_{\mathrm{CM}} - V'_{\mathrm{CM}} \tag{1.4}$$

1.2 Design Process in Multi-Component Systems and Proposed EMC Design Flow

This section describes the design process in the brush motor drive system as one example of multi- component systems and proposes the flow of the EMI countermeasure method in this study. Finally, an overview of the proposed design method and its purpose and motivation will be presented in this thesis.

1.2.1 Design Process in Multi-component Systems and Proposed Design Flow

Multi-component systems have been increasing in the automotive and electronic component fields, and the complexity of Electromagnetic Interference (EMI) problems caused

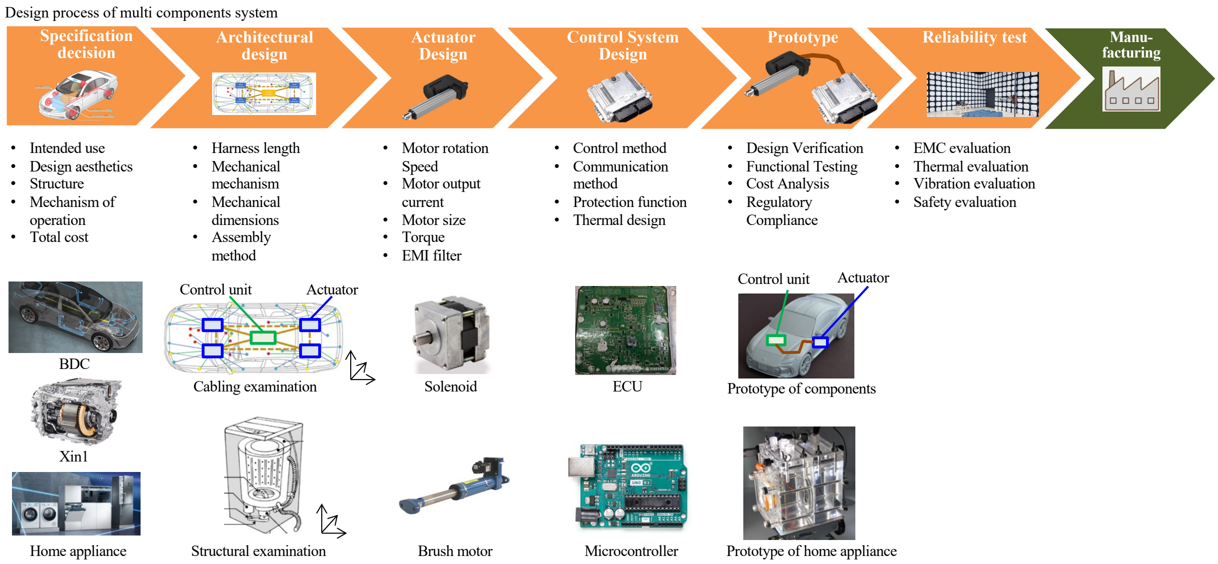

Figure 1.4 Design process example in multi-component systems.

by conducted electromagnetic noise has become an issue. For example, components that connect a single ECU and multiple modules with cables, called Body Domain Control or components that connect a battery, motor, inverter, and transmission in a product called Xin1. An example of the design process for such a multi-component system product is shown in Fig. 1.4.

Firstly, define the basic requirements and functions of the system as a specification decision and clarify objectives, performance criteria, and constraints. Next, in architectural design, cable and structural examinations are designed as the overall structure of the system and the relationships among major components. The detailed design of the actuators (moving elements) in the system includes the design of motors, servos, solenoids, and other drive devices in actuator design. In control system design, ECU and micro controller are developed and implemented as control mechanisms to ensure that the system meets specific operating requirements and required performance. In prototyping, testing is performed to ensure that the product will properly perform the functions in order to assume. This includes integrating the entire system and verifying the operation of each function. Finally, in reliability tests, EMC, temperature, and vibration evaluations are performed to confirm the reliability and durability of the product.

However, these processes are rarely completed in a single cycle, and reliability tests often fail to meet the required performance. The current EMC design process from specification decision to reliability test is shown in Fig. 1.6a. If the EMC test fails, stepping back through multiple stages is usually not permissible in the design process due to its impact on the product specifications. In such cases, EMI problems, if discovered, may require expensive EMI filters, shielding, and ferrite cores, and may extend development cycles, which should be avoided. One of the reasons that reliability tests do not meet

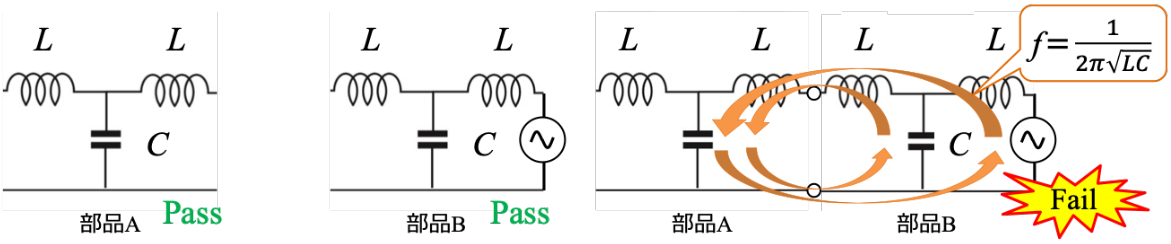

(a) Circuit of individual component (b) Circuit of multi-component system

Figure 1.5 Example of reliability test failure due to resonance in a multi-component system.

the requirements is described. As shown in Fig. 1.5a, each individual component often passes the reliability test. However, these components are composed of multiple parts as shown in Fig. 1.5b, and in this case, the connection of the parts causes resonance and other problems unintended by the designer. As a result, the EMC performance does not meet the requirements, and the reliability test does not meet the requirements, which can be a problem. Also, one of the reasons that reliability tests do not meet the requirements is the possibility of changes in product characteristics due to elemental Design process of multi components system variations or changes in product specifications. By optimizing the design with redundant design before prototyping, it is possible to design a device that satisfies the required performance in reliability tests even if there are element variations or changes in the product specifications [21, 24, 25]. Therefore, optimal design with redundant design before prototyping is important to detect problems in advance and implement improvements efficiently. On the other hand, it is also important to solution method with redundant design after prototyping as well as before prototyping. Even if a large amount of time is spent on the design before prototyping, there are cases in which the EMI test fails due to other factors after prototyping. If the product does not satisfy the requirements, it cannot be sold in the market. Therefore, even in the after prototyping stage, an optimal design method for EMI solution method is effective to prepare for any eventuality. Especially in the case, since it is necessary to shorten the time to market, an efficient and quickly EMI solution method is desired.Thus, it is essential to study efficient countermeasures for EMI design in the design process before and after EMI test. Therefore, it is necessary to have a solution method that can effectively suppress EMI in case of EMC test failures.

Therefore, we propose an efficient design flow as shown in Fig. 1.6b. The study of EMI problems in this thesis applies set based design method such as Preference Set-based Design (PSD) and an optimal design method using ANN for EMI filters in the before prototype stage of the design process. This enables redundant designs that satisfy requirements even when product specifications change or element variations occur [21, 24, 25]. In addition, the application of the RL snubber design method enables countermeasures to be taken even if the EMI test fails after prototyping [26–36]. Appropriate

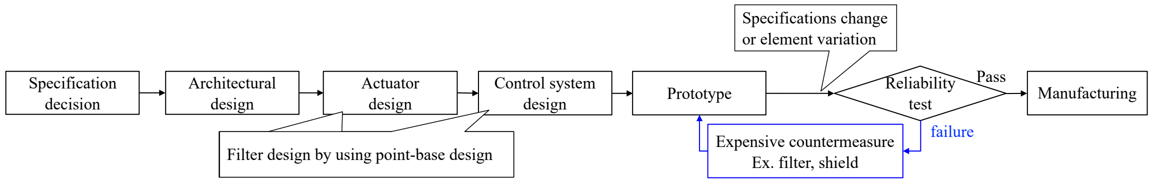

(a) Current design flow

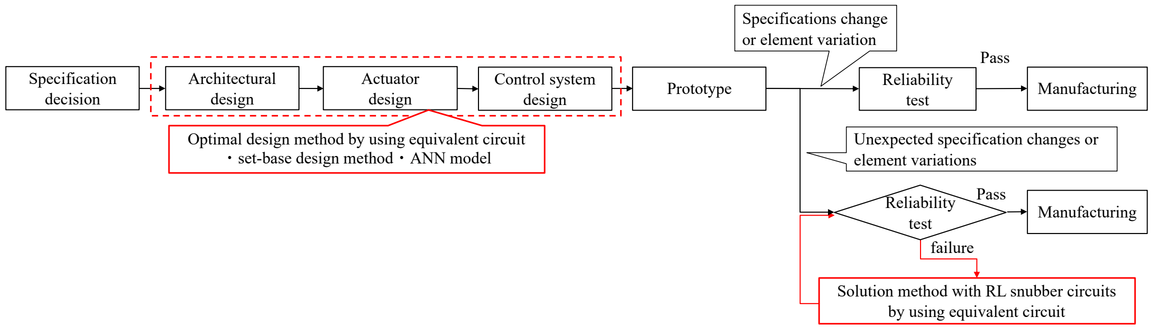

(b) Proposed design flow

Figure 1.6 Design process flow of products in multi-component systems: (a) current and (b) proposed.

design of EMI filters by applying the optimal design method according to the design process is extremely effective in shortening the design process and enables quick and effective noise suppression.

1.2.2 Point-Base Design Method and Set-Base Design Method

This section describes the advantages of applying set based design over point based design methods in the design process in Fig. 5.3.

Conventionally, the point-based design method shown in Fig. 1.7a is often used in the design field for EMI filter design. This is to find the combination of the design parameters x_i and x_j to be passed. The designer searches for a combination that satisfies the requirements by changing the design parameters with the intent. This method seeks a single optimal solution that satisfies multiple requirements. However, when product specifications change or device variations occur, it may be difficult to satisfy the requirements. The reason for this is that there are many elements and components in an electronic device, and their interactions are extremely complex. It is difficult to design for the mutual effects of design changes, which increases the risk of test failures. Therefore, in many cases, countermeasures against EMI problems often involve design iterations and trial-and-error to achieve a design that satisfies the standard, which can take an enormous amount of time. As a solution to such a problem, it is considered effective for EMI filter design to be redundantly designed to obtain not one solution that can satisfy the requirements, but multiple solutions [21, 24, 25].

In contrast to point-based design, the set-based design shown in Fig. 1.7b allows a set

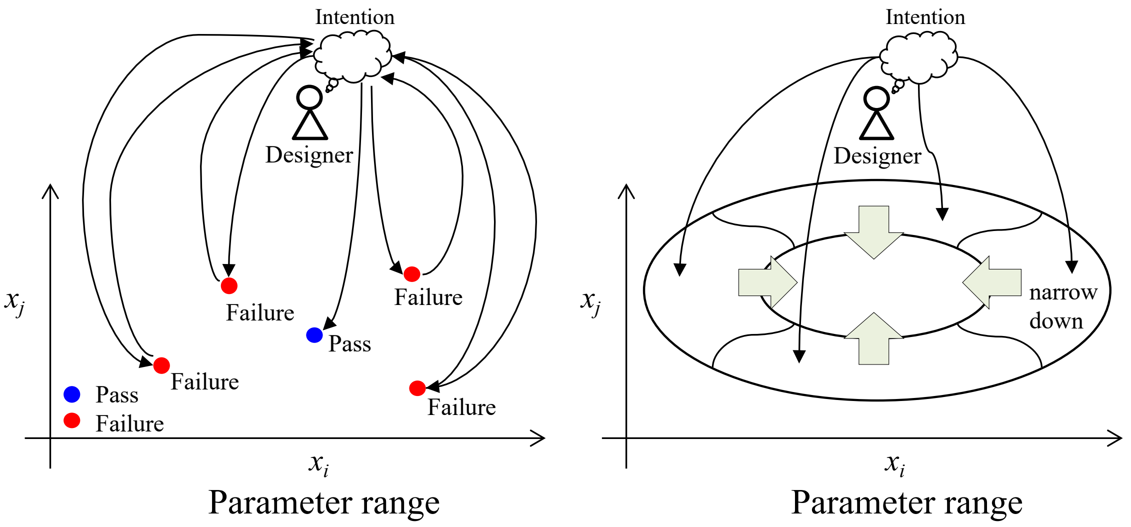

(a) Point-based design method (b) Set-based design method

Figure 1.7 Comparison of point-based and set-based design methods [1, 2].

of design solutions to be obtained as an interval solution, rather than a single solution that satisfies multiple requirements [1, 2]. Therefore, this method can determine the most effective and efficient one combination among multiple solutions and is expected to reflect the designer's intention. In addition, even if product specification changes or element variations occur, the design can be proceeded with consideration of these changes to meet the requirements, reducing EMI without necessitating many design process revisions [21, 24, 25]. In this way, the design can be flexible to design changes. In order to obtain multiple ranges of interval solutions that satisfy multiple requirements, there is a method of all-inclusive search in which all combinations within the design range are calculated. However, the method of calculating all combinations would take an enormous amount of time and would be impractical. Therefore, in this study, we will propose an optimal design method that enables set-based design such as PSD and an optimal design method using ANN.

1.3 Design Procedure by Optimal Design and Solution Method with Equivalent Circuit Model

This section describes the proposed method on optimal design before prototyping and implementation solution after prototyping using equivalent circuit models for multi-component systems.

A multi-component systems consists of many components, each of them affecting each other, increasing the complexity of the EMC design and making it difficult to meet many of the requirements. Therefore, a model is needed that can quickly and accurately evaluate EMC performance with many performance requirements. Equivalent circuit models can represent the characteristics of these complex systems and enable the calculation of design parameters that satisfy the target required performance. At this time, it is essential to construct a highly accurate equivalent circuit model to determine the design parameters that satisfy the requirements in order to prevent redesign in the design process [26, 30, 32, 33, 37, 38]. This is because the accuracy of the model has a significant influence on the calculated filter characteristics, the attenuation characteristics $V_{\mathrm{DMnoiseATT}}$ and $V_{\mathrm{CMnoiseATT}}$. However, using an equivalent circuit model with a circuit simulation tool, EMC performance can be calculated quickly, saving limited time in the design process. However, using equivalent circuit models with circuit simulation tools allows for quick calculations of EMC performance, contributing greatly to saving limited time in the design process [14–18, 26, 30, 32, 33, 37–39].

However, it is difficult to optimize these multiple parameters simultaneously even with an equivalent circuit model, and it is inefficient to repeat the design and simulation process. Thus, it is difficult to design the EMI Filter obtained multiple ranges of interval solutions that satisfy multiple requirements. By using mathematically models, various design can be calculated quickly and the optimal solution can be identified efficiently [1, 2]. Furthermore, many conditions that it is difficult to consider in actual experiments and prototypes can be explored by modeling using simulations. Therefore, Input and output data for modeling is obtained by utilizing desktop simulation tools rather than using actual measurements. At that time, the equivalent circuit model is identified by measuring the impedance to the actual product and d using a 2-D electrostatic field solver [16–18, 39]. This approach allows optimization in the early stages without repeated prototyping and experimentation. This is expected to reduce prototype costs and development time. By modeling the relationship between the obtained design parameters and objective function, and optimizing based on this relationship using software and tools, the interval solution of design parameters that simultaneously satisfy multiple performance requirements can be quickly identified [40]. Therefore, it is possible to solve these problems if multiple design parameters that satisfy multiple performance requirements can be determined quickly, accurately, and over a wider interval solution range. In order to achieve this, we propose to optimize the design and improve design efficiency by creating and modeling an equivalent circuit model of the entire system. As modeling methods, this study proposes a set-based design method using mathematical modeling and a design method using ANN, which is a machine learning modeling.

On the other hand, it is also important to take a solution method in the evaluation after prototyping. This is because there are cases where EMI tests fail due to other factors after prototyping. In such cases, we propose a solution method that uses an equivalent circuit model to solve the problem effectively without rework. In particular, this study proposes a procedure to design RL snubbers using the previously proposed optimal design method [32–35]. By verifying the EMI suppression effect of the RL snubber obtained using the optimization method through actual measurements, the optimal design of the RL snubber

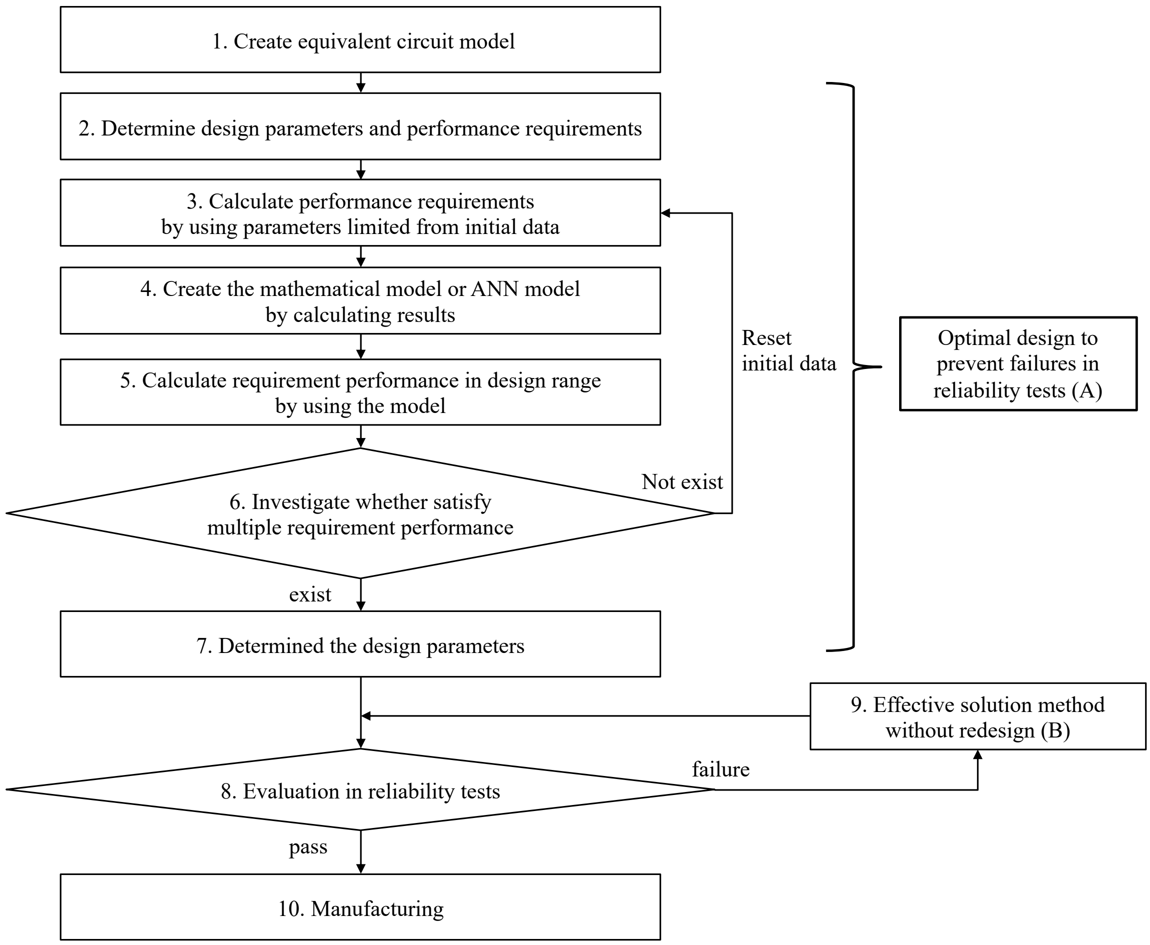

Figure 1.8 The design procedure by using optimal design and solution method with equivalent circuit model.

circuit is practically feasible if it can be determined that the loop of LC resonance of any circuit is an equivalent circuit characterized by the third-order characteristic equation. As a result, by establishing a practical optimal design procedure, the process of problem solving can be more efficient and expedited.

Finally, we propose the design procedure shown in Fig. 1.8, which consists of an optimal design method before prototyping using an equivalent circuit model and a solution method after prototyping.

1. Create an equivalent circuit model of the product. Create circuit models of the entire system, not just the components, to create an accurate model.

2. Determine the multiple performance requirements and multiple design parameters.

3. Determine initial data for design parameters. Calculate performance requirements by using parameters limited from initial data.

4. Using the calculation results of the combination of required performance and design

parameters, create a mathematical model or Artificial Neural Network (ANN) model that represents the relationship between these parameters.

5. Target performance requirements are set, and design parameters that satisfy the requirements are examined using the created model.

6. Investigate whether satisfying the required performance. If there is no satisfactory combination, increase the range or add or change another variable.

7. Determine the design parameters.

8. Evaluate whether the resulting multiple design parameters satisfy the multiple performance requirements.

9. If they fail, allow straight forward design by using effective solution methods without redesign.

10. Proceed to the manufacturing process.

1.4 Explanation of Thesis Structure

As described above, this thesis focuses on systems composed of multiple components and proposes an optimal design method for EMI suppression. The method first constructs an equivalent circuit model of conducted emissions. Next, a mathematical modeling method using the equivalent circuit model is studied, and the optimal design is performed using a set-based design method and an optimal design method using ANN. Finally, the optimal design method of RL snubber is applied to counter noise due to LC resonance generated by other factors.

The thesis is organized as follows in Fig. 1.9. In Chapter 2, EMI problems in brush motor drive systems as example systems composed of multi-component systems and proposed practical countermeasures to solve them are presented. This section describes the noise generation mechanisms and the selection of suppression methods. The specific suppression methods include modification of cable length, modification of filter constants, and application of RL snubber and RC snubber circuits, and the effectiveness of each and how to apply them in the design process are discussed. The design parameters necessary to proceed with the optimal design and the metrics for evaluating requirement performance will also be clarified. In Chapter 3 introduces in detail the modeling of noise sources and the impedance identification method to improve the accuracy of the model for targeted brush motors system. The accuracy of the model has a significant influence on the output of design parameters that satisfy the required performance. In particular, to model the impedance of brush motors more accurately, a measurement method that more accurately accounts for the motors under operating condition is described. In Chapter 4, the details

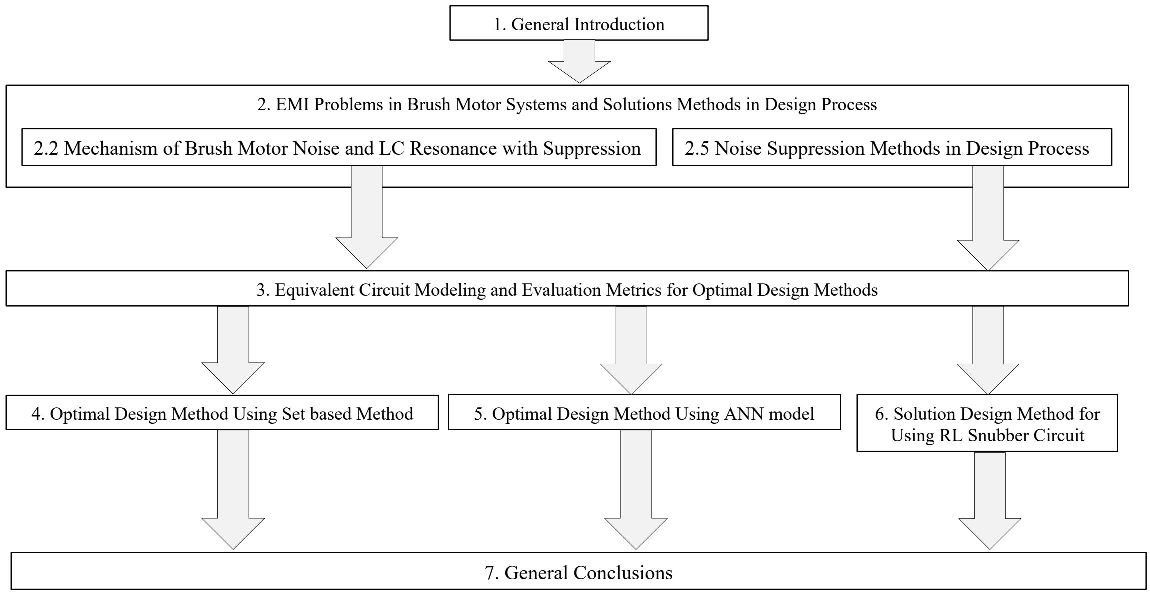

Figure 1.9 Chapter flows of this thesis.

of the set-based design method and, in particular, the application procedure, required initial data, and results obtained when utilizing the set based method are described. Apply the proposed procedure to obtain a range of design parameters and evaluate their validity in brush motor drive systems. Chapter 5 describes the theoretical background of the ANN based design method and the filter design obtained using the created ANN model. For brush motor drive systems, a design method using the ANN model will be used to obtain a wider range of design parameters and to evaluate their validity. In Chapter 6, we evaluate the proposed implementation procedure of the optimal design of the RL snubber circuit as an EMI suppression method when the EMI test fails during prototyping. Conventional proposed optimal methods will be used to explain the applicability of the brush motor drive system, and the suppression effect by actual measurement when implemented will be described.

Chapter 2

EMI Problems in Brush Motor Drive Systems and Solution Methods in Design Process

2.1 Introduction

In recent years, automotive and electronic device designs have become increasingly complex due to factors such as higher efficiency, smaller size, and stricter budgets. In addition, EMI has a serious impact on the performance of electronic equipment, and environmental regulations have become stricter, making efficient EMI suppression filter design essential. In order to efficiently design countermeasures and element tuning to meet these many performance requirements, a method to predict EMI accurately and quickly is needed. Various noise source models have been developed to accurately and quickly predict EMI in the design of automotive equipments and consumer electronics products [8–13]. In particular, several noise source equivalent circuit models have been proposed for brush motors used in automotive and electronic equipments [13–18]. Since electromagnetic noise from micro-arcs generated by the rotation of brush motors is expected to continue to be a problem in the future, the prediction of noise levels and countermeasures are important in EMI reduction [3, 4]. EMI filters are also used as basic components for EMC countermeasures and are widely used in high-speed differential signal wiring, power supply lines, etc [5–7]. In addition, the design of EMI filters is based on the separation of differential mode and common mode [19–23]. In the evaluation of these filters individually and elements individually, a solution that satisfies the requirements for the target value is required. In many cases, the design parameters that satisfy the required values have been obtained by setting the desired values based on the attenuation characteristics of the filter itself or the transmission characteristics of the transmission line. However, in order to market a product, it is necessary to satisfy all of these conditions, taking into account the actual product installation environment, the evaluation environment based on international standards such as CISPR25 and CISPR22 [41–43], and the EMI limitations of the individual manufacturer. The EMI limitations of each manufacturer must also be taken into account. Furthermore, it is not easy to design a circuit that can separate DM, CM and satisfy the required characteristics of each at same time. Therefore, an optimal design focusing only on a simple filter is not practical, and since the parameters of the entire system affect each other, it is necessary to consider the design of the multi-component systems, including the parameters that affect it.

In EMI suppression design, it is important to design EMC considering the multi-component systems at the initial stage, such as before prototyping. Even if each individual component achieves its EMI rating, this may not be achieved due to interactions between components during the evaluation of the entire system after prototyping the design process. In this case, it is often difficult to undo the design of the component because the design process is already in progress in many phases. As a result, additional filter elements may be introduced to avoid rework, which results in increased costs. Therefore, it is essential to study the entire system in the early stages to avoid such problems. Thus, by taking an EMC design approach that takes into account the entire system interaction from the initial stages of the product design process, the performance and quality of the product can be improved. This will prevent rework and failures in later stages, lead to efficient product development, and increase competitiveness in the competitive marketplace.

Therefore, this thesis establishes a multi-objective design method to optimize the EMC design including the multi-component systems, which allows for consideration in the initial stage. The objective is to obtain multiple design parameters (including non-filter parameters) that simultaneously satisfy multiple performance requirements with high accuracy, high speed, and a widely range of interval solution. Previous set-based design methods examined methods to obtain a single range solution. Focusing on the optimal design of the individual filter, the S-parameters were evaluated to satisfy the target value at a given frequency with respect to the transmission characteristics. This method was able to obtain one interval solution [44–47]. However, if these techniques are to be applied in a more practical application, it is essentially necessary to include design parameters other than the filter. Furthermore, it is desirable to be able to obtain wider range of interval solutions.

The remainder of this chapter is organized as follows. Section 2.2 introduces the mechanism of brush noise generation in brush motors reported in previous papers and the objective of this study. An explanation is given regarding the occurrence of LC resonance, where the application of brush noise countermeasures increases EMI. Section 2.3 discusses the generation of LC resonance when brush noise reduction measures are applied, and the degradation of EMI filter characteristics using the parameters of DM, CM attenuation characteristics. Finally, Section 2.4 describes suppression methods to simultaneously suppress EMI increase by resonance and brush noise. In addition, these solution methods are summarized. Section 2.5 summarizes the main points and concludes the chapter.

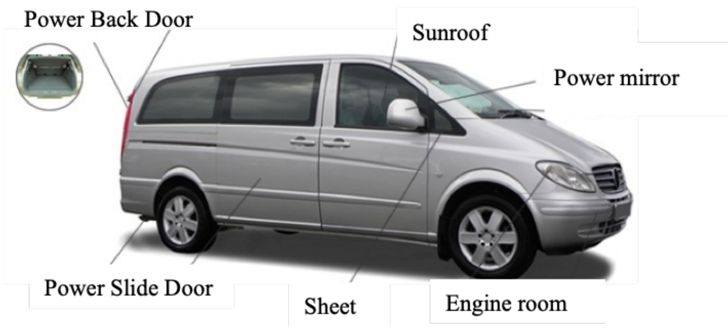

Figure 2.1 Products using brush motor drive systems installed in automotive [3].

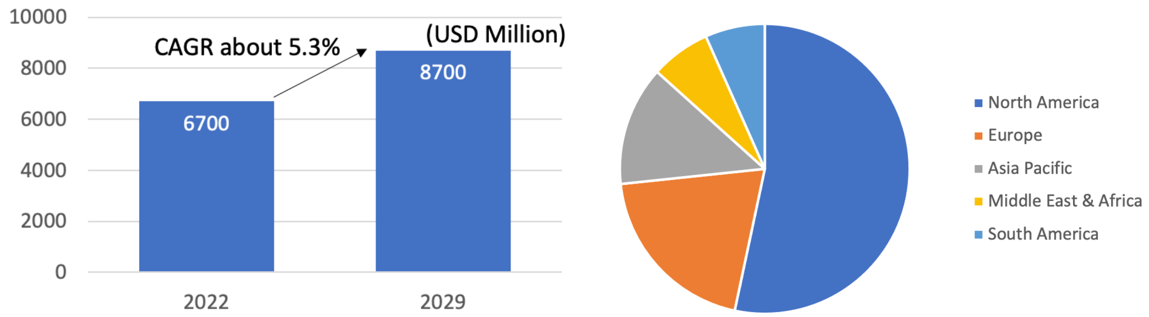

(a) Measure in investment and business (CAGR) of Brush motor market

(b) Brush motor market expand to world in the future

Figure 2.2 Brush motor market in the future [3,4].

2.2 Mechanism of Brush Motor Noise and LC Resonance with Suppression

This section introduces the mechanism of brush noise generation in existing brush motors and the purpose of this study. The EMI increase by resonance caused by the LC resonance that occurs when brush noise countermeasures are applied is also explained. In addition, we will explain how to evaluate the entire system in a brush motor drive system.

The application area of brush motors in the automotive area is used in products such as sunroofs, seats, and power sliding doors in Fig. 2.1. Specifically, the Fig. 2.2a, Fig. 2.2b shows the future expansion of the brush motors [3,4]. A commonly used measure in investment and business (CAGR), which indicates the average annual growth rate of revenue, sales, and market size over a given period, is expected to increase by 5.3 % toward 2029 in Fig. 2.2a [3,4]. There are also many developments in each country and in each company. In addition, the application area of brush motors in brush motors in the field of home appliances has been also used in products such as vacuum cleaners, fans, washing machines, and power drills, and is expected to expand in the future in Fig. 2.2b [3,4]. Accordingly, due to micro-arcs generated by brush motors, electromagnetic noise at the

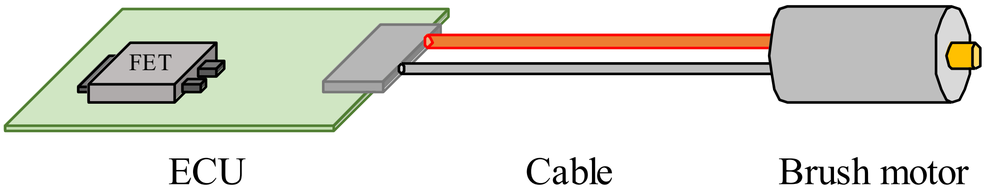

Figure 2.3 brush motor drive systems.

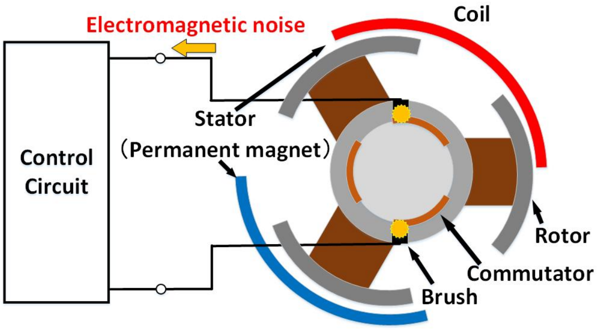

Figure 2.4 Internal structure of brush motors and brush noise generation.

mechanical interface is expected to continue to be a problem in the future. To suppress electromagnetic noise, EMI filters inside brush motors are installed. A brush motor drive system driven by a control electronic control unit (ECU) is called a brush motor drive system shown in Fig. 2.3. In this system, both the brush noise generated in brush motors and the switching noise generated by the PWM-controlled power semiconductors in the ECU are sources of EMI [8–11, 13, 15–18]. This chapter mainly describes the means of suppressing brush noise generated in brush motors during rotation, while the solution method to LC resonance by other reason are described in the latter part of the chapter.

2.2.1 Mechanism of Brush Noise Generating from Brush Motors

This section details the EMI that occurs during the operation of direct current (DC) motors. First, the mechanism of brush noise generated by brush motors is explained.

A brush motor is a type of electric motor that uses brushes and commutator components. A schematic cross-sectional diagram of a brush motor with three phases is shown in Fig. 2.4. Regardless of the type of power source, the rotating force of an electromagnetic motor is the Lorentz force generated by the action of the current and the magnetic field. Unlike alternating current, the direction of the current in direct current is not reversed, so the positional relationship between the current and the magnetic field changes with rotation in a direct current motor. Therefore, switching must be performed at the timing when the positional relationship between the current and the magnetic field reverses, and the direction of the current must be reversed to continuously generate rotational force in the same direction. In other words, during motor rotation, the commutator performs the

Figure 2.5 Brush motor used in the study (Produced by Igarashi Electric Works).

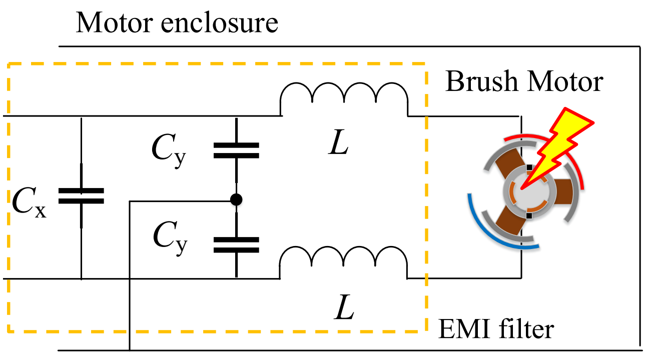

Figure 2.6 Diagram of a brush motor with EMI filters inside brush motors.

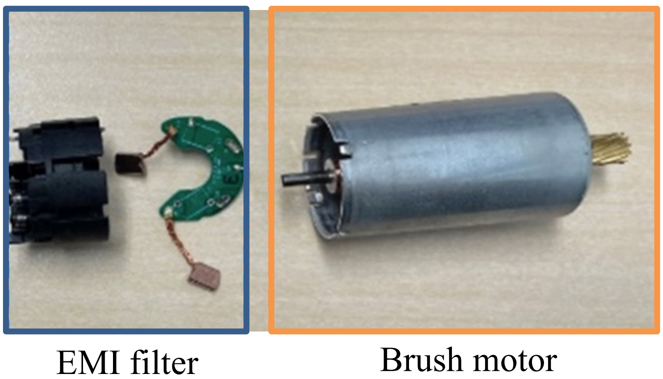

Figure 2.7 Actual brush motors with EMI filters inside brush motors.

process of switching the direction of the current through the brushes. This is done at the mechanical contact point between the brushes and commutator. When a power supply is connected to the motor, the brushes and commutator come into contact with each other, current flows through the coil, and a magnetic field is generated, which repels or attracts the permanent magnet, resulting in rotational motion. Brush noise is generated when the brushes and commutator make contact.

Recent studies have characterized the generation and propagation of micro-arcs by specific parameters. These have been found to be influenced by the geometry of the armature, the design of the brushes and collector, as well as the load torque and applied voltage of the motor. For example, they propagate as DM currents through the internal structure and windings of the motor and as CM currents through the magnetic core, shaft, and casing, as shown in Fig. In other words, these differential mode and common mode currents are generated, so it is important to take these measures.

Therefore, a filter inside the brush motor is generally used to suppress brush noise. An actual photograph of the brush motor used in this thesis is shown in Fig. 2.5 Methods to reduce brush noise include adjusting brush pressure, selecting appropriate brush materials, and keeping the commutator surface smooth, but in general, an EMI filter such as the one shown in Fig. 2.6 is installed. In this Fig. 2.5 case, this method is made possible by installing an ECU for the filter inside the brush motor as shown in the Fig. 2.7. The filter circuit is shown in the figure and consists of three major components: X capacitor C_{x}, Y capacitor C_{y}, and coil L. The X capacitor is considered capable of suppressing differential mode noise, while the Y capacitor is considered capable of suppressing common mode noise.

2.2.2 LC Resonance in brush motor drive system

The previous section described EMI suppression methods for brush noise generated by brush motors. In this section, we explain the EMI problem using the brush motor drive system that is the subject of this study as an example. The EMI suppression is not for the brush motor itself, but for the entire system, such as the brush motor drive system, Internal EMI filters for brush motors must be designed not only to suppress brush noise, but also to take into account the increase in other EMI. In order to do so, we will first explain the evaluation environment of international standards used to evaluate EMI in a system such as a brush motor drive system.

Fig. 2.8 illustrates a block diagram of the motor noise evaluation system where a brush motor (SX-17665-01, Igarashi Electric Works) is connected to Artificial Mains Network (AMN) via a parallel two wire cable for 12 V DC power supply and is placed at 50 mm above the system ground. The brush motor should be a 6-pole, neodymium magnet, 4-slot type. This AMN is used to measure the conducted EMI produced by the brush motors and the ECU at the CM and DM propagating through the wiring and ground to the power supply. In this study, the control ECU is represented by considering only the electrolytic capacitors for the inside impedance. At this time, EMI filters are installed inside brush motors. Brush motors are generally located inside brush motors enclosures,

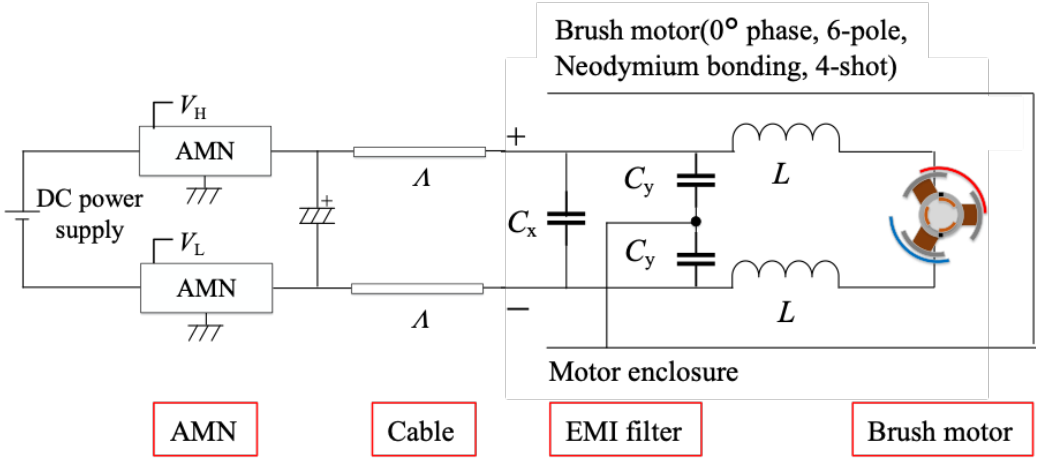

Figure 2.8 Block diagram of motor noise evaluation system (CISPR25).

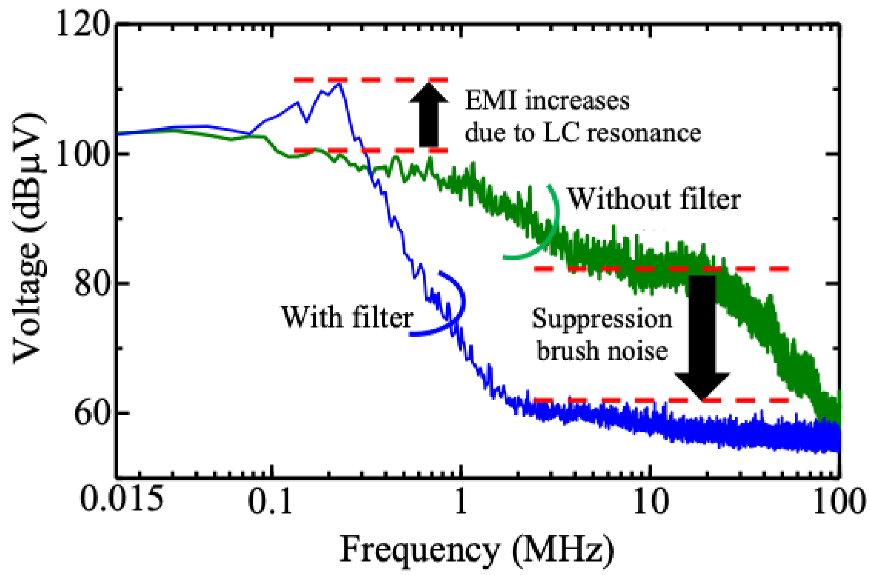

Figure 2.9 Conducted emission tests (CISPR25) for brush motor drive system.

and the connection to the enclosure may be made by filters inside filters.

Next, the increase in EMI when brush motors are installed in brush filters will be discussed. Fig. 2.9 shows the evaluation results when the system as a whole is evaluated in the CISPR25 evaluation environment described in Fig. 2.8. First, brush noise generated by brush motors can be reduced by installing a filter inside the brush motor to reduce EMI after 10 MHz. But when the system is examined as a whole, EMI increases due to the influence of the harness. This increase in EMI in carrier frequency bands such as the AM band is manifested by LC resonance between the capacitor in the EMI filter and the parasitic inductance (ESL) of the cable. In other words, this indicates that the filter installed to suppress brush noise from 1MHz to 10MHz, but on the other hand, LC resonance is generated when the entire system is evaluated. In this case, the capacitors of C_x and C_y in the EMI filter resonates with the parasitic inductance (ESL) of the cable in the LC resonance, and an increase in EMI becomes apparent in the carrier frequency band such as the AM band. This resonance cannot be avoided. Therefore, EMI filters for automotive brush motors are designed, since a resonance between the capacitance of the filter and the parasitic inductance of the power-line cable occurs, not only the brush noise but also the resonance must be simultaneously suppressed.

This indicates that it is necessary to design not only to satisfy the required performance of the filter attenuation characteristics of a single filter, but also to satisfy the required performance of the entire system. Furthermore, this is something that occurs in any product, regardless of the brush motor drive system, and it is necessary to find design parameters that can suppress EMI, not just for the filter itself, but for the entire system complexity. These explanations also suggest that changes in specifications, such as variations in cable length or filter parameters etc., can affect the filter characteristics when evaluated for the entire system. It is desirable to have redundant design that enables design to satisfy the required performance even when small variations or specification changes occur. It is difficult to obtain multiple parameter values that can satisfy multiple performance requirements for the entire system, and in many cases it takes an enormous amount of time. The objective of this thesis is to obtain multiple design parameters (including non-filter parameters) for such a system that simultaneously satisfy multiple performance requirements fast, accurate, and widely range. This makes it possible to implement effective EMI suppression design while a rapid design process is required. In addition, enabling redundant design that can adapt to changes in product specifications and variations in elements will help design process to be carried out without rework.

2.3 Evaluation Method with Noise Attenuation Characteristics

This section describes the case in which the EMI filter characteristics degrade when the filter is mounted on a brush motor, as described in the previous section. Next, the target performance requirements and design parameters of the brush motor system focused on in this thesis are defined.

First, a circuit with only the design parameters that are the target of this study is shown in Fig. 2.10. Design parameters of the built in EMI filter are C_x, C_y, and L. This is because the EMI filter has a large impact on the noise attenuation, and the cable length Λ also has an influence on the entire system design.

Next, to evaluate the EMI filter characteristics in this thesis, the DM voltage V_H - V_L and CM voltage $V_H + V_L$ at the noise terminals of the AMNs shown in Fig. 2.4 are used. The performance of the filter is evaluated by the attenuation of the DM and CM voltages with and without the filter for a cable length of 2 m as shown in Fig. 2.11. As an example, the attenuation characteristics are shown for the case of Attenuation of C_x, C_y, = 15 nF, L = 1 μH, and Λ = 2 m. The blue spectrum is the attenuation characteristic of DM noise. The green spectrum is the attenuation characteristic of CM. For example, in the case of Fig. 2.11, we can see that the noise reduction is achieved above 10 MHz. On the other hand, the DM noise shows that the noise is worse below 1 MHz. This indicates characteristic degradation due to resonance generated by the cable and capacitors, This indicates that the requirements are not met in DM noise.

In other words, the EMI filter characteristic at 10 MHz $\leq f \leq$ 30 MHz has a reduction effect of about 20 dB or more, but at 0.1 MHz $\leq f \leq$ 1 MHz, the resonance between the capacitance and the cable inductance causes a noise increase problem. Therefore, to avoid this problem, we decided to satisfy 10 dB of attenuation from 10 MHz to 30 MHz, where brush noise is prominent, and -5 dB of attenuation from 0.1 MHz to 1 MHz. Even if the resonance frequency is shifted outside the target frequency, the value is set to -5 dB because the value may not be satisfied depending on the edge of the resonance frequency. Table 2.1 shows the required performance for the above mentioned DM and CM attenuation.

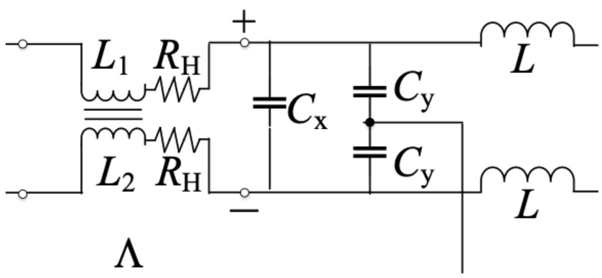

Figure 2.10 Cable length and EMI filter using the design parameters.

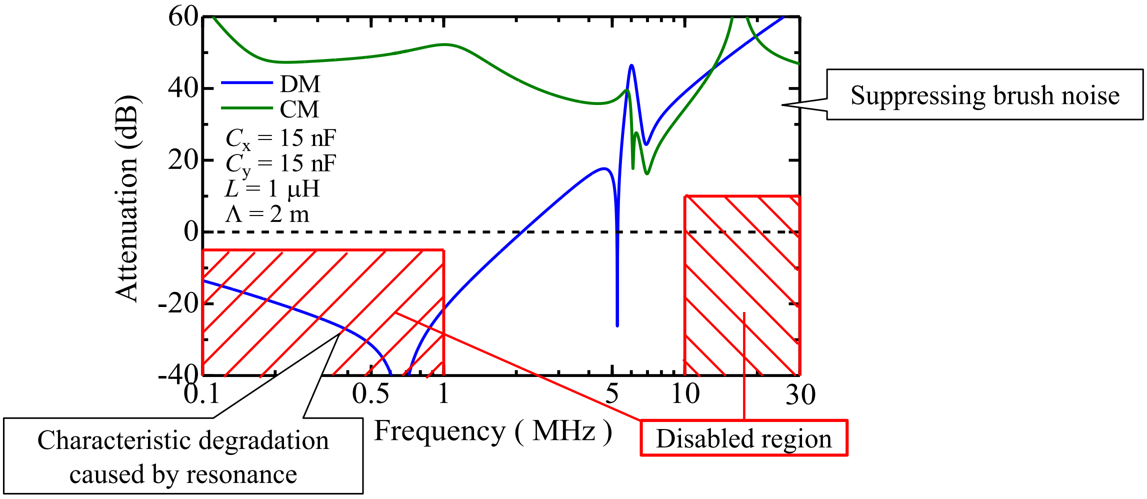

Figure 2.11 DM and CM attenuation in C_{x}, $C_{\mathrm{y}} = 15$ nF, $L = 1$ μH, $\Lambda = 2$ m attenuation.

Table 2.1 Required performance for DM, CM attenuation.

Frequency	$V_{\mathrm{DMnoiseATT}}$ and $V_{\mathrm{CMnoiseATT}}$
0.1 MHz – 1 MHz	-5 dB or more
10 MHz – 30 MHz	10 dB or more

In other words, the goal of this study is to obtain a wider range solution of design parameters for C_{x}, C_{y}, and L each of which satisfies all four of these performance requirements with good accuracy. Redundant designs are necessary in this case because the cable length and filter parameters can vary when manufacturing a motor system. The target tolerance for redundant design parameters is $\pm$ 5% for resistors generally used in the E24 series or lower. Also, capacitors and coils are generally used with a tolerance of $\pm$ 20%.

2.4 Noise Suppression Methods in Design Process

This chapter describes methods for simultaneously suppressing brush noise and LC resonance. The suppression methods have different levels of difficulty in implementation at each phase of the design process, and these will be organized and explained. The design process for brush motor drive systems and the countermeasure methods of suppression are shown in Fig. 2.12.

First, each process in the product design process for a brush motor drive system, one of the multi component systems is described in Fig. 2.12. In the initial phase, the product design concept, product specifications, and target cost of each component are determined. Next, specifications for the mechanical components are determined. Specifications such as body size and shape are determined, as well as cable specifications for the placement of the motor and ECU. Drive unit components are then selected to meet the operating requirements of the mechanical components. For example, depending on the operation of the mechanical components, it is decided whether brushless motors or solenoids are used to enable performance. For brush motor drive systems, brush motors are selected that satisfy the torque performance, speed, current, and other requirements to meet the specifications of the mechanical components. At this time, each brush motor is individually tested in accordance with international standards to design an internal EMI filter. Then, the specifications of the control ECU to control this drive unit are determined. The specification of the control ECU determines, for brushless motors, the energizing method of the 3-phase AC drive, and so on. For the brush motor drive system, the drive system such as H-bridge circuit, low-side switching circuit, relay drive, etc. are determined. Finally, reliability tests including EMC are conducted on the ECU prototype, and if the EMC test fails, it is difficult to redesign the design process before prototyping. Stepping

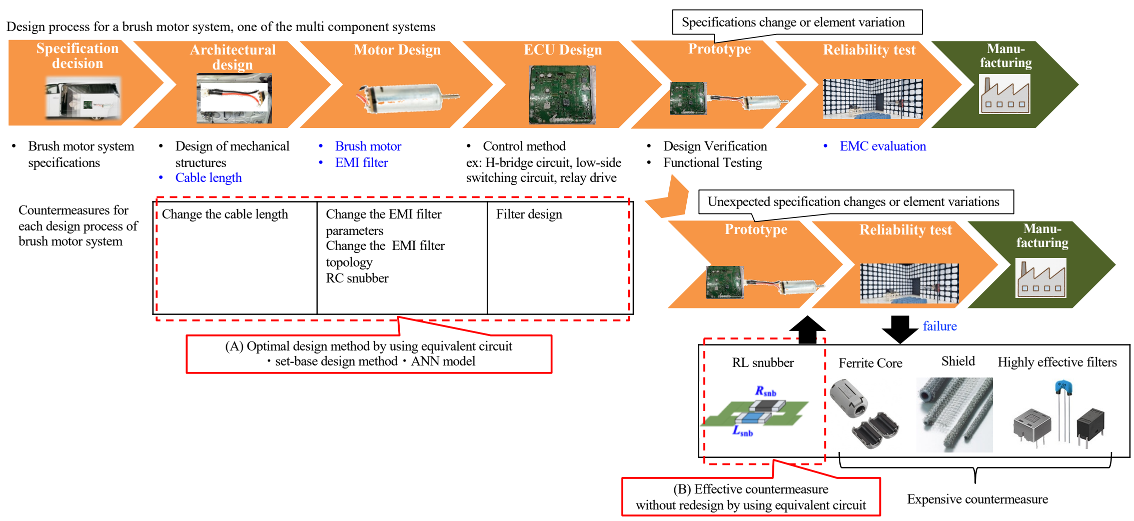

Figure 2.12 Countermeasures to LC resonance in each design process of brush motor drive system.

back multiple steps in the design process should usually be avoided because of its impact on vehicle specifications. Therefore, ferrite cores, shielding, and filters with high effective filtering of noise attenuation are generally used as countermeasures in place. However, these countermeasure methods are expensive and should basically be avoided.

Next, regarding the design process, methods that can suppress both brush noise and LC resonance in brush motor drive systems are described for each phase in Fig. 2.12. In this thesis, we examine (A) the optimal design method for the design parameters before prototyping and (B) the countermeasure method after prototyping. In the initial stage of design, it is important to design EMC under the condition that there are no restrictions on design parameters in Fig. 2.12. In (A), the objective is to establish a multi-objective design method to obtain multiple design parameters (including those other than filter parameters) that simultaneously satisfy multiple performance requirements with high accuracy, high speed, and a wide interval solution range. Since there are few constraints on design parameters before prototyping, the optimal design method enables multi-objective design with redundant design. This allows the design process to be carried out without rework through redundant design that can handle changes in product specifications decision and element variations. In the design process of brush motor drive systems shown in the figure, the cable length is designed in architecture design and the EMI filter is designed in motor design. Therefore, it is desirable to be able to obtain as wide an interval solution range as possible that simultaneously satisfies multiple required performances from a wide range of design parameters at the stage of these decisions. In particular, if design parameters can be determined that can handle changes in product specifications decision and element variations, there is no need to perform rework in the design process. However, there are cases where reliability tests inevitably fail due to unexpected specification changes or element variations, or due to the accuracy of the model. To prepare for such cases, it is desirable to find a countermeasure method that minimizes rework and costs even after prototyping. In such cases, ferrite cores, shields, and highly effective noise attenuation filters are often used, but these should be avoided as much as possible due to mounting size and cost restrictions. The RL snubber circuit is practical as a countermeasure because it does not require many design processes before prototyping and can be considered inside the ECU. The RLsnubber can be installed in series with the resonant loop of the ECU simply by going back before prototyping. Therefore, in brush motor drive systems, RL snubbers are highly consistent with the design process and are employed in this thesis. Thus, the realization of the optimal design method and countermeasure method for each of (A) and (B) can contribute to an efficient design that satisfies the EMC performance.

2.5 Conclusion

This chapter introduces the brush motor drive system as an example of one of the multi-component systems to which the optimal design will be applied in this study. The brush noise generated in this system, its suppression method, and the associated increase in EMI are described. The internal EMI filter in a brush motor drive system must suppress not only the brush noise but also the resonance because of the resonance between the filter and the parasitic inductance of the power line cable. Therefore, using the filter design in brush motors system as an example, differential mode and common mode noise levels were investigated. The results showed that the brush noise was reduced above 10 MHz, but on the other hand, the filter was degraded below 1 MHz. This indicates characteristic degradation due to resonance generated by the cable and filter, which means that the design must not only satisfy the filter characteristics of a single component, but also the performance requirements of the entire multi-compornent systems. This also occurs in any product, regardless of whether it is in brush motors or not, indicating that it is important to find design parameters for EMI suppression that take the entire multi-component systems into consideration.

Therefore, using the brush motor drive system as an example in this thesis, we explained the importance of obtaining design parameters with high accuracy and wide range to satisfy multiple performance requirements simultaneously in the early stage of prototyping. The redundant design that can accommodate specification changes and element variations can reduce the need to go back to the early stage of design. In addition, the importance of optimal design of RL snubber circuits was explained in the case of EMI problems after prototyping. By enabling a straight-forward suppression method without trial and error, rapid design measures can be taken. The performance requirements and design parameters used in the optimal design method to be applied from Chapter 4 onward are also defined. It was shown that the above approach enables efficient EMC design for multi-component systems.

Chapter 3

Creating Equivalent Circuit Modeling for Optimal Design Methods and Countermeasure

3.1 Introduction

Chapter 2 explained the mechanism of noise generated by brush motors and how to suppress it by installing filters inside brush motors as well as the EMI increase by resonance of LC generated by filters installed with brush filters. Several countermeasure methods in the design process were also introduced. In addition, it was shown that it is not easy to determine multiple design parameters that satisfy multiple performance requirements. The objective of this thesis is to use optimal design methods to obtain more accurate and wider range of interval solutions for brush motor drive systems. This chapter describes an equivalent circuit model for the entire system evaluating the conducted emissions of brush motors. The advantage of the equivalent circuit model is that it saves cost and time in fabricating and testing the actual prototype, and allows many design parameters to be quickly explored. This allows us to quickly obtain the calculation data to apply the set-based methods and ANN models described in Chapters 4 and 5 to the optimal design of the brush motors system. In practical applications, it is necessary to consider not only the filter but also the system as a whole, taking into account the mutual influence of many parameters. Furthermore, brush motors are particularly important to model in this study, and we will explain how to model them in stationary and dynamic conditions, how to measure their impedances and create equivalent circuits for each, and verify their implementation. The set-based method and the design parameters to be applied to the ANN model and the performance requirements will also be described.

While RLC circuits are sufficient for modeling brushless motors, such circuits cannot be reproduced in brush motors. Therefore, in brush motors, EMI models have so far been developed using the detailed structure model [16–18, 39] and the macro model [14, 15]. The detailed structure model attempts to correspond the actual structure of the motor to the model structure and to treat it with a detailed equivalent circuit model. In their paper [16–18, 39], a method is proposed to automatically generate high-frequency models of DC motors. The proposed software model generator generates an equivalent circuit to reproduce the high-frequency impedance and radiation spectrum of a typical DC motor in the frequency range of 150 kHz to 1 GHz. The impedance and radiation spectra can be calculated from armature geometry, winding radius, and position and orientation within the motor casing, which are structural and material properties that significantly affect the degree of interference.This allows analysis to minimize EMI without the need for actual measurements, even in the design phase of motors where prototypes and measurements are not yet available.

The macro model is also based on the Norton equivalent circuit [14, 15]. The brush motors are modeled as current sources that are sources of EMI, and their impedance model is built in parallel. This macro model does not model the detailed behavior of a particular component or subsystem, but only describes the input-output relationships. This approach is used to simulate large systems and circuits, omitting details to capture the overall behavior. The model has been used to estimate conducted EMI generated by filtered DC motors and has been validated on several DC motors. In previous studies, modeling of brush motors has been limited to creating models based primarily on structural and material properties or behavioral models in a standstill state. However, from the perspective of the supplier handling the entire system, structural and material properties are confidential information of the brush motor manufacturer, and CAD drawings and material information are difficult to obtain. Even in environments where brush motors can be evaluated, behavioral models of brush motors in a stopped state cannot adequately represent the internal impedance during dynamic condition. Therefore, a method using a network analyzer together with two current probes was previously proposed for this purpose [48]. The conventional proposed method [48, 49] is that a current is applied from Port of the network analyzer to the closed loop of the wire harness via the current injecting probe, and the output of the current receiving probe is measured at anothrer Port. This can measure the motor impedance in operation conditon at noncontact. However, because the conventional method assumes a quasi-TEM propagation mode, it is necessary to construct parallel wiring harnesses with spatial spacing sufficiently small compared to the wavelength.

In this study, an accurate noise source equivalent circuit model of brush motors is essential for the practical application of our optimization method. Since the discharge phenomenon occurring in brush motors is in a dynamic condition, it is desirable to model the impedance not only under the stationary condition but also dynamic condition for more accurate modeling. The noise source equivalent circuit model to be constructed must be able to accurately predict not only differential mode but also common mode. Therefore, we construct a new brush motor drive system model in brush motors based on this information. Firstly, we identify the internal impedance of the brush motor at motor standstill as a base. Next, the internal impedance of the noise source equivalent circuit during brush motor operation is identified. In this study, the AMN assuming bias T is used to measure the impedance under dynamic conditions by measuring the AMN's terminating resistance with a network analyzer. Even in operation, the network analyzer is not powered. The impedance of the load under dynamic condition can be obtained by finding the F-matrix of the entire system including the AMN and the load and subtracting the impedance of the AMN. Then, in order to evaluate the brush motor drive system, the equivalent circuit modeling of the entire system in conducted emission evaluation system including the impedance of the surrounding area including brush motors will be explained. Finally, to verify the accuracy of the model, noise prediction is performed to confirm the prediction accuracy of DM noise and CM noise.

In this chapter, an equivalent circuit model is created to obtain data from circuit simulation in order to apply the set-based design method and ANN model. In brush motors system as an example, design parameters and performance requirements are defined as a preliminary preparation for optimal design. The structure of this chapter is as follows. Section 3.2 first describes the entire structure of the equivalent circuit model for the entire system targeted in this study. Next, Section 3.3 focuses on brush motors and describes how to model them in brush motors under stationary and dynamic conditions. The model accuracy in brush motors is important for the optimal design presented in Chapters 4-6, as it is highly dependent on the design accuracy. Section 3.4 defines the design parameters and required performance values for the optimal design method applied from Chapter 4 onward. Section 3.5 concludes the chapter with a summary of important points.

3.2 Creation of Based Equivalent Circuit Model in Conducted EMI System

In order to perform efficient calculations on a desktop for optimal design, equivalent circuit modeling is used in this study. This section presents the measurement system of the brush motor drive system, summarizes the points and measurement methods considered in its construction, and presents its equivalent circuit. Conducted EMI measurement methods and the measurement methods and equipment used for each modeling are described. In particular, each parameter in the equivalent circuit model of brush motors was identified by measuring each one individually with a VNA.

3.2.1 Environment for Evaluating Electromagnetic Interference

The evaluation of conducted EMI has many limitations that affect its accuracy. Factors such as the wire arrangement of the connection between the spectrum analyzer, the test equipment (EUT), and the load or power supply can change the EMI measured under the same dynamic conditions. Therefore, to realize reproducible measurements, certain aspects related to the test equipment specified by EMC standards must be taken into account. A block diagram of the evaluation system in this study is shown in Fig. 3.1, which is a separate mechanical and electrical system in which brush motors (SX-17665-01, Igarashi Denshi Seisakusho) and a control ECU are connected by a cable. In order to assume practical design situations, an evaluation environment following CISPR25 [43] conducted interference tests is used.

The evaluation environment is connected to the ECU via an AMN with a cable for a 12V DC power supply. This AMN is used to measure the conducted EMI produced by the brush motors and the ECU at the CM and DM propagating through the wiring and ground to the power supply. In this study, the control ECU is represented by considering only the electrolytic capacitors for the inside impedance. The brush motors are installed 50 mm above the system ground with a parallel 2 wire cable (= 2 m) from the ECU. At this time, EMI filters are installed inside brush motors. Brush motors are generally located inside brush motors enclosures, and the connection to the enclosure may be made by filters inside filters.

3.2.2 Creating the Equivalent Circuit Model for Evaluation System and Brush Motor

In order to be able to calculate the brush noise attenuation characteristics by the EMI filter as the required performance, the present evaluation system is represented as an equivalent circuit in Fig. 3.1. This equivalent circuit is divided into the AMN, the cable, the installed with brush filters, and the brush motor.

First, the parameters of the AMN (TNW-1502) are generally used parameters, and

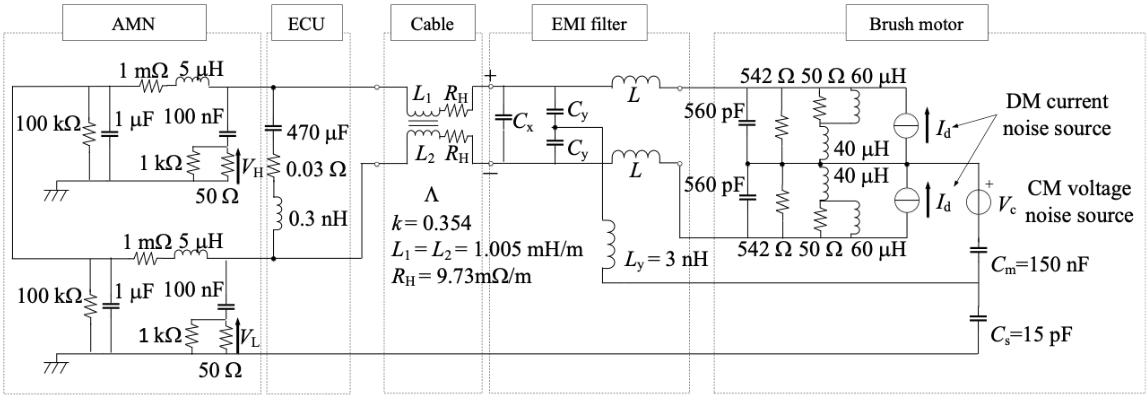

Figure 3.1 Equivalent circuit model of evaluation system in brush motor drive system.

Table 3.1 Measurement equipment used for the impedance identification

Parameter	Specification
Network analyzer	Agilent E5061B
Height of wire harness	50 mm
Calibration kit	85033E
Line impedance stabilization Network	TNW-1502
DC stabilized power supply	PW16-5ADP

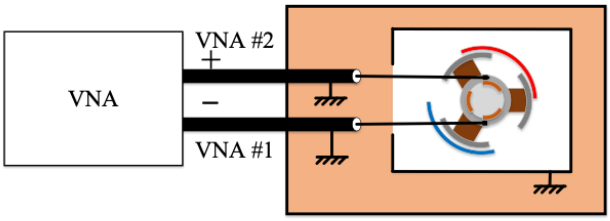

Figure 3.2 Method of measuring internal impedance of brush motors using VNA.

the reference results are as follows. Furthermore, during the evaluation, the spectrum analyzer is connected via a harness to the 50 Ω of the AMN, which will be the V_H and V_L. The parameters of the cable were calculated using 2-D electro stationary field calculation software. The cable is modeled 50 mm away from the system GND, A commonly used AWS cable of 1.25 sq. is assumed, and the cross-sectional structure is linear mm and coated mm. This gives $R_H = 9.73\ \Omega/\text{m}$, $L_1 = L_2 = 1.005\ \text{mH/m}$, and $k = 0.354$.

Next, we then discuss the identification of the equivalent circuit model in brush motors. In this section, each parameter in the equivalent circuit model of brush motors was identified by measuring each one individually with a VNA. The measurement equipment used for the impedance identification is shown in the Table 3.2.2. A description of the stationary impedance measurement method for brush motors, the measurement environment, and the VNA used will be presented. First, the stationary internal impedance of brush motors is measured by connecting the measurement port of the VNA directly to

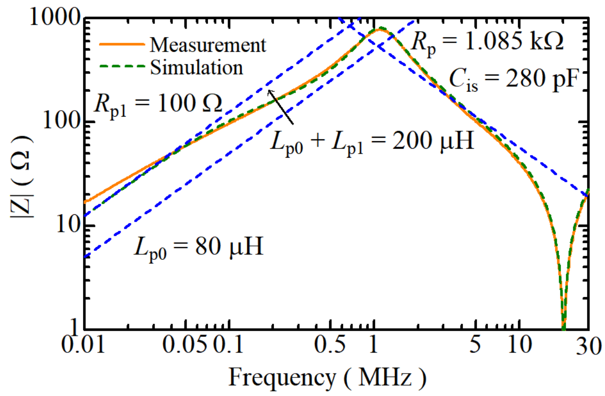

Figure 3.3 Circuit simulation results for brush motor not installed with brush filters.

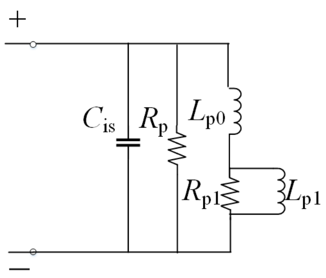

Figure 3.4 Equivalent circuit model of DM impedance of brush motors.

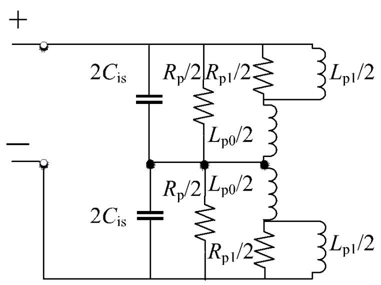

Figure 3.5 Extended equivalent circuit model for DM impedance of brush motors.

the in brush motors by VNA measurement as shown in Fig. 3.2. The DM impedance in brush motors is shown in Fig. 3.3. This is the input impedance seen on the motor side from the ports of the + and - terminals of the brush motor not installed with filters. By fitting the effective inductance of the coil and the capacitance between the coils, a circuit model like the one shown in Fig. 3.4 was created. The capacitance between the coil and the coil is C_{is}, and R_p is used as the resistance due to magnetic losses. The inductance of the coil is considered to be inductive from 0.01 to 1 MHz, since it is clear that the change in inductance of the coil is not 20 dB/decade. Therefore, the inductance was identified more accurately by fitting using R_{pn} - L_{pn} [16–18, 39].

The resistance and inductance of the equivalent circuit in brush motors were halved and the capacitance was doubled, as shown in Fig. 3.5. Furthermore, by dividing the circuit into series, it was extended so that the filter characteristics can be evaluated when a 1V noise source is inserted. Next, the equivalent circuit in brush motors including CM impedance is shown in Fig. 3.6. In order to represent the CM impedance in brush motors alone, it is necessary to model the parasitic components as shown in Fig. 3.7. Therefore, the parasitic capacitance C_s between the motor and the system ground was identified

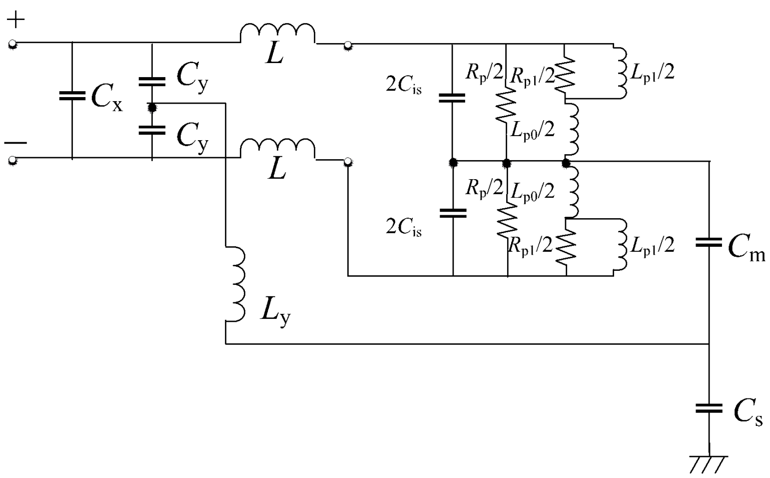

Figure 3.6 Equivalent circuit of brush motor including CM impedance.

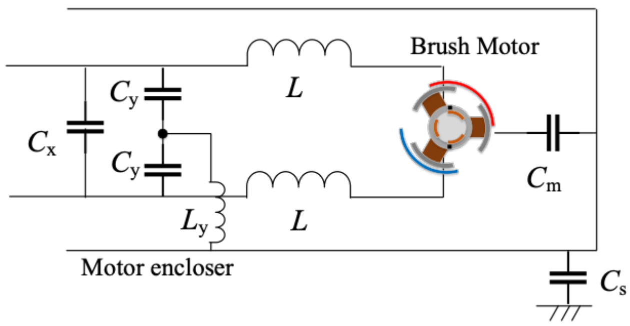

Figure 3.7 Pontic picture of parasitic components in brush motor.

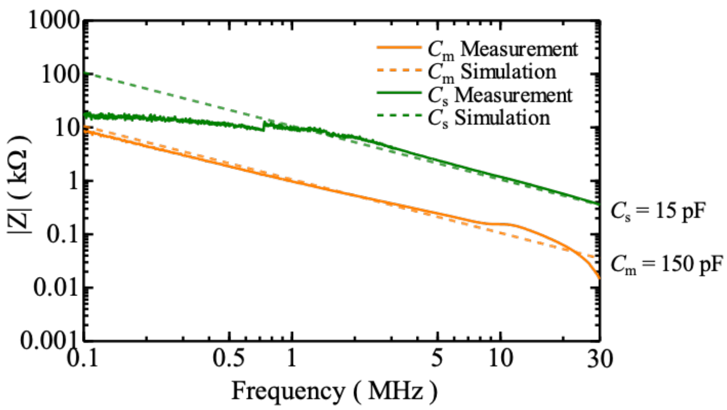

Figure 3.8 Comparison of measured and Simulation result for C_m and C_s.

from a 1-port measurement with the + and - terminals lumped together and the system GND as a port. The parasitic capacitance C_m and inductance L_y between the motor coil and the enclosure were identified by measuring the + and - terminals together and both terminals of the motor enclosure shown in Fig. 3.8.

In order to evaluate the filter characteristics of DM and CM noise, a noise current source equivalent model was adopted for DM noise and a noise voltage source equivalent model for CM noise in the noise source equivalent circuit model of brush motors shown in Fig. 3.1, where a 1 A current source and a 1 V voltage source were inserted as noise sources for DM noise and CM noise respectively. A voltage source of 1 V is inserted as a noise source for CM noise. Inside the filter studied in this thesis, the circuit that constitutes the EMI filter is composed of a typical X capacitor C_{x}, Y capacitor C_{y}, and coil L.

3.3 Proposed Measurement Procedure for Identifying Dynamic Impedance

In the previous section, regarding the equivalent circuit model of the brush motor, each parameter was identified by measuring each individually with VNA. In this section, we propose a method and procedure for impedance measurement using AMN in brush motors under dynamic conditions in order to improve the accuracy of the equivalent circuit model of brush motors.

This section describes the identification method under the dynamic condition and examines the modeling accuracy under the stationary and dynamic conditions. In the previous section, the identification method was easy because the impedance was measured with the brush motor in a stationary state. However, since the brush motor noise is generated in the dynamic condition, it is necessary to identify the brush motor noise source and impedance under the dynamic condition. However, it is difficult to measure the brush motor in the dynamic condition because the power supply is applied to the brush motor, which may cause a power feed to the VNA and an inflow of brush noise. Therefore, we will explain how to measure the impedance under the dynamic condition. Fig. 3.9 shows the punch picture of the brush motors and the parameters that make up the noise source model in brush motors. The parameters are then identified using the flowchart shown in Fig. 3.10.

First, 1. obtain the S-parameters of the measurement system. Fig. 3.11 shows a measurement system in which the working internal impedance is identified using a VNA. In order to simultaneously supply power to the motors and suppress the inflow of brush noise into the VNA, power is first supplied in brush motors via the AMN. Then, the internal dynamic impedance is measured from the high-frequency port of the AMN. A 20 dB attenuator (ATT) is inserted between the RF port of the AMN and the VNA to reduce brush noise. Fig. 3.13 shows the block diagram of the modeling target including

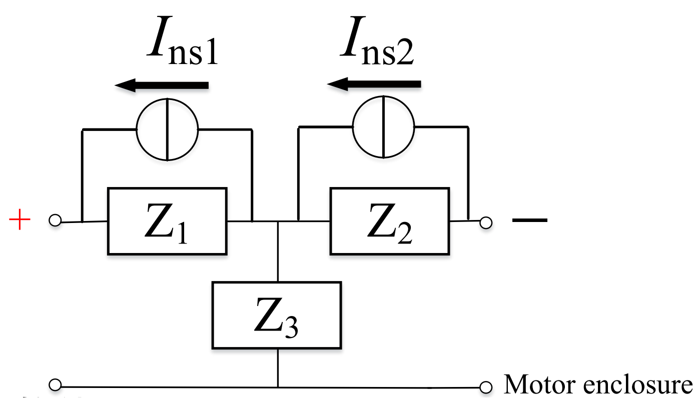

Figure 3.9 Equivalent circuit of noise source and brush motor impedance.

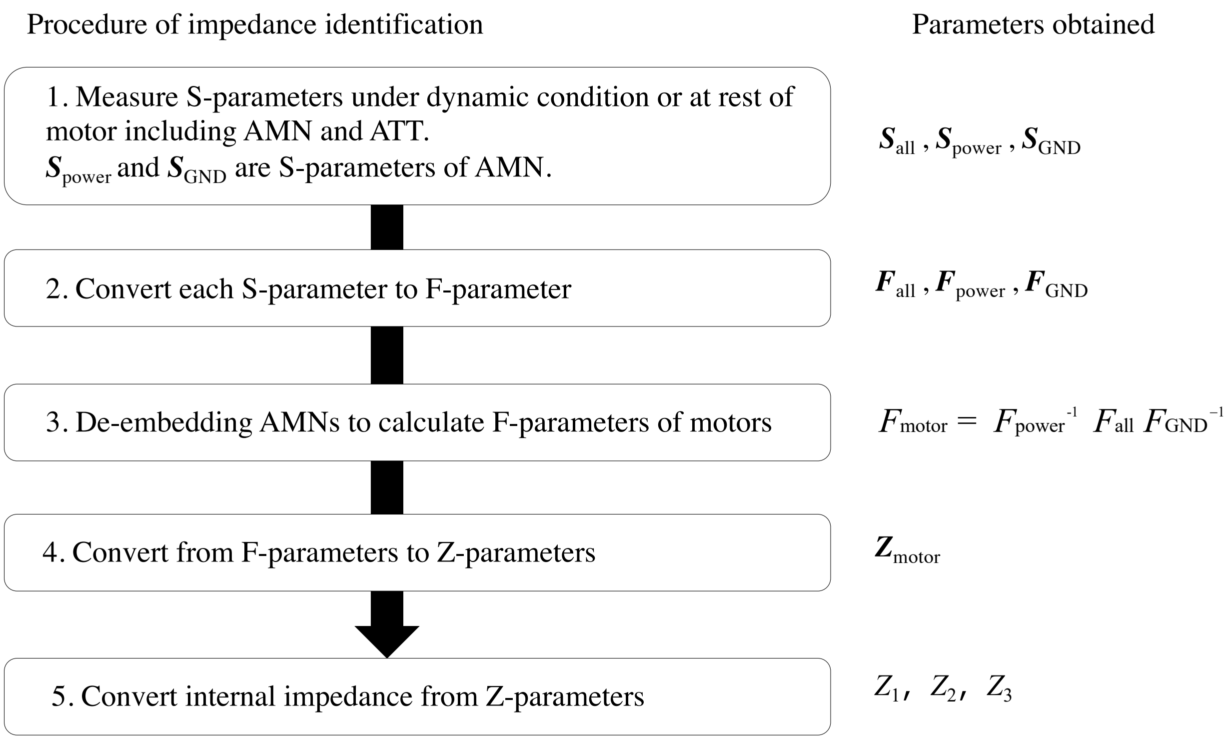

Figure 3.10 Procedure of impedance identification using VNA with AMN.

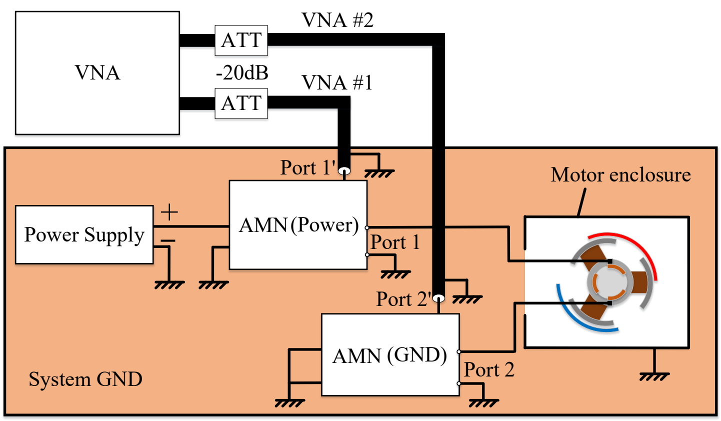

Figure 3.11 Impedance measurement system for brush motors.

AMN as seen from the port of VNA.

Therefore, measure the AMN and the overall S-parameters. Next, 2. S-parameters are converted to F-parameters. Then, 3. S-parameters obtained from the 2-port measurement by VNA are converted to F-parameters using the following equation.

$$F_{\text{all}} = F_{\text{power}} \cdot F_{\text{motor}} \cdot F_{\text{GND}} \tag{3.1}$$

Where F_{power} and F_{GND} are the F-parameters of the AMN on the power and GND sides, and F_{motor} is the F-parameters of the motor to be obtained. If F_{power} and F_{GND} are

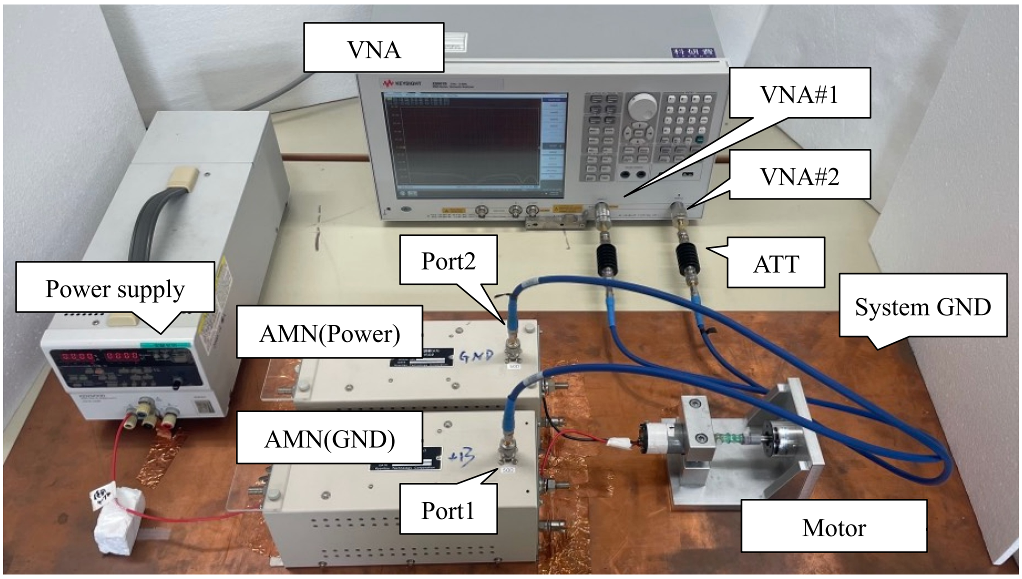

Figure 3.12 Measurement environment of brush motor impedance under dynamic condition.

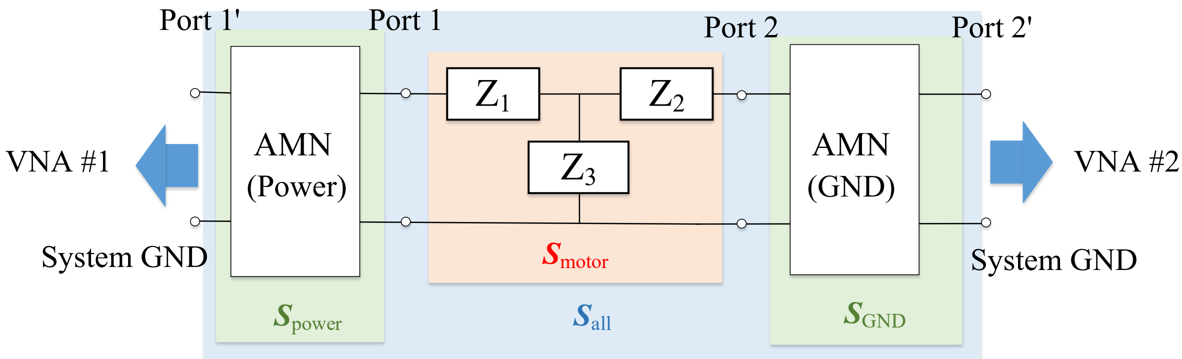

Figure 3.13 Impedance parameters of brush motors under dynamic condition.

obtained by another VNA measurement, F_{motor} can be obtained by de-embedding the AMN part and using the following equation.

$$F_{\text{motor}} = F_{\text{power}}^{-1} \cdot F_{\text{all}} \cdot F_{\text{GND}}^{-1} \tag{3.2}$$

Then, 4. F_{motor} is converted to Z-parameters. Finally, by converting 5. T-type equivalent circuit to Z_1, Z_2, and Z_3, that is, the dynamic internal impedance, it is possible to identify the brush motors in brush motors in operation.

3.4 Identification of Impedance in Brush Motor in Dynamic and at Rest

This section describes that the validity of the procedure described in the previous section is validated using static elements. Impedance measurements in brush motors under stationary conditions are performed in order to compare the results with those of the section 3.2. This is because an equivalent circuit model of brush motors with good accuracy is essential for practical use in the optimization design method described in Chapter 4 and thereafter.

3.4.1 Verification of the Procedure that Identified the Impedance of the Static Lead Element.

In this section, we verify the validity of the proposed method using static elements, resistors and capacitors with lead wires. Combinations of elements to be inserted in Z_1, Z_2, and Z_3 are shown in Table.3.4.1. The impedance is identified by the procedure in Fig. 3.10 with the elements inserted in Z_1, Z_2, and Z_3 in the Fig. and the DC stabilized power supply connected, but no voltage applied.

The results of leaded resistors and capacitors identified by the proposed measurement method are shown in the Fig. 5.3. The black dotted line is the true impedance of the device identified using a VNA. The solid-colored result is the impedance measured by the measurement system without AMN shown in the Fig. 5.3. The colored dotted line is the impedance obtained by the proposed method. The black dotted line and the solid colored line are in good agreement at all frequencies. The capacitors are inductive at low frequencies above 20 MHz, but there is a slight discrepancy between the test fixture results and those of the proposed method. In the proposed method, Z_1, Z_2, and Z_3 are combined by soldering, which changes the length of the lead wires, which in turn changes the ESL. At low frequencies below 0.5 MHz indicate that the accuracy deteriorated in the range indicated. At this time, 1000 Ω resistors and 1 nF capacitors resulted in low accuracy due to their high impedance. This could be due to the ESL of the lead wires and the use of alligator clips.

Table 3.2 Combinations used to validate the proposed measurement method.

Combination No	Z_1	Z_2	Z_3
No.1	10 Ω	10 Ω	10 Ω
No.2	100 Ω	100 Ω	100 Ω
No.3	1 kΩ	1 kΩ	1 kΩ
No.4	1 nF	1 nF	1 nF

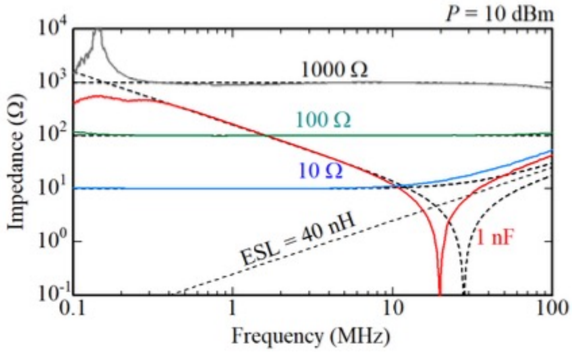

(a) Result of brush motor impedance Z_1

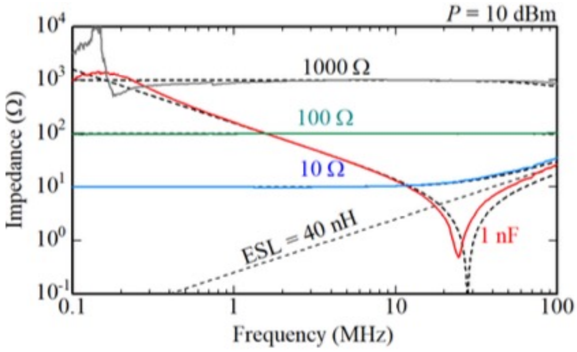

(b) Result of brush motor impedance Z_2

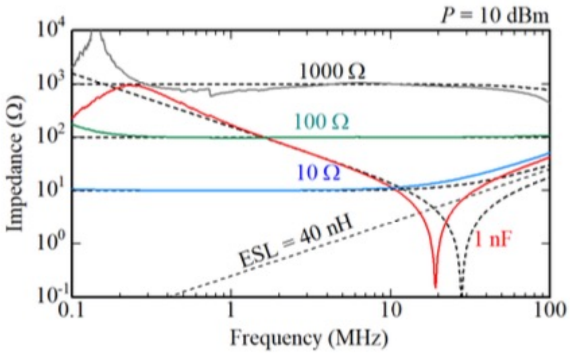

(c) Result of brush motor impedance Z_3

Figure 3.14 Impedance of resistors and capacitors obtained by the proposed method.

3.4.2 Identifying Impedance of Brush Motor under Dynamic Condition and at rest

The proposed design method and procedure were applied to measure the impedance of brush motors under stationary and dynamic conditions. Fig. 3.15 and Fig. 3.17 are the frequency characteristics of Z_1 and Z_3 of the brush motor under stationary and dynamic condition, respectively, and Z_2 is omitted because it is almost identical to Z_1. The equivalent circuit model can also be expressed as in Fig. 3.19.

Firstly, result of brush motor impedance Z_1 and Z_2 under dynamic condition in Fig.

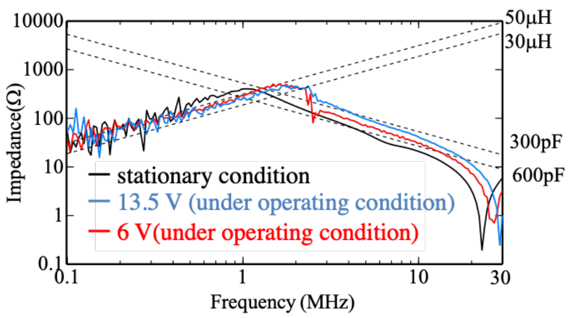

Figure 3.15 Magnitude of impedance Z_1 and Z_2.

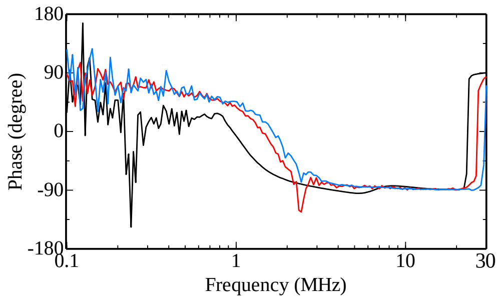

Figure 3.16 Phase of impedance Z_1 and Z_2.

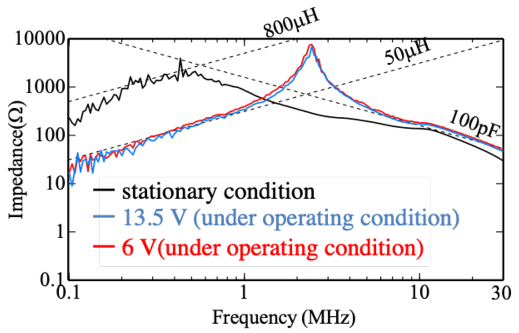

Figure 3.17 Magnitude of impedance Z_3.

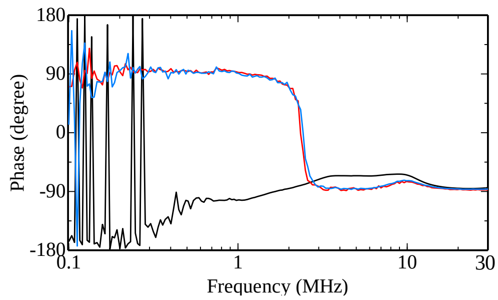

Figure 3.18 Phase of impedance Z_3.

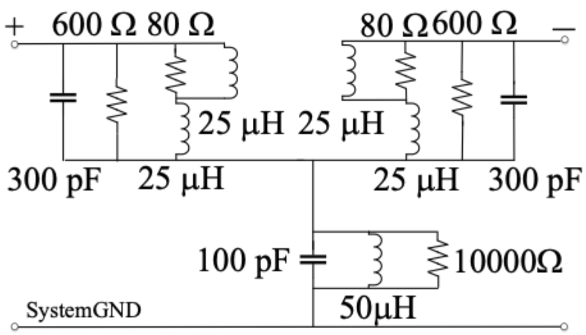

Figure 3.19 Equivalent circuit of brush motor including CM impedance under dynamic condition.

3.15, Fig. 3.16 are described. The validity of the identification method was confirmed since the impedances of the spectra of $C_{\mathrm{is}} = 280$ pF, $L_{\mathrm{p0}} = 80$ μH measured in the section 3.2 and $Z_1 = 300$ pF, $Z_1 + Z_2 = 60$ μH measured by the proposed design method also showed similar impedances. Also, this confirms the validity of the identification method, since the impedance was generally similar to the $C_{\mathrm{m}} = 150$ pF spectrum measured in section 3.2 at 1 MHz and beyond.

Next, the impedance Z_3 of brush motor is explained in Fig. 3.17, Fig. 3.18. Z_3 under stationary condition were compared with and without AMN, and a difference was observed below 0.4 MHz for Z_3 at stationary. However, other than that, the results generally agreed with each other, confirming the validity of the identification method. The next comparison was made when 0 V, 6 V, and 13.5 V DC were applied via AMN, and Z_1 did not show much change. However, Z_3 was smaller under 1 MHz in operation than stationary conditions. As a result, the impedance under stationary conditions generally agreed with the evaluation method proposed in the previous section, confirming the validity of the measurement method using AMN. Furthermore, the proposed evaluation method showed that the impedance under dynamic conditions changed at Z_3, which confirms that the accuracy of the impedance measurement has improved. Finally, the equivalent circuit of the brush motors under dynamic condition, created using the obtained Z_1 - Z_3, is shown in Fig. 3.19. In next section, this equivalent circuit will be used to identify noise sources in the brush motor and to verify the accuracy of the impedance of the brush motor under stationary and dynamic conditions.

3.5 Verification of Impedance of Brush Motor in Dynamic Condition in Non-powered

In this section, we identify the noise sources in the brush motors and verify the accuracy of the impedance of the brush motors under stationary and dynamic condition. To investigate the accuracy of the impedance in brush motors, validate it by predicting noise current sources.

Two brush motors are prepared in brush motors for impedance accuracy verification. Two types of motors are used, one is Motor A with no filter installed and the other is Motor B with a filter installed. The equivalent circuit model of the brush motors under dynamic conditions shown in Fig. 3.20 and the equivalent circuit of the identified EMI evaluation environment shown in Fig. 3.19 are used to predict the noise voltage. Therefore, the noise current source calculated using the Z_{A} obtained for Motor A is used to validate the prediction of Motor B installed with the filter.

Firtly, obtain the actual measured values of V_{Hmeas} and V_{Lmeas} for motor A without filter, which represent V_{H} and V_{L} in the measurement environment shown in the Fig. 3.21. The measured environment in that case is shown in Fig. 3.21, and the measurement conditions are shown in the Table 3.5.

Next, using the equivalent circuit model of Motor A under dynamic condition in Fig. 3.1 EMI evaluation environment, insert I_{ns1}, $I_{\mathrm{ns2}} = 1$ A and calculate the transfer impedance Z_{A} from the following equation.

$$\begin{bmatrix} V_{\mathrm{Hmeas}} \\ V_{\mathrm{Lmeas}} \end{bmatrix} = \begin{bmatrix} Z_{11} & Z_{12} \\ Z_{21} & Z_{22} \end{bmatrix} \begin{bmatrix} I_{\mathrm{ns1}} \\ I_{\mathrm{ns2}} \end{bmatrix} \tag{3.3}$$

$$\mathbf{Z_A} = \begin{bmatrix} Z_{11} & Z_{12} \\ Z_{21} & Z_{22} \end{bmatrix} \tag{3.4}$$

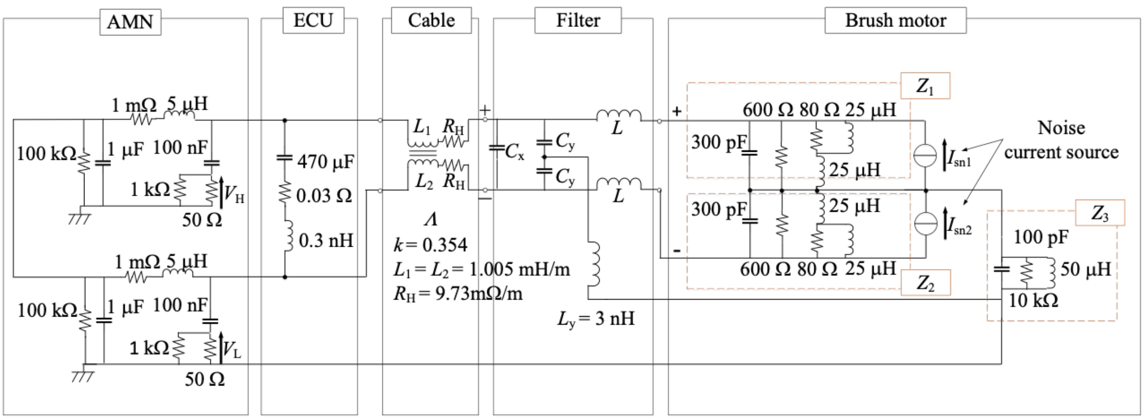

Figure 3.20 Improved Equivalent circuit model of evaluation system in brush motor drive system.

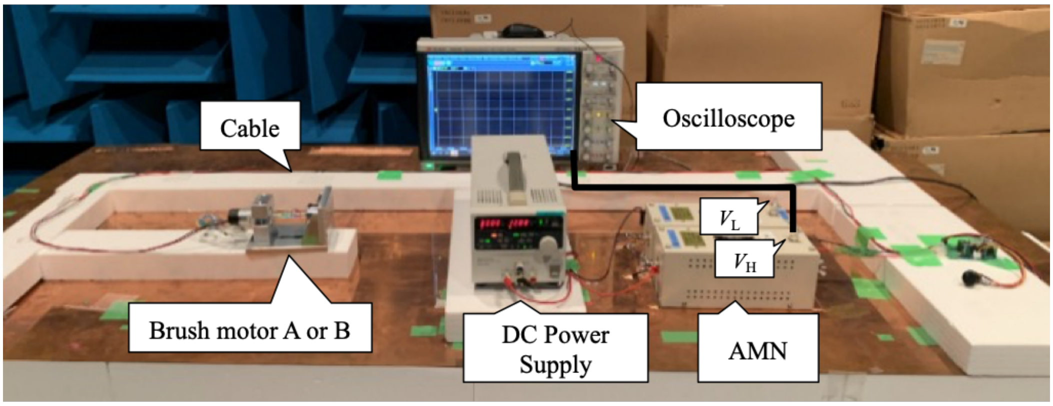

Figure 3.21 Actual measurement environment for verifying the impedance of the identified brush motors.

Table 3.3 Measurement conditions for brush motor noise

Parameter	**Specification**
Frequency range	0.1 MHz - 30 MHz
Length of wire harness	150 mm
Height of wire harness	50 mm
Oscilloscope	DSO-S104A
Sampling rate	100 MSa/s
Sampling points	10 kpts
Line impedance stabilization Network	TNW-1502
DC stabilized power supply	PW16-5ADP

$$\begin{bmatrix} I_{\mathrm{ns1}} \\ I_{\mathrm{ns2}} \end{bmatrix} = \mathbf{Z}_{\mathbf{A}}^{-1} \begin{bmatrix} V_{\mathrm{Hmeas}} \\ V_{\mathrm{Lmeas}} \end{bmatrix} \tag{3.5}$$

Then, using the inverse matrix of the transfer impedance Z_{A} and the actual measurement results of V_{Hmeas} and V_{Lmeas}, calculate the noise current sources I_{ns1} and I_{ns2} from the following equations.

Finally, using the noise current sources I_{ns1} and I_{ns2} obtained using the following equations, predict the actual measurement results of V_{Hmeas} and V_{Lmeas} at motor B installed with the filter. The filter condition for motor B is C_{x}, $C_{\mathrm{y}} = 1$ nF, $L = 0.6$ μH, $\Lambda = 2$ m.

$$\begin{bmatrix} V_{\mathrm{Hpredict}} \\ V_{\mathrm{Lpredict}} \end{bmatrix} = \mathbf{Z}_{\mathbf{B}} \begin{bmatrix} I_{\mathrm{ns1}} \\ I_{\mathrm{ns2}} \end{bmatrix} \tag{3.6}$$

The measured and predicted results of DM noise and CM noise using V_{H} and V_{L} are shown in Fig. 3.22 and 3.23. DM noise is calculated using V_{H} - V_{L}, while CM noise is calculated using $V_{\mathrm{H}} + V_{\mathrm{L}}$. As for the DM noise prediction results, they generally agreed with the measured results, and the predicted results for the dynamic state were closer to the measured results. As for the CM noise prediction results, the predicted errors were closer to the measured results than the measured results, with errors of more than 20 dB

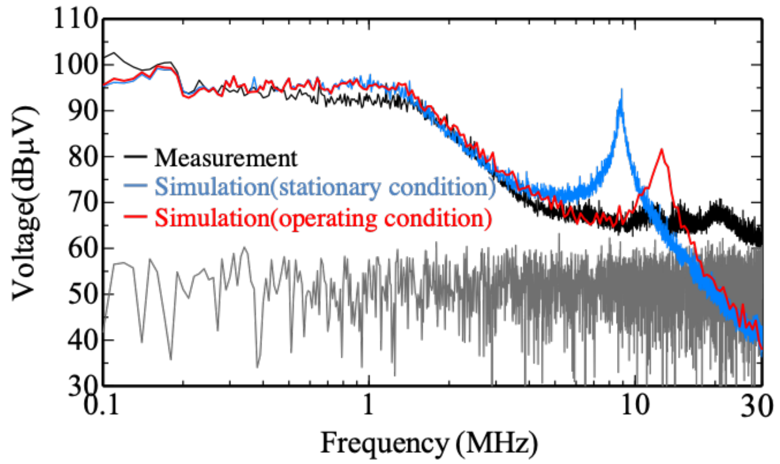

Figure 3.22 Comparison of measured and simulated results in DM noise.

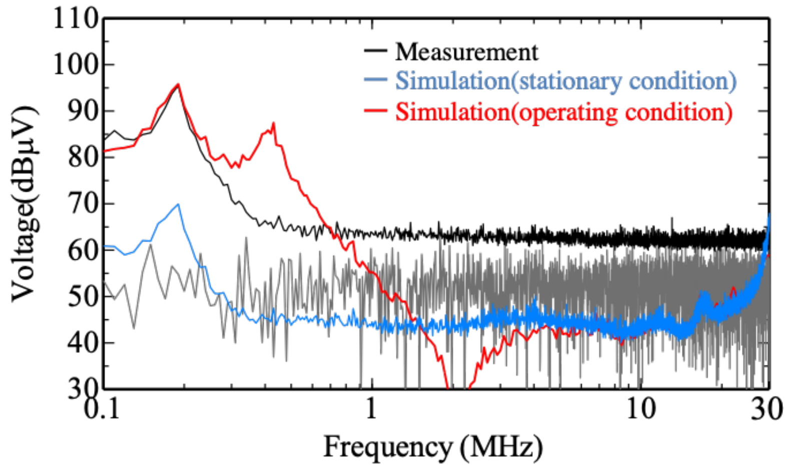

Figure 3.23 Comparison of measured and simulated results in CM noise.

for the low frequency portion below 1 MHz. The results confirm that the CM noise was underestimated by the internal impedance identified at motor standstill because the CM noise increases as Z_3, which contributes to the CM noise, becomes smaller.

Thus, the identification of the internal impedance of active brush motors by VNA using AMN confirmed that Z_3 decreases at low frequencies in brush motors compared to the internal impedance in stationary operation. In addition, the equivalent circuit model improved in accuracy because the noise level in the dynamic model increased to the measured level at low frequencies, whereas the stationary model underestimated the noise in predicting the CM noise voltage.

Chapter 4

Optimal Design Method Using Set-based Method

4.1 Introduction

The product design process often requires finding a solution that simultaneously satisfies multiple performance objectives, sometimes with conflicting requirements. In addition, it is important to have a design methodology that allows for the development of products at low cost and in a short period of time. The main approaches in the field of mechanical design to achieve these goals include design parameters and set-based design [50]. As a traditional method, point-based design is a design method that sets initial values for multiple design parameters and repeatedly modifies (tries and errors) the variables in pursuit of the optimal design solution. This method finds a single optimal solution that satisfies multiple requirements.

The point-based design method is often used in the design phase because it is often easy to understand and intuitive for many engineers and designers. However, the designer repeats trial and error of design and analysis until the desired design conditions and specifications are satisfied based on the designer's experience. Also, in many cases, the complexity of the many elements and components inside an electronic device can make it difficult to satisfy multiple requirements due to their interaction. As a result, EMI problems are often addressed through design back and trial-and-error, the current design is that it takes time and costs a lot of money to find the optimal design solution. In addition, changes in product specifications and variations in devices may occur during the design process. In such cases, the risk of test failure increases due to the effects of complex interactions caused by changes in the parameters of a single element. In this case, the size, length, and shape of motors and cables are generally determined before the prototype of the design process. Therefore, if an EMC test fails on an ECU prototype, stepping back to the design process, such as changing the motor or wiring, is not allowed because it will affect the vehicle specifications.

As a solution to this problem, it is important to optimize the design of EMI countermeasures including the entire system before prototyping in the design process. In addition, there is no single design solution that can satisfy multiple requirements, and redundant design is considered to be more effective. Therefore, in designing brush motors and cables for this project, it is desirable to obtain a range of design parameters that satisfy multiple performance requirements in order to prevent design process back after prototyping. When design parameters that satisfy the required performance are obtained as a range of interval solutions the most effective and efficient one can be selected among multiple solutions, which is expected to reflect the designer's intention. In addition, even if product specifications are changed after prototyping or element variations occur, the requirements can be met by taking them into account in the design process, making it unnecessary to reconsider the design. In this way, design parameters that satisfy the requirements can be obtained as a range of solutions, which enables flexible design and saves design time.

Therefore, an approach has been proposed as set-based design, in which design parameters and required performance are considered in a range, and the range of design parameters is narrowed down to satisfy multiple required performance. In this set-based design, in contrast to point-based design, a set of design solutions can be obtained as a range of interval solutions rather than a single solution that satisfies multiple requirements. Within this set-based design, the Preference-Set-Based Design method (PSD) [1, 2] has been examined. The PSD method is characterized by the incorporation of an index called "preference," which quantitatively evaluates the designer's intention with respect to design parameters and performance requirements, while also maintaining design robustness. Formerly in the field of mechanical devices, research on the design of cantilever beams has been pursued [51]. They has applied the PSD method to electrical devices and demonstrated the design of EMI filters [21, 24, 25], differential transmission lines [22], and radio absorbers [52]. Furthermore, in order to simplify the design of filters using the PSD method, they have proposed a design method that utilizes the design of experiments [53] for meta-modeling. It is shown that the number of initial calculations for meta-modeling, such as reducing the maximum number, can be efficiently reduced in the example model considered.

These PSD methods have only been applied to the optimal design of only filters or only for partial designs. However, in the actual design process, it is necessary to perform optimal design of complex systems, such as entire systems, rather than using only filters or partial designs. In this study, a brush motor drive system in an international standard evaluation environment is used as an example, not as a stand-alone filter, and the PSD method is applied to a more practical design situation to satisfy multiple requirements. Therefore, we propose a multi-objective design method that combines an equivalent circuit model and PSD method based on a meta-model. The set-based method based on the meta-model uses a mathematical model in which the performance requirement are a function of multiple filter parameters, so that a range of filter parameters that satisfies the required attenuation characteristics can be determined. In the design of practical products, the values of elements that can be used in practice are discrete, so it is desirable to specify not only a specific value but also an allowable range of values for the elements to be specified as design parameters. From this point of view, the present design method is suitable for the design of practical products. At this time, it is important for designer that multiple parameters that satisfy multiple performance requirements should be obtained as a wider and more accurate range of interval solutions. For this purpose, the modeling accuracy of the required performance and design parameters is important. Since inaccurate modeling does not accurately reflect actual performance requirements or constraints, there is no guarantee that the solution obtained is the true optimal solution, and the search area that may contain the optimal solution may be missed. Depending on the modeling accuracy, it is possible to find a more accurate and wider range of interval solution that satisfies the required performance. Therefore, to achieve this objective, we attempted to obtain a wide range solution by implementing the PSD method twice. This procedure was applied to the PSD design methodology using the design parameters and required performance obtained from circuit simulation. Using a brush motor drive system as an example, the verification was performed to obtain a range of interval solution of EMI filters and cables that satisfy several required performances.

4.2 Proposed Design Method Procedure Using Set Based Method

This section first provides an explanation of the set-based method, followed by an explanation of the meta-modeling applied when using the PSD method.

4.2.1 Set-based Design Method

Many design methodologies have been proposed in development, such as the traditional point-based design that can find one optimal design parameter. On the other hand, the set-based design methods are proposed to treat design parameters and required performances in a range and can narrow down the range of design parameters to satisfy required performances. The fundamental idea of the set-based design method [1, 2] is to consider the various uncertainties in performance and parameters in terms of a set of "sets" that include their range of parameters variation. If a "set" that satisfies one objective performance for each design parameter exists, and if a common range that satisfies all of the multiple required performances exists for that design parameter, then that common range becomes a "set" that satisfies all required performances. However, if this common range does not exist even for one required performance, it is impossible to satisfy all the required performances set by the designer, and it is necessary to change the range of design parameters again. The design parameters are then narrowed down to leave only those solutions that satisfy multiple performance requirements, as shown in Fig. 4.1. By repeating this process, a "set" of design parameters that satisfies multiple required performance can be identified. Therefore, if a common range for all required performances exists, there is a valid solution in the range of design parameters, indicating that an interval solution can be searched for as a "set".

Next, it describes the design procedure using the applied set-based design method.

The flowchart of the conventionally proposed PSD method is shown in Fig. 4.2. The PSD method is a set-based design method that identifies a range of design parameters that satisfy multiple performance requirements. It combines the analysis ranges of design

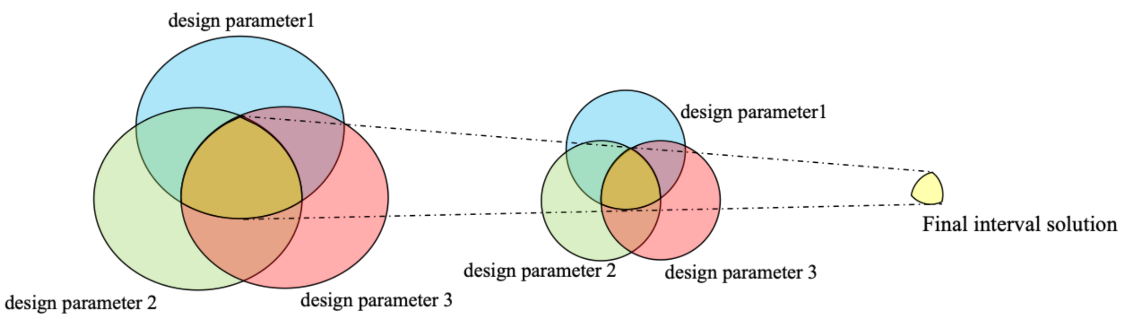

Figure 4.1 Diagram of Set-Based Design Methodology 4.1.

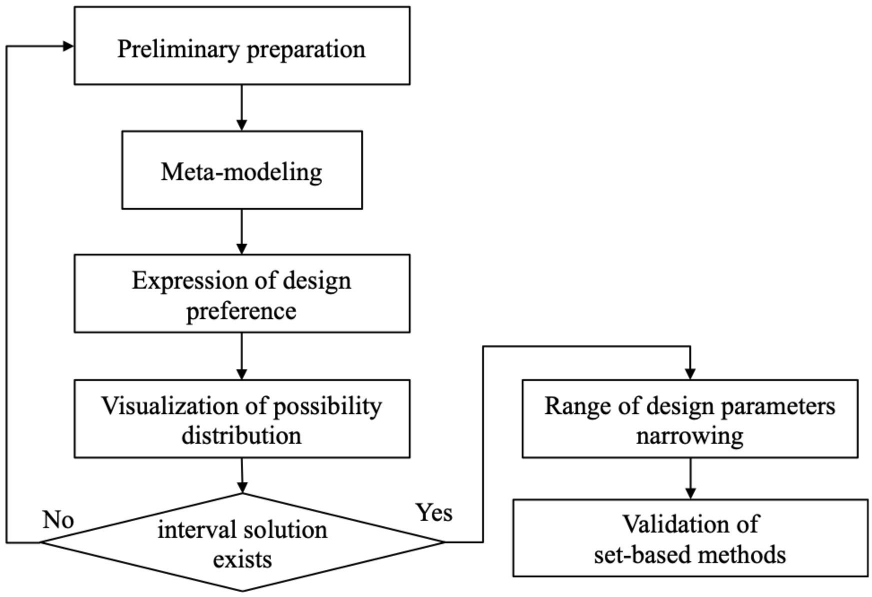

Figure 4.2 Set-Based Design Methodology Procedure.

parameters and performance requirements with weighted preferences to reflect the intentions of the designer. The first step is to determine the initial range of design parameters. Since the analysis is performed within this range, they must be determined based on the designer's intent so that the solution is included. Several patterns of design parameters and their performance data are given within this initial range. For example, in brush motor drive system, it is unknown how the filter characteristics will change when the design parameters are changed. In this case, it is not possible to predict where a wider solution can be obtained. Thus, the initial data should be as wide a range of design parameters as possible. Then, the characteristics of the design objective are approximated by a meta-modeling equation in design using the PSD method. Based on simulation data, approximate equations are calculated in which each performance is represented as having the design parameters as independent parameters. In this term, a response surface methodology (RSM) is used for a this meta modeling. Then, the existence of a range solution is investigated, and the design parameters are narrowed down by using the PSD solver. Finally, the EMI filter characteristics of the obtained design parameters in the range solution are evaluated, and the validity of the design method is confirmed.

4.2.2 Meta-modeling

This section provides an explanation of meta-modeling used in the set-based design method procedure. It expresses the equation(4.1) as a function of the required performance y and the design parameters x as an approximate expression that relates the required performance and the design parameters.

$$y = f(x_1, x_2, \ldots, x_n) \tag{4.1}$$

First, an initial range is set to determine the range of design parameters that can realize the requirements. Then, the relationship between the required performance y and the design parameter x is defined by an approximate expression, and a response surface is created in equation(4.2). Meta-modeling is performed by obtaining the coefficient β of each term from the Response Surface Methodology (RSM) using the values of the initial range.

$$y = \beta_0 + \sum_{i=1}^{k} \beta_i x_i + \sum_{i=1}^{k} \beta_{ii} x_i^2 + \sum_{i<j}^{k} \beta_{ij} x_i x_j \tag{4.2}$$

$$\mathbf{y} = \mathbf{X}\boldsymbol{\beta} + \boldsymbol{\epsilon} \tag{4.3}$$

$$\mathbf{y} = \begin{pmatrix} y_1 \\ y_2 \\ \vdots \\ y_n \end{pmatrix} \tag{4.4}$$

$$\mathbf{X} = \begin{pmatrix} 1 & x_{11} & x_{12} & \cdots & x_{1(k-1)} \\ 1 & x_{21} & x_{22} & \cdots & x_{2(k-1)} \\ 1 & \vdots & \vdots & \ddots & \vdots \\ 1 & x_{n1} & x_{n2} & \cdots & x_{n(k-1)} \end{pmatrix} \tag{4.5}$$

$$\boldsymbol{\beta} = \begin{pmatrix} \beta_1 \\ \beta_2 \\ \vdots \\ \beta_n \end{pmatrix} \tag{4.6}$$

$$\boldsymbol{\epsilon} = \begin{pmatrix} \epsilon_1 \\ \epsilon_2 \\ \vdots \\ \epsilon_n \end{pmatrix} \tag{4.7}$$

In this case, the design parameters are in different units and need to be normalized. By making all the orders of the design parameters the same order, the design parameters can be evaluated with equal orders. This allows the sensitivity of the design parameters to the required performance to be expressed in terms of the coefficient β'. It can be expressed by the following equation(4.8),(4.9).

$$\bar{x} = \frac{x - x_{\mathrm{MIN}}}{x_{\mathrm{MAX}} - x_{\mathrm{MIN}}} \tag{4.8}$$

$$y = \beta'_0 + \sum_{i=1}^{k} \beta'_i \bar{x}_i + \sum_{i=1}^{k} \beta'_{ii} \bar{x}_i^2 + \sum_{i<j}^{k} \beta'_{ij} \bar{x}_i \bar{x}_j \tag{4.9}$$

LEVEL	x_1	x_2
1	$x_{1.\mathrm{MIN}}$	$x_{2.\mathrm{MIN}}$
2	$x_{1.\mathrm{MID}}$	$x_{2.\mathrm{MID}}$
3	$x_{1.\mathrm{MAX}}$	$x_{2.\mathrm{MAX}}$

In this study, the data of $V_{\mathrm{DMnoiseATT}}$, $V_{\mathrm{CMnoiseATT}}$ used for meta-modeling is obtained from circuit simulations with three values (minimum, middle, and maximum) for each set of design parameter inputs. These values are used as design parameters with each parameter normalized by three levels as shown in the Table 4.2.2. In doing so, the response surface is created by defining the relationship between the required performance y and the design parameter x as an approximate expression. In this case, the method uses the sum of the first order term, the second order term, and the mutual term.

4.3 Application of Set Based Design Method

This section describes the flow of the design methodology using the set-based method in brush motors system as an example.

The application of the design procedure using the set-based method in this paper is shown in Fig. 4.3. Since brush motor drive systems are complex with many parameters, it is difficult to determine the initial range. Therefore, the set-based design procedure is applied twice, as shown in Fig. 4.4. The first time, the analysis is performed with a wide initial range to see where the interval solution can be obtained. Then, based on the interval solution obtained, the initial range is reconsidered and the set-based design method is applied for the second time. The initial range in the second set-based design method is several times wider than the range solution obtained in the first set-based design method. This is because if the design range is wide in the first set-based design method, the approximation accuracy in the initial wide range may result in a narrow interval solution. Therefore, this method is necessary to obtain a wide range of solutions. In the case of meta-modeling with a wide initial range, the approximation accuracy may be low, because this may result in a narrower design range solution that satisfies the requirements. If an interval solution cannot be obtained even after applying the first set-based method, the first initial range is reconsidered.

The procedure 1 is to determine the initial range, which is the design range. As mentioned above, the initial range is defined as a wide initial range. In this case, a wide enough initial range is determined for the four design parameters. Since the ESL of the cable also affects the attenuation characteristics considered in this study, the filter design parameters include the cable length in addition to the filter element parameters. In the brush motor drive system shown in this example, the initial range is determined as wide

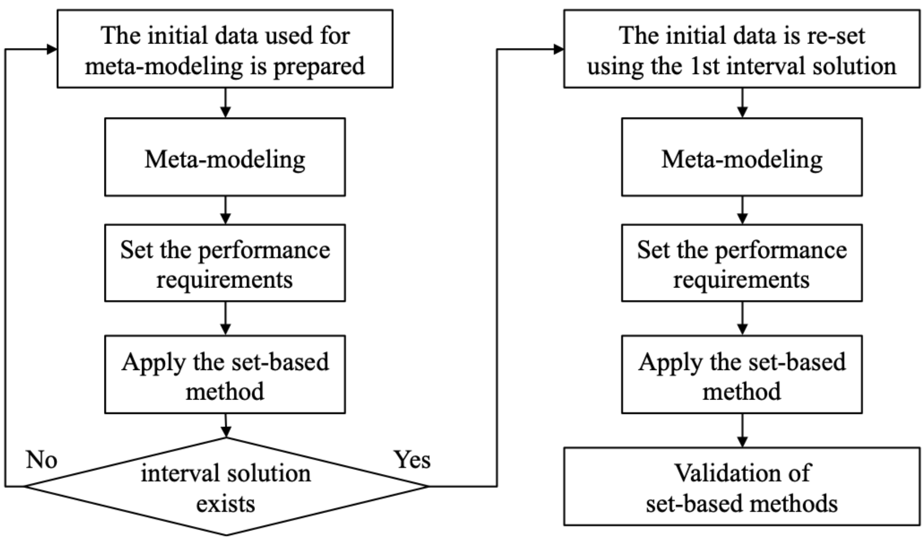

Figure 4.3 Procedures of the set-based design method in this study.

Table 4.1 3 levels of initial data for applying set-based method to brush motor drive system

	C_x(nF)	C_y(nF)	L(μH)	Λ (m)
Level 1	0.5	0.5	0.1	1.7
Level 2	5	5	1	2
Level 3	20	20	3	2.3

Table 4.2 Normalization of initial data in brush motor drive system

	C_x	C_y	L	Λ
Level 1	0.1	0.1	0.1	0.85
Level 2	1	1	1	1
Level 3	4	4	3	1.15

as shown in the Table 4.1. In order to create an approximate equation using the response surface method that relates the requirements to the design parameters, if the orders of each design parameter are different, they cannot be evaluated equally. When performing set-based design for brush motor drive systems with different orders of design parameters, it is necessary to apply normalization. Therefore, the equations explained in the previous section are used to normalize the design parameters. Each parameter in the Table 4.1 is used to normalize each parameter shown in the Table 4.2.

Next, as procedure 2, the required performance is determined. as described in section 3.5, the required performance of the filter design is a total of four kinds of attenuation characteristics of DM and CM noise at low frequency (0.1 MHz $\leq f \leq$ 1 MHz) and high frequency (10 MHz $\leq f \leq$ 30 MHz), respectively, as shown in the table. In other words, a wider range solution of design parameters that satisfies these four performance requirements is obtained.

Next, we explain the meta-modeling method as procedure 3. An approximate equation is determined as a meta-modeling of the relationship between the required performance of the attenuation characteristics and the design parameters. In this process, the at-

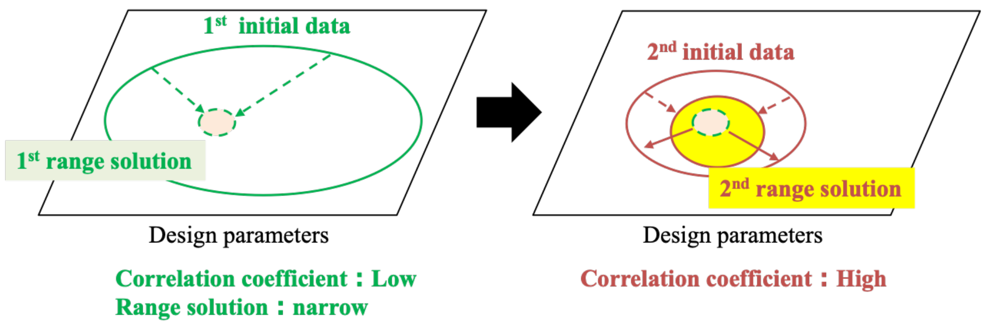

Figure 4.4 Punch diagram of the expansion of the range solution by implementing the set-based design method twice 4.1.

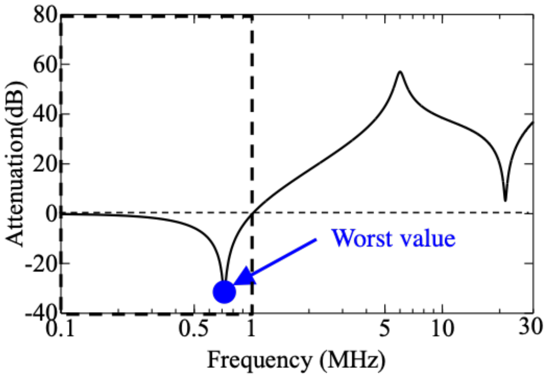

Figure 4.5 Example of worst-case DM attenuation $V_{\mathrm{DMnoiseATT}}$ at low frequencies

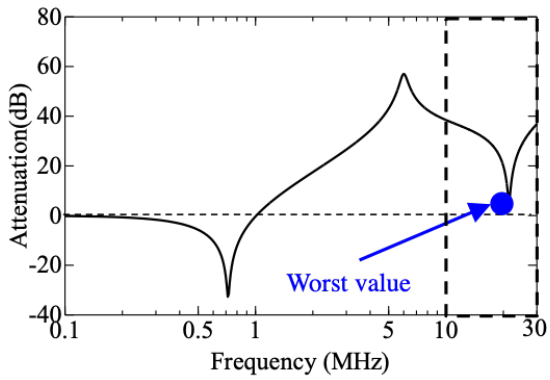

Figure 4.6 Example of worst-case DM attenuation $V_{\mathrm{DMnoiseATT}}$ at high frequencies

tenuation characteristics are calculated using circuit simulation as the reference data for determining the approximate equation. At this time, the equivalent circuits identified by actual measurement of the impedance of the brush motor and the measurement environment, respectively, as shown in Section 3.3, are used to calculate the circuit simulation. Then, 81 combinations of MAX, MID, and MIN are calculated by circuit simulation at the three levels shown in the table. One of the 81 calculation results, $V_{\mathrm{DMnoiseATT}}$ spectrum of attenuation characteristics obtained from the equivalent circuit, is shown in the figure. It shows the worst value of DM attenuation at each of the frequencies defined in the performance requirements (low frequency (0.1 MHz $\leq f \leq$ 1 MHz) and high frequency (10 MHz $\leq f \leq$ 30 MHz)) as blue dots. This means that 81 worst-case DM attenuation values can be obtained for low frequency (0.1 MHz $\leq f \leq$ 1 MHz) and 81 worst-case values for high frequency (10 MHz $\leq f \leq$ 30 MHz). Thus, 81 combinations of design parameters and 81 worst-case values can be used to determine an approximate equation for the worst-case DM, CM attenuation $V_{\mathrm{DMnoiseATT}}$ and $V_{\mathrm{CMnoiseATT}}$ at low frequencies (0.1 MHz $\leq f \leq$ 1 MHz) through meta-modeling.

Using the data on the attenuation characteristics at the element values varied by the three levels shown in Table 4.2, approximate equations for y shown in Section 4.2 are obtained using the response surface method with the element values as parameters, as second-order polynomials expressed as the sum of the second-order term, first-order term, and alternating terms. As a result, two types of approximate equations for DM attenuation are created for low frequency (0.1 MHz $\leq f \leq$ 1 MHz) and high frequency (10 MHz $\leq f \leq$ 30 MHz), and two types of approximate equations for CM attenuation are created for low frequency (0.1 MHz $\leq f \leq$ 1 MHz) and high frequency (10 MHz $\leq f \leq$ 30 MHz). In other words, four approximate formulas are prepared in total. Then, using the meta-modeling approximations for each of the four performance requirements, an interval solution for the design parameters that satisfies these four performance requirements is obtained.

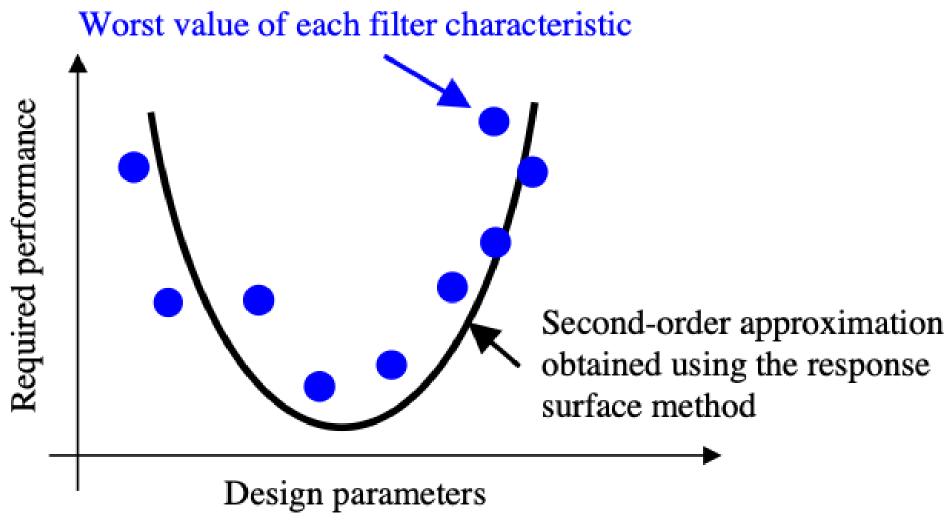

Figure 4.7 Approximation by quadratic equation in response phase method.

Finally, investigate whether an interval solution satisfying the required performance has been obtained as procedure 4. If no interval solution is obtained after applying the first set-based method, reconsider the first initial range. The brush motor drive system targeted in this study is very complex and has many local solutions due to the existence of many parameters. Therefore, during meta-modeling, a wide initial range of design parameters includes a range that cannot be expressed by a second-order function, and the match between the approximate equation and the attenuation characteristics obtained by circuit simulation is reduced. In other words, the correlation coefficient between these characteristics becomes low, and as a result, a sufficiently wide range solution may not be obtained. Therefore, in brush motor drive systems, meta-modeling is limited to the range of the obtained solution, and meta-modeling is performed again to improve the accuracy of the meta-modeling and obtain a wider range of solutions. At that time, the initial range for the second set-based design method is set using a range that is several times wider than the range solution obtained by the first set-based design method. Then, a wider range interval solution is obtained by applying the set-based design method a second time.

4.4 Validation of the Proposed Method

In this section, we investigate the effectiveness regarding the results obtained using the procedure in the previous section. It will be verified whether the obtained interval solution satisfies the required performance. We examine whether a wide range of solutions can be obtained by performing the set-based design twice, and whether the proposed method can be applied to practical situations.

First, the interval solutions obtained by the first set-based design method using this meta-modeling are shown in Table 4.4.

Next, using the range solution obtained from the first set-based design method, the range solution for the design parameters to be used in the second set-based design method is narrowed down as shown in Table . In this study, the initial range of the second set-based design method is set to be four times the obtained range solution.

Then, the second set-based design method is applied using the initial range solution set in Table 4.4. The interval solution obtained by the set-based design method with the second meta-modeling is then shown in Table 4.4.

Next, the validity of the obtained interval solutions is evaluated. In order to verify whether the interval solution shown in Table 4.4 satisfies the required performance, the attenuation characteristics were calculated for 81 combinations of filters with three different maximum, average, and minimum values of element values. The DM and CM noise attenuation calculated for 16 combinations using the minimum and maximum values of the four design parameters in the interval solution are shown in Fig. 4.9, Fig. 4.8.

Since the results in Fig. 4.9 and Fig. 4.8 are in the minimum to maximum value range, it can be confirmed that the obtained interval solution satisfies all the required performances with respect to the DM and CM noise attenuation characteristics. Therefore, it can be seen that the interval solutions obtained by the second set-based design

Table 4.3 Range solution for the first application of the set-based design method.

	C_x(nF)	C_y(nF)	L(μH)	Λ (m)
Range of interval solution	0.5–0.9	2.15–2.55	1.49–1.55	2.28–2.3

Table 4.4 Initial data for the second application of the set-based design method

	C_x(nF)	C_y(nF)	L(μH)	Λ (m)
Level 1	0.5	0.7	1.28	2.24
Level 2	0.7	2.35	1.52	2.3
Level 3	2.35	3.95	1.76	2.34

Table 4.5 Range solution for the first application of the set-based design method

	C_x(nF)	C_y(nF)	L(μH)	Λ (m)
Range of interval solution	0.5–1.5	2.5–4	1.5–1.8	2.24–2.3

Table 4.6 Correlation coefficients and required performance

	1st set-base method	2nd set-base method
$V_{\mathrm{DMnoiseATT}}$(0.1 MHz–1 MHz)	99.43%	99.99%
$V_{\mathrm{DMnoiseATT}}$(10 MHz–30 MHz)	98.78%	99.98%
$V_{\mathrm{CMnoiseATT}}$(0.1 MHz–1 MHz)	98.18%	99.99%
$V_{\mathrm{CMnoiseATT}}$(10 MHz–30 MHz)	99.69%	99.97%

method shown in Table are more widely obtained than those obtained by the first set-based design method shown in Table . Also, as shown in Table , the interval solution obtained a range of more than 9% with respect to the average value. Therefore, elements that satisfy the interval solution can be selected by using elements with an accuracy of 5% or less. Therefore, it was confirmed that practical design parameters can be obtained. The ability to obtain a range of design parameters is a significant feature of the set-based design method.

Finally, the accuracy of meta-modeling using the first and second set-based methods is discussed. A scatter diagram showing the correspondence between the results of the circuit simulation and the meta-modeling equation obtained by the response phase method is shown in Fig. 4.10, Fig. 4.11. In the ideal response phase, the actual values and the response phase perfectly match, resulting in a straight line with slope 1 and intercept 0 (wavy line in the figure). However, there is an error with the actual result, and the correlation coefficient of the meta-modeling equation is small, which means that the approximation is inaccurate. In such cases, the interval solution may not satisfy the required performance. In this study, the correlation coefficients in each frequency range were greater than 98%. The correlation coefficients in each frequency domain in the case of the first set-based design method are shown in Fig. 4.10. The correlation coefficients in each frequency domain for the second set-based design method are shown in Fig. 4.11. The correlation coefficients of the approximate meta-modeling equations used in the first

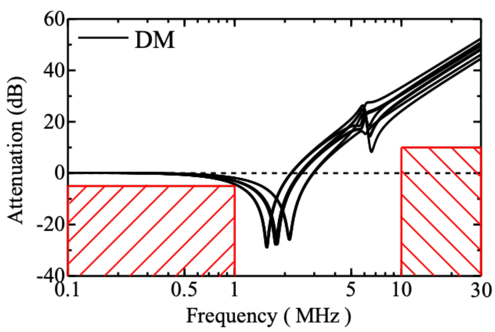

Figure 4.8 Evaluation of DM attenuation($V_{\mathrm{DMnoiseATT}}$) using a range solution with applications of the set-based design method twice.

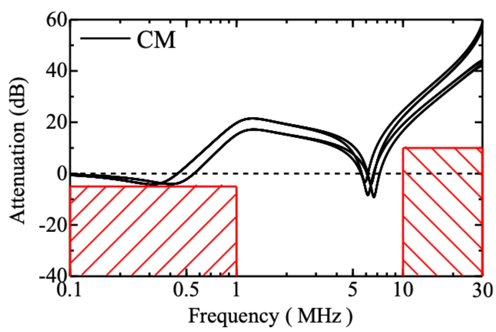

Figure 4.9 Evaluation of CM attenuation($V_{\mathrm{CMnoiseATT}}$) using a range solution with applications of the set-based design method twice.

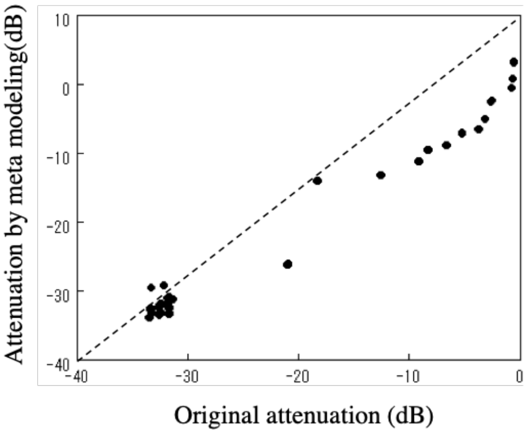

(a) $V_{\mathrm{DMnoiseATT}}$ (0.1 MHz – 1 MHz) of correlation coefficients with first set-based method

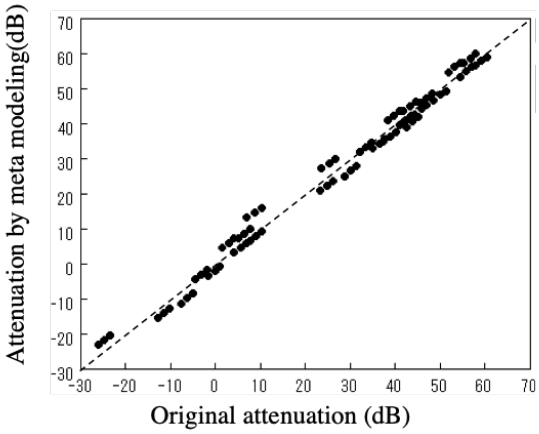

(b) $V_{\mathrm{DMnoiseATT}}$ (10 MHz – 30 MHz) of correlation coefficients with first set-based method

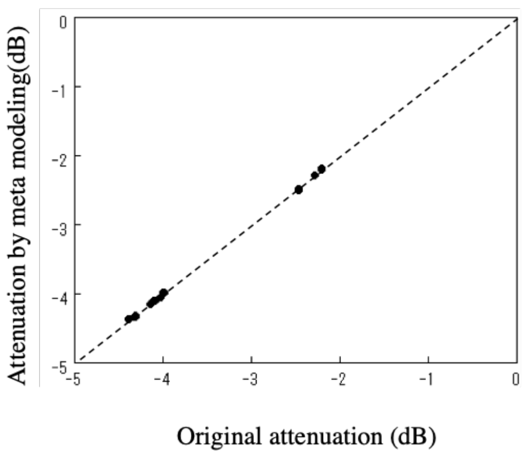

(c) $V_{\mathrm{CMnoiseATT}}$ (0.1 MHz – 1 MHz) of correlation coefficients with first set-based method

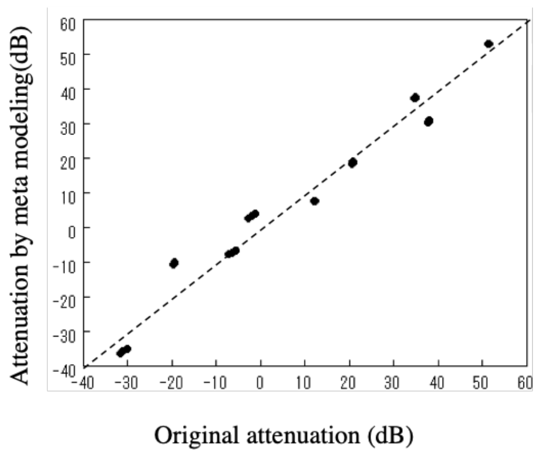

(d) $V_{\mathrm{CMnoiseATT}}$ (10 MHz – 30 MHz) of correlation coefficients with first set-based method

Figure 4.10 Correlation coefficients of the meta-models.

and second times are shown in Table 4.6. It is confirmed that the correlation coefficients for the four performance requirements increased when the set-based design method was applied in the second round compared to the first set-based design method. The correlation coefficients of the meta-models were improved by the set-based methodology in the first and second times. This is because the second meta-modeling creates a model specific to the first interval solution and allows for a more detailed characterization of the data in that range. Furthermore, the increase in the density of data around that interval solution would have increased the accuracy of the meta-modeling approximation equation, and focusing on a specific range would have increased the entire accuracy because the approximation equation would have been generated with the most relevant data. This allowed a wider range solution to be obtained by conducting set-based twice. In conclusion, we

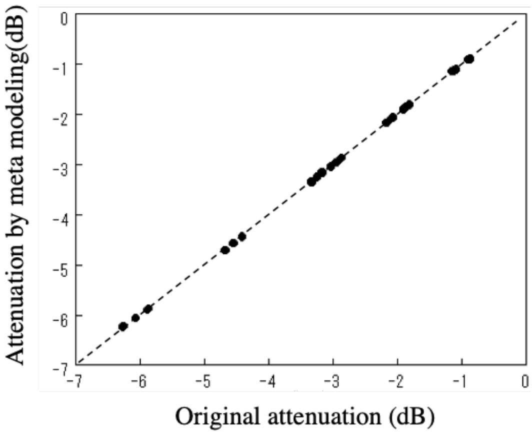

(a) $V_{\mathrm{DMnoiseATT}}$ (0.1 MHz – 1 MHz) of correlation coefficients with second set-based method

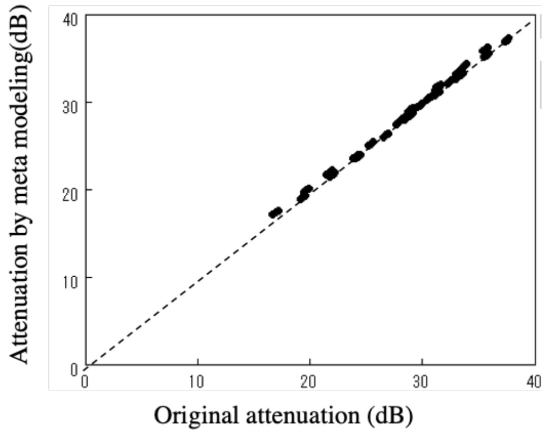

(b) $V_{\mathrm{DMnoiseATT}}$ (10 MHz – 30 MHz) of correlation coefficients with second set-based method

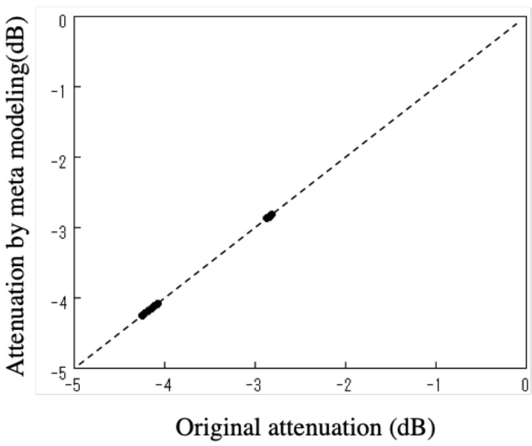

(c) $V_{\mathrm{CMnoiseATT}}$ (0.1 MHz – 1 MHz) of correlation coefficients with second set-based method

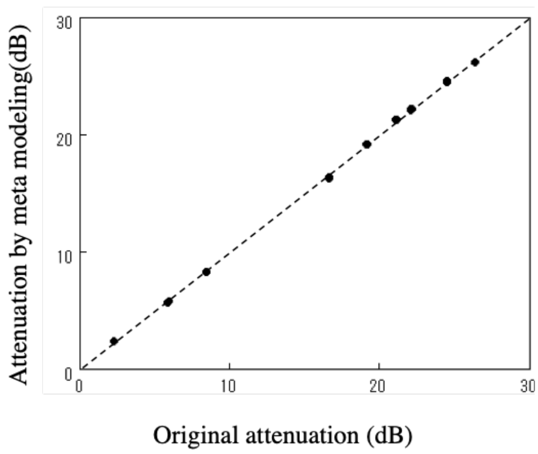

(d) $V_{\mathrm{CMnoiseATT}}$ (10 MHz – 30 MHz) of correlation coefficients with second set-based method

Figure 4.11 Correlation coefficients of the meta-models with the second set-based method.

were able to confirm the effectiveness of the set-based design method for brush motor drive system.

4.5 Conclusion

In this chapter, we proposed design method and procedure using a multi-objective design method that combines equivalent circuit modeling and meta-modeling. In brush motors system as a design example, the EMI filter characteristics of DM noise and CM noise are considered as the required performance, and the values of circuit parameters satisfying each of them are determined, and the interval solution is obtained by meta-modeling. The response phase method was used for meta-modeling, where each of the four required performances was expressed in terms of the first and second terms of each design parameter, as well as in terms of alternating terms. In this study, the set-based design method is applied twice as the design method to perform meta-modeling and computation of the interval solution. By applying the method twice, the correlation coefficient of the approximate equation obtained by meta-modeling can be made higher, and a wider interval solution is obtained. This allows the first meta-modeling to calculate the interval solution with a wide initial data range, and the second to obtain the interval solution more widely. The second meta-modeling increased the correlation coefficient, indicating that it is obtained accurately and widely. Finally, to demonstrate the validity of the proposed method, it was evaluated for 81 combinations of filter parameters in the interval solution. All combinations satisfied the required performance, confirming the effectiveness and validity of the proposed method.

Chapter 5

Optimal Design Method Using ANN Model

5.1 Introduction

In Chapter 4, we studied optimal design methods for determining filter constants that satisfy multiple performance requirements in brush motor drive systems. Focusing on the PSD method, which is one of the set-based design methods, we were able to obtain one range solution that satisfies the required performance by applying it to the brush motors system, the target circuit. However, when there are multiple local solutions, this is not necessarily the optimal (widest) range solution. The range of the interval solutions was not large enough for practical designs, it was difficult for the PSD method to find an optimal filter parameter set in such a restricted interval solution. The modeling accuracy was not always high, the one of reasons are that since the response phase method was used for modeling, approximated by a second-order function. Also reason is that the filter characteristics were given as the worst value rather than the frequency spectrum. This indicate that the system of interest in this study has many different interval solutions, and the relationship between design variables and required performance may be very complex. In such cases, modeling accuracy is not always high when the worst-case value in this relationship is approximated by a second-order function due to the limitations of the PSD solver. Therefore, detailed and accurate modeling is required with respect to this relationship between design variables and required performance in order to obtain a broader range of solutions. Thus, by using the other method, such redundant solutions are needed to cover a wider feasible range of design parameters and meet an assortment of different lead time and price goals. Therefore, in Chapter 5, we apply the ANN model, which can enable highly accurate modeling, and investigate whether it is possible to search for complex multiple interval solutions.

In this thesis, we focus on the modeling method by using Artificial neural network (ANN). ANN is a type of computational model that mimics the workings of neurons in the human brain; ANNs have the ability to learn based on large amounts of data and solve problems such as prediction and classification. ANN is a viable alternative, which can be used for fast evaluation of EMI filter behavior. ANN emulates a given device or a circuit after learning the device or circuit behaviors through an optimization process referred to as training [54]. In particular, ANNs have the ability to model nonlinear relationships and complex behavior, making them applicable to many applications and design issues. In addition, once the ANN model is trained, it can rapidly compute outputs for new input data, greatly speeding up the design iteration process and simulation.

A number of work have introduced several optimal design methods using ANNs in EMC analysis and as an alternative to simulation. Several optimal design methods using ANN are explained. Firstly, the approach for reverse modeling of EMC analysis by predicting radiated EMI due to structure has been proposed. This thesis indicates that EMI is predicted by using the height and size of the dielectric and structure as variables. When radiated sources are difficult to identify, it is difficult to effectively address the EMI problem using previous analysis and design methods. As for electromagnetic model, in order to simulate the high-frequency coupling behavior, accurate structure parameters and physical parameters are required, which are usually hard to obtain. What is more, electromagnetic model needs long time simulation and lots of calculation resources. But by using the ANN model, we have been able to achieve higher accuracy in less time than the full wave simulation solver. It has also been shown to significantly reduce memory requirements [55]. They has proposed the ANN modeling method for EMC analysis of ECUs and shielded enclosures. Next, in order to optimize filter parameters rapidly, an efficient modeling method of EMI filter is demanded. ANN has been successfully applied in modeling of printed circuit board (PCB) [54, 56, 57], which offers a valuable reference for modeling of EMI. This method is faster and more effective than previous methods and allows modeling with limited training data. Study results show that the ANN model is faster and uses less memory than traditional EMC simulations. Other methods exist to predict S-parameters in ECUs with microstrip lines, using the distance between wires and dielectric thickness as inputs. This has confirmed that the ANN algorithm can be used to optimize the design of meander lines [54, 56, 57]. In addition, ANNs are also used to predict time waveforms in circuit operation and to predict the response of devices and circuits. For example, one method uses design variables in circuit diagrams to predict the nonlinear behavior of circuits and perform dynamic modeling in a continuous time domain. This is done by using ANN models, which are independent of circuit details and have been shown to be capable of building models from input and output data [40]. For example, the use of physics-based FET models is computationally time consuming, but the use of ANNs has been shown to overcome this and allow for efficient optimization [58].

Thus, through these studies, we can confirm that the ANN model has shown its effectiveness in a wide variety of problem domains in electrical and electronic engineering. In particular, it is capable of rapid computation, reduced memory usage, and highly accurate prediction from limited data. Even for problems that take a long time or do not require the accuracy of previous methods, the ANN model can provide rapid and highly accurate results. In particular, it has been shown to respond effectively to complex problems such as design optimization and nonlinear behavior prediction.

Therefore, in Chapter 5, we examine optimal design methods using ANNs to enable rapid calculations and highly accurate modeling from limited data. Only a single interval solution was determined by performing predictive calculations using the ANN, so we take a machine learning approach here to obtain multiple interval solutions, where filter characteristics are interpolated using limited data corresponding to each design parameter's minimum and maximum values. After training with the limited initial data, fine interpolation is applied to help identify multiple interval solutions. Proposed Design method by predicting filter characteristics using the ANN model [59, 60].These are the optimal designs related to the filters alone, and the ANN model is created as training data by measuring several combinations of filters. Using the ANN model, the optimal combination of design parameters is obtained. However, it only finds one optimal combination of design parameters, and it has not been examined whether it is possible to search for multiple local solutions. It is also necessary to design filters for the entire system. Therefore, we apply the ANN model to investigate whether it is possible to search for multiple interval solutions. In this case, we used as teacher data the frequency response of the filter, which was not used when we applied the PSD method to predict complex characteristics. Then, in order to obtain a wider range of interval solutions, ANN training data will be increased to improve the modeling accuracy.In addition, we will investigate the modeling accuracy in the case of training with magnitude values and in the case of training with Real part (Re) , Imaginary (Im) [61] in order to predict the spectra.

In this chapter, section 5.2 first describes the method and procedure for finding a range solution for the filter parameters using the ANN model. Section 5.3 describes the structure of the ANN model, including input/output data and the training model. Section 5.4 describes the validity of the prediction model using the ANN model, Section 5.5 confirms the validity of the obtained results, and Section 5.6 describes efforts to improve the prediction accuracy of the modeling accuracy when the training method is changed. Section 6 describes our efforts regarding how to improve the prediction accuracy of the modeling accuracy when changing the learning method. In particular, the superiority of training with Mag or Re and Im in predicting spectra or increase in initial data has not been examined. Therefore, we conducted a survey on training data when predicting spectra. Finally, the range of interval solutions obtained by applying the ANN model will be validated in order to examine the certainty of the obtained range solutions.

5.2 Proposed Design Method Procedure Using ANN Model

5.2.1 Proposed Design Method using ANN Model

In this section, we explain the mechanism of the range of filter parameters solution search combined with machine learning using the ANN model. Only a single interval solution was determined by performing predictive calculations using the set based design method in chapter 4, thus it was difficult to find an optimal filter parameter set in such a restricted interval solution. Therefore, in order to obtain a wider range solution with higher accuracy for multiple design parameters that satisfy multiple required performance, in addition to the set-based method, the method shown in Fig. 5.1 can be considered as a method to perform full finding and extract using combinations of parameters in the design range. For example, multi-objective optimal design has multiple input and output results, which are expressed as design parameters x_1, x_2... x_{q} and required performance y_1, y_2... y_{q}, respectively. In other words, it is necessary to find a combination of values of x_1, x_2... x_{q} that satisfies all the required performance y_1, y_2... y_{q}. The combination of design parameters that satisfies all performance requirements can be represented by the blue dots in Fig. 5.1. Then, by finding multiple interval solutions from the extracted combinations, a wider range solution can be found.

However, in circuit simulation, it is not practical to find finely search in the design range to the necessary all combinations for the design, because of the large amount of memory used and the huge amount of time required for many combinations that take a long time to analyze at one time. Therefore, we considered that multiple design parameters and multiple performance requirements can be accurately modeled using the ANN model to compute the full finding more quickly.

Previous papers have reported that higher accuracy can be obtained in a shorter time than with circuit simulation solvers [54, 56, 57]. There are also reports that modeling can be performed with limited training data, resulting in faster and more effective calculations

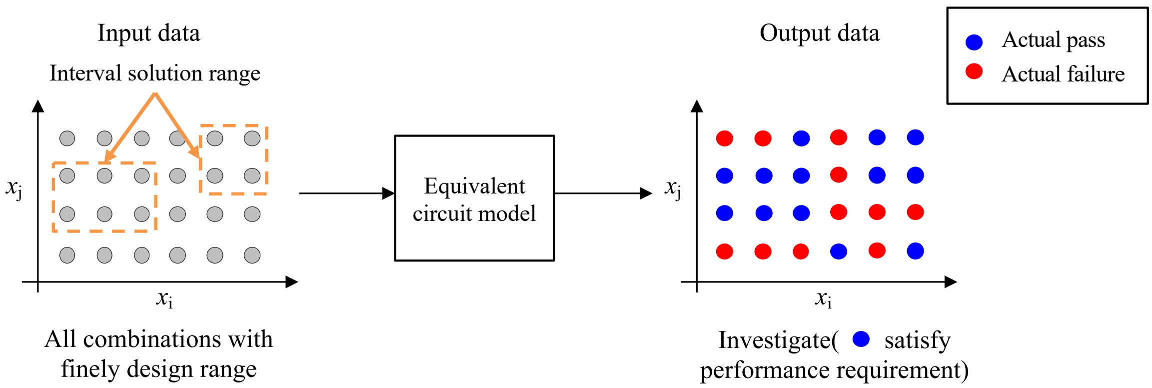

Figure 5.1 Full finding method by using the circuit simulation.

[59, 60]. Also, proposed design method by predicting filter characteristics using the ANN model [59, 60] have been reported. These are the optimal designs related to the filters alone, and the ANN model is created as training data by measuring several combinations of filters. Using the ANN model, the optimal combination of design parameters is obtained. However, it only finds one optimal combination of design parameters, and it has not been examined whether it is possible to search for multiple local solutions. Therefore, we thought that by replacing the calculation of the full search with ANN instead of circuit simulation to compute a huge amount of combination data in a short time with high accuracy, we could possibly find a range solution much faster than conventional methods. Therefore, with reference to previous papers [54, 56, 57, 59, 60], we will investigate an optimal design method using ANN that enables rapid calculation and highly accurate modeling from a limited amount of data.

5.2.2 Procedure for Interval Solutions Range Using ANN Model

We explain the mechanism of the range of filter parameters solution search combined with machine learning using the ANN model for the equivalent circuit model. Although it is possible to perform highly accurate modeling by using an ANN model, we do not want to spend a lot of time acquiring training data for the ANN model. Therefore, the training data for the ANN model should be calculated data obtained by using entire circuit simulation with the required performance as the design parameters. During the set-based design method in Chapter 4, the worst value in the frequency range of the required performance was used to approximate it to a quadratic function using the response phase method. The application of the ANN model will improve the modeling accuracy of the relationship between the required performance and the design parameters. Therefore, we used as teacher data the frequency response of the filter, which was not used when we applied the PSD method to predict complex characteristics. Furthermore, the total calculation time can be reduced by using only a limited amount of data from the initial range. The training data and the type of data have a large influence on the modeling accuracy. Therefore, considerations regarding the data to be trained are discussed in the latter half of Chapter 5. After training with the limited initial data, we take a machine learning approach here to obtain multiple performance requirements interpolated to each design parameter's minimum and maximum values. Then, using the combinations obtained by the ANN model that investigate to find for multiple interval solutions. Multiple interval solutions can then be combined to obtain the widest range of interval solutions. As a results, the optimal combination of design parameters for multiple design parameters that satisfy multiple required performance can be determined.

The procedure of Fig. 5.2 below shows the flow how the filter characteristics are estimated using the ANN model trained by an equivalent circuit model.

1. Obtain the filter characteristics corresponding to the design parameters located at the maximum and minimum boundaries of the design range and inside the design

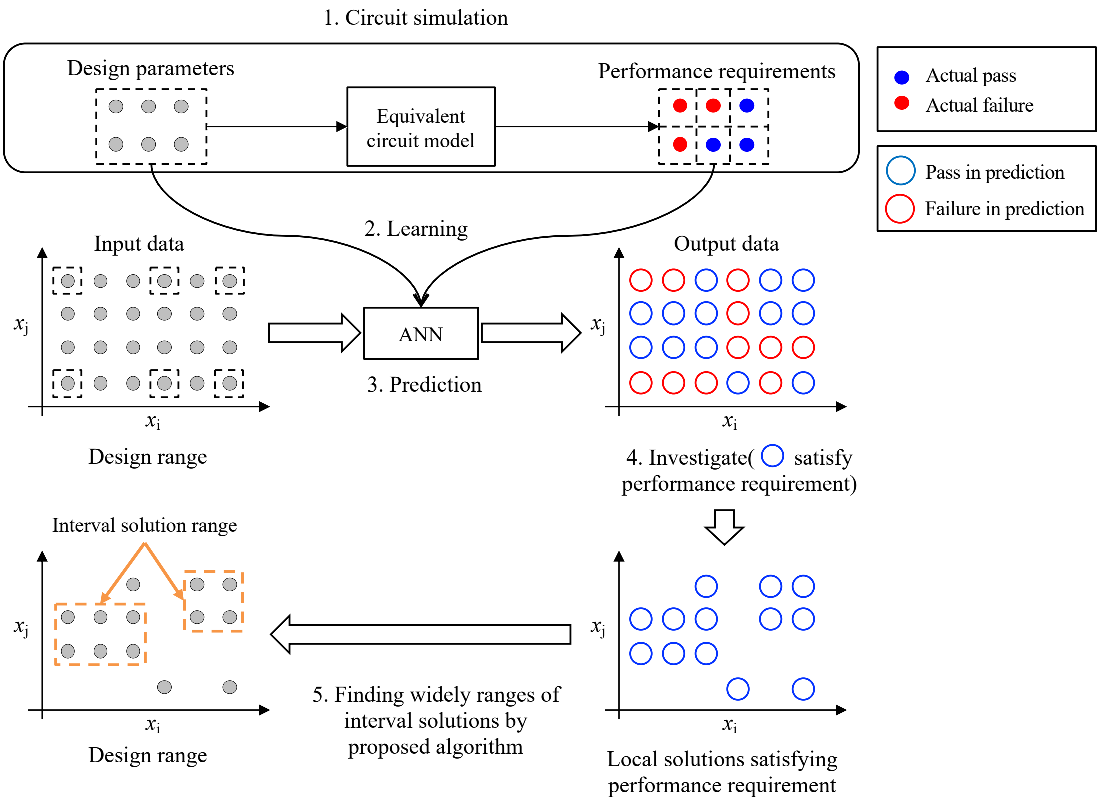

Figure 5.2 The procedure for the range of the interval solutions using the ANN model trained by equivalent circuit model.

range by circuit simulation using an equivalent circuit model.

2. Feed the obtained pairs of design parameters and filter characteristics as training data to the ANN for training.
3. The design parameters, which are finely divided within the design range, are given to the ANN model as input data, and the filter characteristics estimated by the ANN model are output.
4. The ANN model determines whether the required performance is satisfied or not.
5. For filter characteristics that satisfy the required performance, pairs of design parameters are obtained, and finally the ranges of interval solution can be found by using proposed algorithm.

5.2.3 Accurate Interval Solution Ranges Predicted in Multi-Objective Optimal Design

This section describe the evaluation of the accurate of the interval solutions range obtained by ANN model.

Table 5.1 Confusion matrix of actual and prediction

		Actual	
		Pass	Failure
Prediction	Pass	TP	FP
	Failure	FN	TN

To prepare it, as details of multi-objective optimal design method by ANN model, an overview of multi-objective optimal design using the meta-modeling and explains how to evaluate the interval solution range obtained by the prediction. For example, Fig. 5.3a shows two-dimensional representation of the combinations of values of two design parameters x_1 and x_2 obtained by the prediction results in the case of satisfying and not satisfying multiple performance requirements. In procedure 4 in Fig. 5.2, all combinations of design parameters can be represented as prediction results of a gridded set shown in Fig. 5.3a. The blue circles that are predicted to satisfy the required performance are shown as "Pass in prediction", while the red circles that do not satisfy the required performance are shown as " Failure in prediction". In procedure 5 in Fig. 5.2, the interval solution range for the design parameters values that satisfy the required performance is shown as the orange dashed rectangle. In this case, the interval solution for x_1 can be expressed as $R_1 = 2$ and that for x_2 as $R_2 = 4$. In this way, it can be shown that the redundant design can be realized by obtaining interval solution range that satisfy the multiple required performances.

Next, Fig. 5.3b shows an example of design parameters x_1 and x_2 obtained as the range of true interval solutions (which cannot actually be obtained). In the figure, the blue dots that satisfies the required performance is represented as " Actual pass", while the red dots that does not satisfy the required performance is represented as " Actual failure". The black dashed rectangle indicates the interval solution range of the design parameters that satisfies the required performance. In this case, the interval solution for x_1 can be expressed as $R_1 = 6$ and that for x_2 as $R_2 = 5$. In other words, this interval solution range indicates the true interval solution range we originally want to obtain. In reality, the range of interval solutions in Fig. 5.3b is wider than the range of interval solutions obtained by the prediction in Fig. 5.3a. This is because the error occurs in the prediction result compared to the actual result due to the influence of the approximation by modeling.

Fig. 5.3c is given by superimposing Fig. 5.3b on Fig. 5.3a . Four elements represented the relationship between actual and prediction results can be generally shown by confusion matrix in Table 5.2.3. The elements of TP, FP, FP and FN are also shown in Fig. 5.3c and it is found that the FNs reduce the range of interval solutions in prediction. In addition, based on the confusion matrix, when the number of each classification is N_{TP}, N_{TN}, N_{FP} and N_{FN} the accuracy itself can generally be expressed as the following equations in the equations (5.1)-(5.3).

- **TP (True Positive)**: The number of predicted results that are pass (Positive) and the actual result is pass.
- **FP (False Positive)**: The number of predicted results that are pass (Positive) and the actual result is failure.
- **FN (False Negative)**: The number of predicted results that are failure (Negative) and the actual result is pass.
- **TN (True Negative)**: The number of predicted results that are failure (Negative) and the actual result is failure.

$$\text{Accuracy} = \frac{N_{\text{TP}} + N_{\text{TN}}}{N_{\text{TP}} + N_{\text{TN}} + N_{\text{FP}} + N_{\text{FN}}} \tag{5.1}$$

$$\text{Precision} = \frac{N_{\text{TP}}}{N_{\text{TP}} + N_{\text{FP}}} \tag{5.2}$$

$$\text{Recall} = \frac{N_{\text{TP}}}{N_{\text{TP}} + N_{\text{FN}}} \tag{5.3}$$

However, these indicates are only accuracy indicates for individual combinations of design parameters values and are not sufficient evaluation for obtaining wider range of interval solutions. Therefore, it is necessary to investigate how the obtained interval solution range actually distributed with respect to the actual range solutions, as well as their sizes. To solve this problem, we propose a new algorithm to find interval solution ranges from the prediction results of design parameters that satisfy the required performance, and investigate the relationship between the size of the obtained interval solution range and the value of the confusion matrix given by TP, FN, FP, TN. As shown in Fig. 5.3a, there are many interval solutions. To obtain a wider range of interval solutions, if we simply use the product of the interval solutions for each parameter ($R_1 \times R_2$ in Fig. 5.3a) as a measure, the length range of interval solutions for the design parameters may be unequal, which is not suitable as a solution. Therefore, in this study, V shown in the following equation (5.4), is used as an index of equality in length so that the magnitudes of each parameter are not unequal. This should provide a well-balanced and large interval solution range for each design parameter.

$$V = \frac{\prod_{i=1}^{p} R_i}{\sum_{i=1}^{p} R_i} \tag{5.4}$$

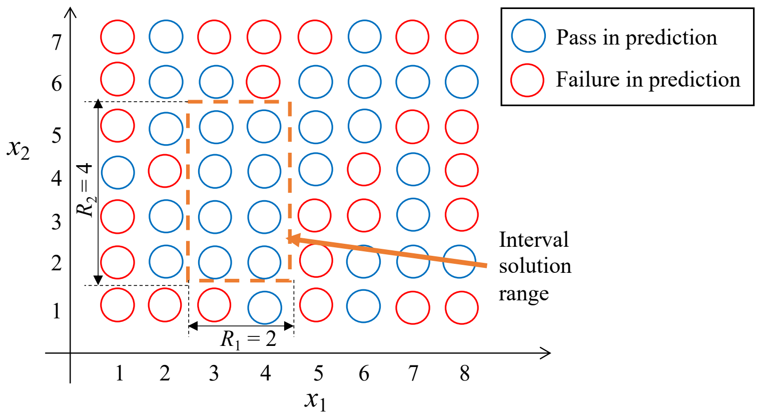

(a) Example of prediction results

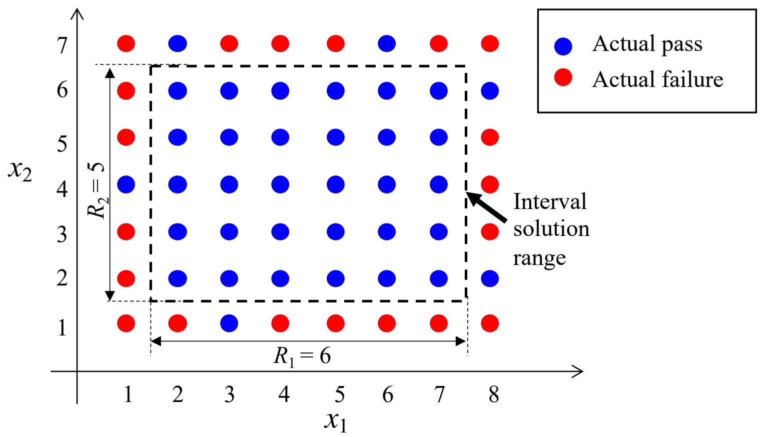

(b) Example of actual results

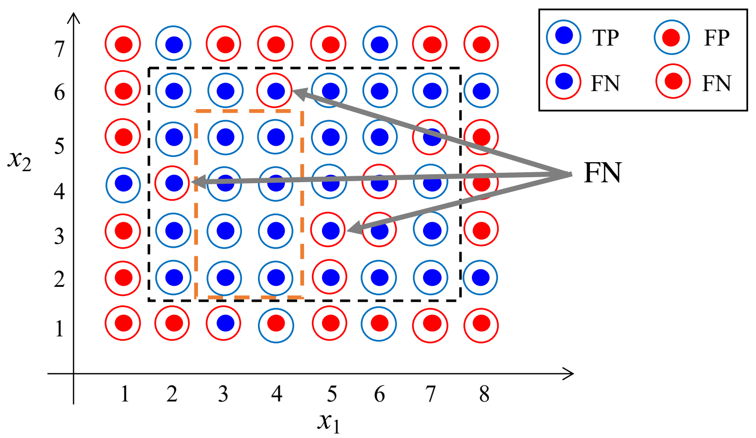

(c) Superimposing Fig. 5.3a on Fig. 5.3b

Figure 5.3 Example of the combinations of values of design parameters and range of interval solutions in pass or failure.

5.3 ANN Model

This section describes the learning method used in this paper for the ANN model, which is procedure 3 described in the previous section. To use an ANN model for training, it is necessary to determine the input and output parameters, the structure of the ANN and the training method. Their setting of the ANN model is important in order to obtain a wide range of designs that satisfy the required performance, because the modeling accuracy of the required performance and design parameters needs to be improved.

Firstly, the input and output parameters detail used in this thesis are described. For ANN training, a numerical matrix of input data and output data corresponding to the input data, called a dataset, is required. Therefore, as in Chapter 4, an equivalent circuit model was created using a circuit simulator DM and CM attenuation characteristics were analyzed, and data was collected. The input data are the design parameters and the output data are the filter characteristics. In particular, the input parameters of ANN are C_x, C_y, L and Λ. When training the ANN model with the design parameters and filter characteristics as the teacher data, all design parameters are set to several levels.These input parameters and the corresponding output parameters from the circuit simulation were used as the training data. Therefore, the training data for ANN consist of the same DM and CM voltage attenuations (3479 frequencies between 100 kHz and 30 MHz) and combinations C_x, C_y, L and Λ.

Next, explain the structure of the ANN, training method and the number of neurons in the ANN model. Fig. 5.4 shows the structure of the ANN used in this study. The training was based on the structure of a 3-layer MLP. We decided to use the paper[59, 60] as a reference. The first layer consists of input neurons, which send data to the second layer, and then output neurons to the third layer. There are four neurons for the first layer, because of the input data of design parameters of C_x, C_y, L and Λ. And the 3,479 for the first hidden and output layers, and 1,740 for the second hidden layer.

The 3479 output layers were matched to the number of points in the frequency spectrums. The output parameter is the frequency response of the filter, and the number of neurons in the output of the ANN, 3479, corresponds to the number of equally spaced frequency points on the logarithmic axis in shown Fig. 5.5. The same number for the

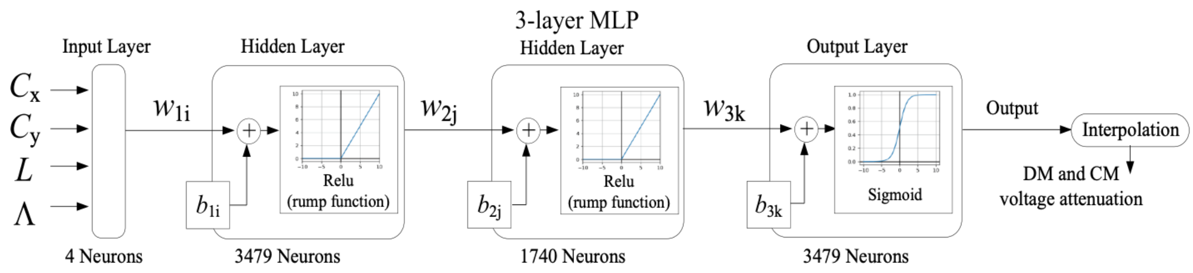

Figure 5.4 ANN structure used in this thesis.

Table 5.2 Artificial neural network training parameters

Parameter	Value/Description
Number of epochs	100
Optimization method	A mini-batch stochastic gradient descent method
Batch size	10
Loss function	Mean squared errors
Input data	Normalized waveform
Learning rate	0.001

Table 5.3 Caluculation environment details for ANN training

Parameter	Value/Description
Calculation Software	Anaconda
CPU	Intel(R) Core(TM) i5-10400
GPU	Nothing
RAM	16GB

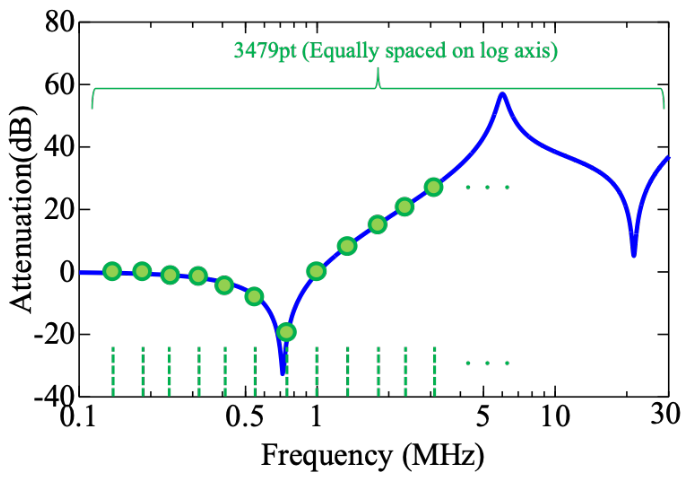

Figure 5.5 Ideal switching signal and actual switching signal.

second hidden layer was calculated as half, referring to a previous paper[59, 60]. Then, the activation functions of the hidden layer and the output layer are sigmoidal and linear functions for each layer, respectively. Used sigmoidal functions, which are suited for error back propagation, and Relu functions, which are computationally efficient. A mini-batch stochastic gradient descent (SGD) method updates the weight w and bias b at each epoch in Fig. 5.4. The size of the mini-batch is 10. The mini-batch SGD method selects a small subset of data (referred to as a "mini-batch") at random and uses this subset to compute the gradient and update the parameters. This method strikes a balance between the characteristics of pure SGD and traditional gradient descent. Because the size of the mini-batch offers a compromise between computational speed and gradient stability, mini-batch SGD is frequently employed in real-world deep learning training. One of its main advantages is its memory efficiency since it doesn't necessitate loading the entire dataset at once. Consequently, this study utilized the mini-batch SGD method for ANN training.

Finaly, the structure of the ANN described above and the parameters used in the training method are shown in Table 5.2. Table 5.3 also shows the PC settings used in the calculations using the ANN model.

5.4 Application and Validation of ANN Model

In this Chapter, interval solutions are found using combinations extracted results satisfying requirements and compares them with the range solutions obtained in Chapter 4. Apply the design procedure using the ANN model to extract the interval solution. Furthermore, the accuracy of the ANN model created in this Chapter 5.3 will be verified.

5.4.1 Application of the ANN Model for brush motor drive system

First, the same dataset used in Chapter 4 was used to construct the characteristic prediction ANN in this section. The input data for training to the ANN model were the filters C_x, C_y and L and the cable lengths Λ that affect the EMI noise. Next, the output data were the attenuation characteristics of the filters and the spectrum of the attenuation characteristics. In other words, the spectrum of the attenuation characteristics of DM and CM noise with C_x, C_y, L and Λ as design parameters is used as the teacher data for training the ANN. The spectra of the attenuation characteristics are obtained from a circuit simulator (AWR Microwave Office) that uses the equivalent circuit calculated in Chapter 4. In this section, in order to reduce the total calculation time, using only a limited amount of data from the initial range. Therefore, Table4.1 in Chapter 4 shows the level 1 (minimum), level 2 (middle), and level 3 (maximum) design parameters for the three levels of C_x, C_y, L and Λ used in the training data. In other words, 81 (=3^4) pairs of input-output data is used as teacher data and similar to Table 4.1 in Chapter 4. The 81 (=3^4) input data and the 81 combinations $\times$ 3179 points output data are used as training data to predict DM attenuation and CM attenuation.

All filter characteristics in the finely design range are predicted by using the ANN model. We calculated the DM and CM attenuations using the trained ANN for 1.44 million combinations. To predict the filter characteristics using the trained ANN model, C_x, and C_y are divided into 40 and L, and Λ is divided into 30 between level 1 and level 3 for each design parameter, as shown in Table 5.4. This means that the design range for each parameter is divided with high resolution. Fig. 5.6, Fig. 5.7 shows the results of the prediction graph, in which the prediction results of 1.44 million filter characteristics are overlaid. Then investigated whether they satisfy the performance requirements (5 dB between 0.1 MHz and 1 MHz, 10 dB between 10 MHz and 30 MHz) in similar

Table 5.4 Setting up a combination with a finely detailed design range

	C_x(nF)	C_y(nF)	L(μH)	Λ (m)
Min	0.5	0.5	0.1	1.7
Max	20	20	3	2.3
Division	0.5	0.5	0.1	0.02
Division Number	40	40	30	30

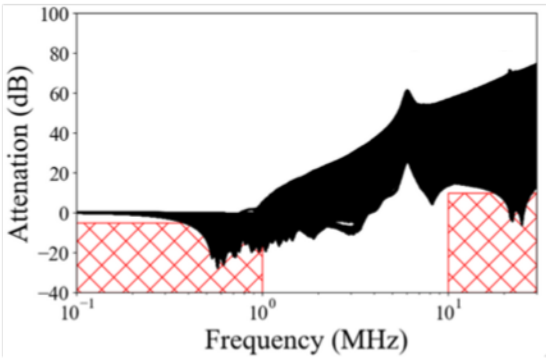

Figure 5.6 1.44 million filter characteristics overlaid DM prediction results.

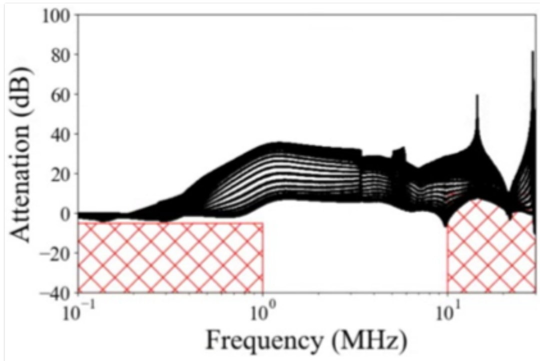

Figure 5.7 1.44 million filter characteristics overlaid CM prediction results.

Table 5.5 Example of multiple interval solutions range obtained using 3 levels of initial data.

	C_x **(nF)**	C_y **(nF)**	L **(**μ**H)**	Λ **(m)**
Resultant set 1	0.5-1.5	2.5-4	1.5-1.8	2.24-2.3
Resultant set 2	0.5-1.5	1.5-2.5	1.3-1.5	1.7-2
Resultant set 3	2.5-3.5	1.5-2.5	2-2.5	1.7-2

Chapter 4. In this case, Fig. 5.8, Fig. 5.9 shows the results of about 10,000 could be extracted predictions of filter characteristics that met the required performance. Finaly, by extracting each multiple combinations of design parameters from these about 10,000 results, multiple interval solutions are obtained.

Finaly, the optimal design method using the ANN model proposed in this study will be used to investigate the obtaining of multiple interval solutions that satisfy the performance requirements. Table 5.5 summarizes the three interval solutions we found, including the same solution as Chapter 4 (resultant set 1), which suggests the current approach expands the range of solutions and enhances the feasibility of design. Furthermore, compared to the set-based design method, the ANN model has improved the accuracy of modeling the relationship between design parameters and performance requirements. In addition, it was confirmed that several interval solutions were obtained that were wide enough to allow the selection of E12 and E24 series elements. Therefore, it can be said that the design method in this study broadens the range of solutions and improves the practicality of the design. Multiple range of interval solutions satisfying the required performance were found, and the ANN model was used to find multiple interval solutions, which was our initial goal. As a result, we confirmed the validity of this method was confirmed since multiple interval solutions were obtained by using the ANN model.

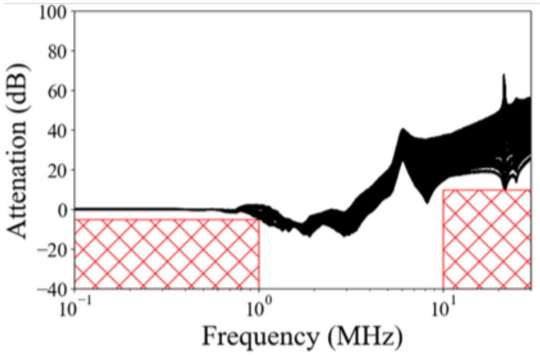

Figure 5.8 Extracted results satisfying requirements from 1.44 million DM prediction.

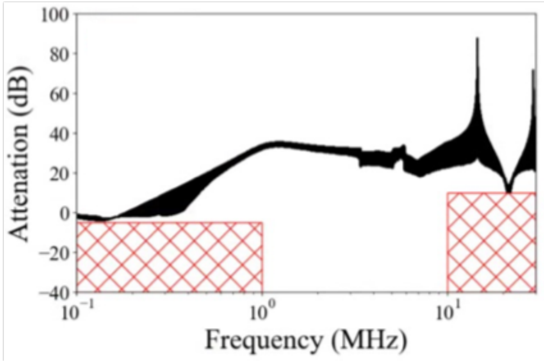

Figure 5.9 Extracted results satisfying requirements from 1.44 million CM prediction.

5.4.2 Validation of the ANN Model Accuracy

In this section, the applied ANN model will be validated using mixed matrices such as TP and FP as well as the precision, recall rate and the voltage of range V that are used. In order to examine more accurate ANN model, we compare the prediction results using ANN models with the actual circuit simulation results. To explain issues related to the ANN model training method and input/output data, and to describe efforts to improve the accuracy of the prediction more.

Table 5.12 obtained by calculating the elements of Table 5.6 shows the accuracy of the ANN. Accuracy and Precision are high at 98.1 % and 97.6 %, respectively, but Recall is low at 27.8 %. This indicates that after dividing the initial data into 3 levels, 97.6 % of the combinations predicted to satisfy the demand and those predicted not to satisfy the demand actually satisfied the requirements. However, this is sufficiently larger than the number that did not satisfy the requirement originally. Most of the predicted results are judged not to satisfy the requirement. Therefore, the percentage of the correct results will increase accordingly. The reason for this is that the total number of TN and FP as the number of requirements not satisfied in this system is large, and the percentage of correct answers is correspondingly high.

Next, as indicated by the precision, 97.6 % of the combinations predicted to meet the requirements actually met the requirements. This indicates that almost all of the predictions were accurate for the total number of combinations that actually met the requirements. This high precision of fit allowed the design to avoid rework and meet the requirements to the extent that they were met, resulting in the desired results. On the other hand, the recall rate was only 27.8 %, and only about 30 % of all correct solutions were obtained as a range solution. This suggests the need to increase accuracy in the design process through the exploration of a wider range of solutions. It is expected that more correct solutions will improve the accuracy and efficiency of the design process by considering a larger number of correct solutions as range solutions. From the relationship

Table 5.6 Confusion matrix with 3 levels of initial data

		Actual	
		Pass	Failure
Prediction	Pass	TP = 10756	FP = 265
	Failure	FN = 27931	TN = 1449048

Table 5.7 Accuracy parameters of ANN obtained by calculating confusion matrix with 3 levels of initial data

	Initial data 3-level
Accuracy	98.1 %
Precision	97.6 %
Recall	27.8 %

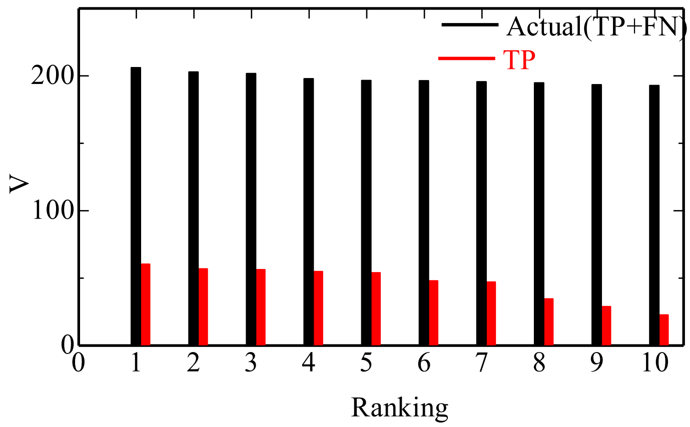

Figure 5.10 Ranking of the range of interval solutions with large values of V.

between the precision and recall based on the confusion matrix and the size of the range, it is found that low recall does not result in wide range solution. This suggests that the prediction accuracy of the ANN model will be increased by reducing False Negative (FN) and increasing True Positive (TP). In addition, the Fig. 5.10 shows the top 10 cases with the largest V between the actual range solution and the resulting predicted range of interval solutions. A value of V in TP that is considerably smaller than the value of V in Actual. From the above, it is clear that the range of interval solutions cannot be found due to the lack of sufficient TP.

We achieved to find the range of interval solutions and calculate the range size; we know low recall does not result in wide range solution. This suggests that the prediction accuracy of the ANN model will be increased by reducing FN and increasing TP. In next section, we aim to improve the accuracy of the modeling so that the FN parameter combinations will be converted to TP.

5.5 Improvement of ANN Model Accuracy by Increasing Training Data

In this section, we aim to improve the accuracy of the modeling so that the FN parameter combinations will be converted to TP. we first consider increasing the number of input/output data to improve the modeling accuracy.

5.5.1 Verification of ANN Model Improvement Effectiveness

It is expected that the spectrum can be trained more accurately by increasing the number of combinations by dividing the initial data more finely between the maximum and minimum values. For the training data, combinations of the design parameters C_{x}, C_{y}, L and Λ with 3 and 5 levels, respectively, are prepared. In the case of 3-level data, the table described in the previous section is used. In the case of 5-level data, the values are equally spaced between the minimum value of level1 and the maximum value of level5. C_{x}, C_{y}, L and Λ for the case where the initial data is divided into 5 segments are shown in Table 5.8. In other words, in the case of the initial 5-division case, 625(=5^4) pairs of input/output data are used as training data.

5.5.2 Evaluation the accuracy parameters of the ANN model

In this section, we evaluate the effectiveness of the ANN model in improving the design methodology. In addition, we verify that the filter characteristics in the range solution estimated by the ANN model met the performance requirements.

Table 5.9 obtained by calculating the elements of Table 5.10 shows the accuracy of the ANN. Accuracy and Precision are high at 98.8 % and 79.0 %, respectively, Recall also is high at 71.5 %. This indicates that the initial data divided into 5 levels, 79.0 % of the combinations predicted to meet the requirement actually met the requirement. 71.5 % of the combinations that actually met the requirement were combinations that were predicted to meet the requirement. Thus, the evaluation was conducted by changing the number of initial data in 3 and 5 levels, and the results showed that the precision of fit was high in the case of 3 levels. In the case of 5 levels, the recall rate was found to be higher. This may be due to the fact that the number of combinations satisfying

Table 5.8 5 levels of initial data for applying ANN to brush motor drive system

	C_{x} (nF)	C_{y} (nF)	L (μH)	Λ (m)
level 1	0.5	0.5	0.1	1.7
level 2	5	5	1	1.84
level 3	10	10	1.8	1.98
level 4	15	15	2.4	2.12
level 5	20	20	3	2.3

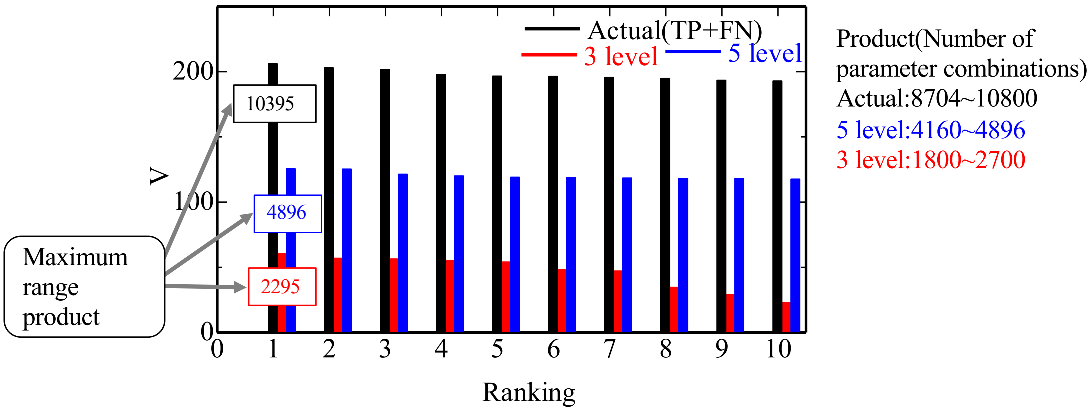

Figure 5.11 The size V of interval solution range obtained by using new developed algorithm.

Table 5.9 Confusion matrix with 5 levels of initial data

		Actual	
		Pass	Failure
Prediction	Pass	TP=27679	FP=7368
	Failure	FN=11008	TN=1441945

Table 5.10 Accuracy parameters of ANN obtained by calculating confusion matrix with 3 levels of initial data

	Initial data 3-level	**Initial data 5-level**
Accuracy	98.1 %	98.8 %
Precision	97.6 %	79.0 %
Recall	27.8 %	71.5 %

the requirements increased in the case of 5 levels, while the number of combinations not satisfying the requirements also increased. This suggests that the ANN models were able to finely estimate the boundaries that did not satisfy the requirements, resulting in an increase in TP and at the same time an increase in FP. Therefore, since it is difficult to evaluate this confusion matrix alone to obtain a wide interval solution, which is the objective of this thesis, we use the value obtained as the size V of the interval solution for the evaluation.

The results of calculating the size of interval solution V using new developed algorithm are shown in Fig. 5.11. It computes the interval solution size V from the 3-level and 5-level TP parameter combinations and sorts them in descending order. Firstly, these are this top 10 cases with the largest V between the actual range solution and the resulting predicted range of interval solutions. A size of V in TP from the 3-level that is considerably smaller than the size of V in Actual. Thus, it was clear that the range of interval solutions cannot be found due to the lack of sufficient TP in the case of the 3-level because FN are many combinations in the case of 3-level. In the other hand, the interval solution range was expanded by reducing FN in the case of 5-level. This means that although the precision is reduced by using 5-levels, the interval solution range obtained by using 5-levels is expanded for the actual interval solution range. Therefore, the validity of using 5-level input data is obtained.

5.6 Improvement of ANN Model Accuracy by Using Re and Im

In this section, we will study improving modeling accuracy how to another method in order to obtain more accurate and wider interval solutions that satisfy the required performance obtained using ANN. In previous studies, magnitude values of attenuation were used for training data. However, since the data changes rapidly around the frequency where resonance occurs, prediction accuracy is expected to be reduced. Therefore, in this section, we attempt to improve the prediction accuracy by training ANN using values that are divided into both real and imaginary parts instead of magnitude values.

5.6.1 Accuracy Improvement Method using Re and Im by Comparison of Prediction and Actual Results by ANN

In order to examine more accurate ANN model, the prediction results using ANN models are compared with the actual circuit simulation results. To explain issues related to the ANN model training method and input/output data, and to describe efforts to improve the accuracy of the prediction more.

Firslty, a comparison of the DM attenuation spectrum obtained using the ANN model in the previous section with the spectrum obtained by circuit simulation is shown 5.12. The results clearly show that the prediction accuracy is insufficient for the sharp change in the spectrum around 2 MHz. This is expected to reduce prediction accuracy because data changes rapidly around the resonant frequencies. This is because at resonant frequencies, the values with respect to frequency change significantly, and it is difficult to express them well as a function of design parameters. Therefore, we thought that the recall rate could be improved if the spectrum around this resonance frequency could be predicted

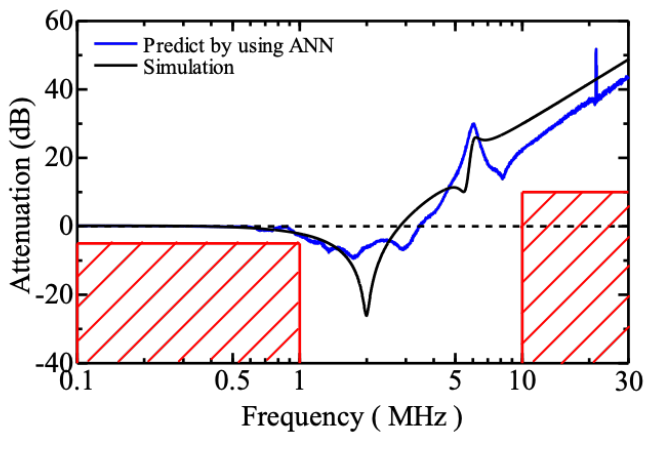

Figure 5.12 Prediction and simulation of DM attenuation in $C_x = 0.5$ nF, $C_y = 4$ nF, $L = 1.3$ μH, $\Lambda = 2.24$ m.

Table 5.11 Confusion matrix with Re, Im of initial data

		Actual	
		Pass	Failure
Prediction	Pass	TP=1810	FP=2286
	Failure	FN=36877	TN=1447027

with higher accuracy. We will reconsider the training data as a method to improve the accuracy of the spectrum at the resonance frequency.

Therefore, it is necessary to accurately predict the dip and peak values around resonant frequencies with large changes in order to more accurately predict the spectrum of attenuation. It has been reported in previous references [61] that by predicting the elements Re and Im, the prediction accuracy is greatly increased as a function of design parameters because the spectrum becomes smooth at the resonance frequency. Smoothly varying data are generally continuous and easy to represent with low dimensional functions with high relevance between data. This makes it easier for the ANN to learn their relationships and more accurate in predicting unknown spectra. Therefore, we will apply these methods with respect to the data in this thesis, and instead of using magnitude for the data used in training, we will predict it by dividing it into its elements, Re and Im. The new proposed training method adding procedure 2.Learning and 3.Prediction in Fig. 5.2 is the following procedure.

1. The spectra of Re and Im, which are the elements before the attenuation Mag, are trained as ANN models, respectively.
2. Using the training data, the Re and Im spectra are calculated for each of about 1.4 million combinations.
3. The Re and Im spectra are used to calculate attenuation and investigate combinations that satisfy the required performance.
4. To evaluate the improvement in modeling accuracy, the model performance is calculated using the confusion matrix and evaluation parameters.

5.6.2 Verification of ANN Model Improvement Effectiveness with Re, Im

The effectiveness of the ANN model in improving the design method was confirmed by using the ANN model obtained from training data using Real, Imaginary. The confusion matrix obtained with Re and Im is shown in the table. In addition, the table shows the results of precision and recall rates calculated using these methods. As a result, the number of TPs was approximately doubled, which reduced the precision and recall rate.

As shown above, the prediction accuracy of the ANN model was reduced when Re and Im were used for training. To examine the reason for this, we will investigate the

Table 5.12 Comparison with the confusion matrix with Re and Im of initial data

	Initial data 3-level	Initial data Re,Im
Accuracy	98.1%	97.4%
Precision	97.6%	44.2%
Recall	27.8%	4.7%

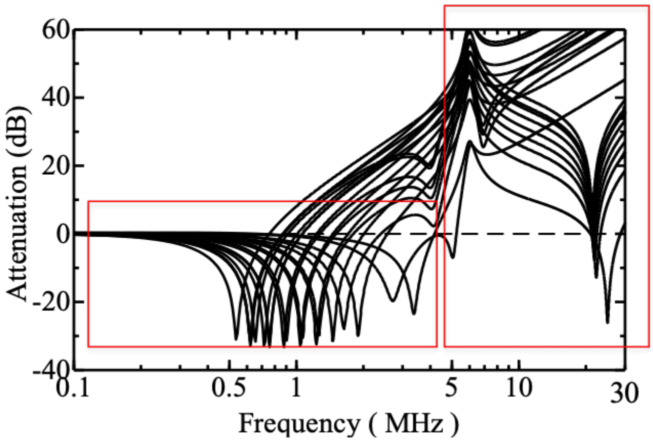

Figure 5.13 Prodected magnitude spectra of DM attenuation selected of 81 combinations.

training data of Re, Im and Mag for the 81 combinations used in the ANN training. The attenuation spectrum used in this training is a combination of Dip and Peak.

First, the magnitude spectra of DM attenuation for 20 randomly selected combinations out of 81 combinations are shown in the Fig. 5.13. Fig. 5.13 shows that the area that changes with each of the 81 combinations generally changes in the area indicated by the red frame. In the red frame, the frequency region from 0.1 MHz to 5 MHz has a value of about 30, while the frequency region from 5 MHz to 30 MHz has a value of about 100.

Next, the Re spectra of the DM attenuation for 20 randomly selected combinations of 81 variables are shown in the Fig. 5.14. Fig. 5.14 shows that the areas that change according to the 81 combinations are indicated by the red and blue frames. The expanded spectrum for the red box is also shown in the Fig. 5.15. This shows that the area in the red box varies with a value of about 2, and the area in the blue box varies with a value of about 6,000. This indicates that the difference in the amount of change on the frequency axis between the red and blue frames is significantly different. This means that in the attenuation spectrum used in training, it is necessary to simultaneously and accurately predict a small change of one digit in the spectrum from 0.1 MHz to 1 MHz and a large change of four digits in the spectrum from 1 MHz to 30 MHz. This has regions of smaller change and regions of greater change when training the Re spectrum of attenuation compared to training the magnitude spectrum of attenuation. However, it is expected that the prediction of large changes will affect the accuracy of the prediction of small changes, resulting in a lower overall accuracy.

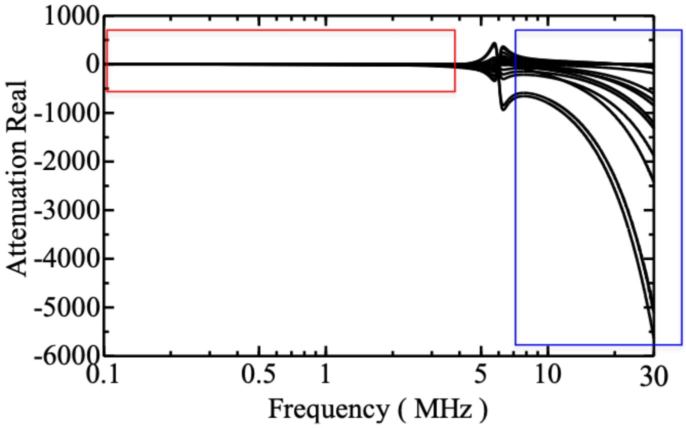

Figure 5.14 Prodected Re spectra of DM attenuation selected of 81 combinations.

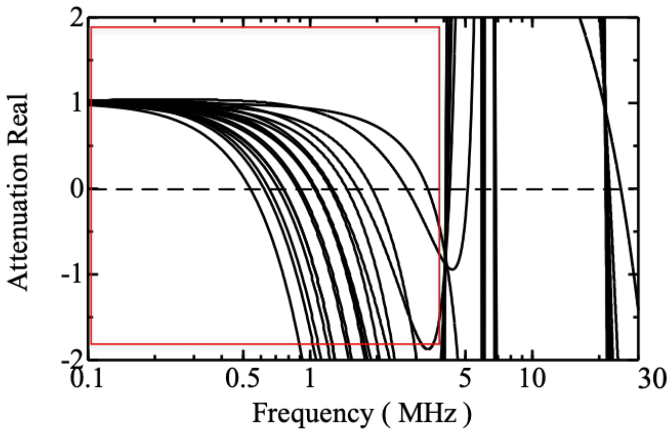

Figure 5.15 Expanding prodected Re spectra of DM attenuation selected of 81 combinations.

In conclusion, in the case of predicting the attenuation spectrum used in this study, training with magnitude is considered to have improved accuracy because the region of change can be narrowed. On the other hand, training using Re and Im, which are the original elements, was shown to be inappropriate. As a result, it was shown that the application of the original elements, Re and Im, was not effective in predicting the attenuation spectrum used in this thesis, and that training in magnitude was more effective in terms of accuracy.

5.7 Conclusion

We explain the mechanism of the range of filter parameters solution search combined with machine learning using the ANN model. Only a single interval solution was determined by performing predictive calculations using the set-based design method, thus it was difficult to find an optimal filter parameter set in such a restricted interval solution. Therefore, by replacing the calculation of the full search with ANN instead of circuit simulation to compute a huge amount of combination data in a short time with high accuracy, we could possibly find a range solution much faster than conventional methods. Therefore, with reference to previous papers [54, 56, 57, 59, 60], we will investigated an optimal design method using ANN that enables rapid calculation and highly accurate modeling from a limited amount of data.

The design parameters and required performance obtained using circuit simulation were trained into an ANN model at three different levels. Utilizing this trained ANN model, the attenuation frequency characteristics of DM and CM for maximum and minimum combinations of design parameters were calculated and verified to satisfy the required performance. For each design parameter, 40 combinations of C_{rmx} and C_{rmy} and 30 combinations of L and Λ were used in the process, for a total of 1,440,000 combinations. We were able to find at least three interval solutions that satisfy the performance requirements, including a single interval solution obtained by our previous approach using preference set-based design. This increased the likelihood that the application of the ANN would find multiple interval solutions and find the optimal solution.

In addition, the need for more accurate prediction of dip and peak values at resonant frequencies was mentioned, and studies were conducted to improve the accuracy of the ANN model accordingly. In previous studies, it has been shown that predicting the Re and Im values improves the prediction accuracy by smoothing the spectrum at the resonant frequencies. However, when applied in this study, it was difficult to predict the values of Re and Im at the same time, because the predicted Re and Im values caused small changes in the spectrum from 0.1 MHz to 1 MHz and large changes in the spectrum from 1 MHz to 30 MHz. Therefore, it became clear that training in magnitude was more appropriate than using the original elements Re and Im. Accordingly, a method was adopted to improve the prediction accuracy of the spectra at the resonant frequencies by increasing the number of training data using magnitude values. Specifically, by increasing the number of input data from 81 ways with 3 levels to 625 ways with 5 levels, we were able to increase the prediction accuracy at the resonant frequencies. This improved prediction accuracy because the peak and dip values at resonant frequencies were found to effectively represent the magnitude spectrum, and the recall rate increased because the frequency region of the correct solution was expanded. However, the precision of fit decreased. This confirmed that the region bordering between failure and pass was more finely predictable, but the results of failures were also judged as pass. Since failure is not acceptable in reliability tests, we confirmed that the three-partitioning method is more practical for the situation in this study. Finally, Table 5.16 compares the training method, training time, and overall time with respect to the optimal design method using the ANN model implemented in this thesis. We were able to establish an optimal design method that is faster, more accurate, and can obtain a wider interval solution by using a set-based design method and an ANN. We confirmed that the interval solution range can be expanded by using the ANN model, and that it is possible to design and select elements that satisfy the range solution.

Figure 5.16 Comparison of optimal design methods used in this thesis.

Full finding	**method**	**PSD method in Chapter 4**	**ANN method in Chapter 5.4**	**ANN method in Chapter 5.5**	**ANN method in Chapter 5.6**
Initial data calculation using Circuit simulation	Calculate 1.44 million combinations By ANN	3 levels(81 combinations)	3 levels(Mag)(81 combinations)	5 levels(Mag)(625 combinations)	3 levels(Re,Im)(81 combinations)
calculation time	144 h	30 sec	30 sec	5 min	60 sec
Meta-modeling or ANN model	-	second-order function, response surface method	ANN model	ANN model	ANN model
Learning time	-	3 min	1 min	3 min	2 min
Interpolation	-	-	Calculate 1.44 million combinations by ANN	Calculate 1.44 million combinations by ANN	Calculate 1.44 million combinations by ANN
Calculation time	-	-	2 h 30 min	2 h 30 min	5 h
All Calculation time including initial data	144 h	20 min	2 h 32 min	2 h 40 min	5 h
Number of interval solutions obtained	Multiple	one	Multiple	Multiple	Multiple
V	193	20	54	160	–

Chapter 6

Solution Design Method for LC Resonance Suppression Using RL Snubber Circuit

6.1 Introduction

Chapters 4 and 5 describe the optimal design method of EMI filters inside brush motors to suppress brush noise in a brush motor drive system. It was shown that EMI filters can be optimally designed to suppress brush noise. In this chapter, we discuss the mitigating solutions for cases in which EMC standards are failed due to increased EMI in the prototype stage. During the ECU design stage or prototyping, EMI may increase due to the electrical connection of the ordered components, which may not satisfy the standard. For example, in the case of products using brush motors, additional product specifications are often added to control the rotation speed and allow the mechanical parts to move freely in conjunction with the motors in ECU design stage. When such a product specification is added, the ECU may be required to control the drive of the brush motor using PWM control. In this system, not only brush noise generated at the brush motor but also switching noise generated at PWM-controlled power semiconductors mounted in the ECU cause EMI such as Fig. 6.1. Brush noise can be suppressed by an EMI filter optimally designed during the brush motor design phase and installed inside the brush motor in Chapter 3 [17, 18]. However, installing an EMI filter inside the brush motor may increase the switching noise in the carrier frequency band, such as the medium wave (MW) band. The reason is that EMI increases due to the LC resonance of X-capacitors inside the motor and the parasitic equivalent series inductance (ESL) of the cable. This means that LC resonance occurs due to factors external to the ECU. As in this example, the resonance that occurs after each ordered component is electrically connected is often not taken into account in the specifications of each component. Therefore, if resonance occurs in the entire system, including the ECU that drives the brush motor, the component manufacturer who sells the system as one system is required to suppress the resonance.

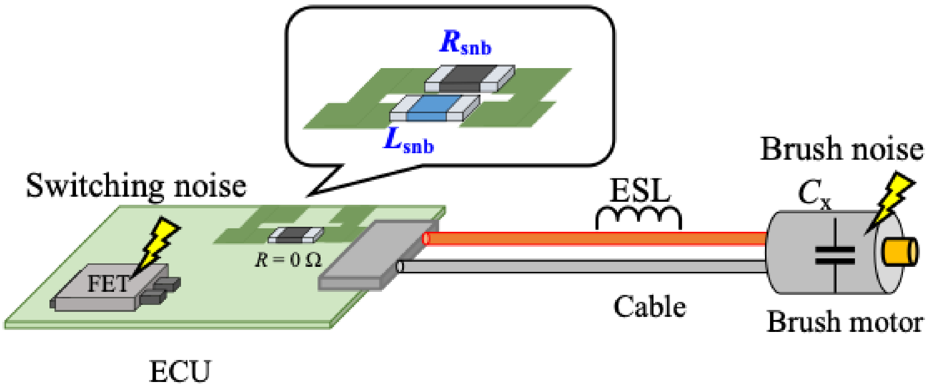

Figure 6.1 Resonance mitigating solutions.

In this case, since the specifications of the EMI filter built into the motor are fixed, resonance suppression by design limited to the drive ECU is required. Therefore, this chapter focuses on LC resonance noise caused by switching noise in brush motor drive systems.

In order to suppress the LC resonance, the solution methods of RC snubber [26] [27] and RL snubber [28–36] circuits are generally used. The RC snubber is a method in which the switching current is bypassed in low impedance by a capacitor and losses are provided by a resistor existing in series. On the other hand, RL snubber is a method in which the switching current is choked by an inductance in a high impedance state and losses are provided by the resistors in parallel. Comparing the resonance suppression effect, the RL snubber is said to be relatively more effective in suppressing resonance because the bypass effect of the RC snubber is reduced by the ESL of the snubber capacitance [30]. Also, the RC snubber circuit must be inserted in parallel with the capacitor generated by the resonance. This is an important design constraint, and if the capacitors that cause LC resonance are mounted in locations that cannot be redesigned, RC snubber circuits cannot be applied. Therefore, for example, the capacitor that is the element of the LC resonance in this project is inside the motor and cannot be changed from the ECU design stage. An RL snubber comprises a pair of resistor R and inductor L, and it can be installed in series with the resonant loop in the ECU to suppress resonance such as a Fig. 6.1. Therefore, the RL snubber can be mounted in the ECU, which is practical because It requires only a single step back to the ECU design stage and is practical.

Previous optimal design methods for RL snubber are described. Two types of methods are generally used to damp LC resonance [26]. First method is that a simple and common way to select optimum parameters from many SPICE simulation results while changing the snubber parameters has been used in previous work [26, 30, 32, 33, 37, 38]. However, considerable trial and error may be required, and determining optimum parameters may be difficult. Second method is that for the RL snubber, second one is a root locus analysis method using a simplified circuit of while resonant circuit [32, 33]. The previous works have shown that a snubber inductance three times greater than the ESL of the entire resonant loop is appropriate. And the optimal resistance is calculated analytically based on the root locus method using a simplified circuit of while resonant circuit. Next, using a simplified resonant circuit, the optimal resistance value is calculated by analytically adjusting the snubber inductance appropriately by simulation-based fitting, based on the Root-Locus method. However, the parameter optimization of this method is also insufficient because the inductance is determined on a rule-of-thumb basis and its inductance is not always optimum for all resonant circuits.

Therefore, our previous work was proposed an optimal design method for RL snubber circuits focusing on LC resonance in synchronous buck converters leading to an increase in EMI. In previous work, a design method was described that optimizes snubber parameters for any damping effect design target using the Q factor. In order to apply RL snubber, the LC resonant loop is simplified and the loop of LC resonance must be extracted to be an equivalent circuit characterized by a third-order characteristic equation. The Q factor is a parameter that expresses the degree of attenuation of the resonance and is often used as a design objective in EMC design. It was analytically derived as a function of the snubber parameters using a simplified equivalent circuit of the resonant loop in the target circuit. Then, contour plots of the Q factor were used for uniquely can determining the optimum parameters.

However, regarding these optimal design method, the procedures for practical design of this method and its evaluation by actual measurement have not been evaluated [32–35]. Establishing a practical optimal design procedure can help make the process of problem solving more efficient and faster. Clear and systematic procedures can help minimize project delays and cost increases. In validating optimal design methods, simulations are based on theoretical models, which must be compared with actual data in practical applications. Therefore, evaluation by actual measurement increases the reliability of the optimal design method because it is based on actual conditions and situations. For example, in the practical application of the optimal design method, it is essential to design based on the thermal constraint for the elements to guarantee the product performance and the fact that the actual elements that can be mounted are discrete elements.

In this study, we propose a procedure to design RL snubber using the previously proposed optimal design method and evaluate it by implementing it in an actual product. The EMI suppression of the RL snubber optimized using the previously proposed optimal methods, and the proposed method was verified by actual measurements. As a result, it is confirmed that an RL snubber can be implemented in practical systems to mitigate LC resonance and suppress EMI using the proposed procedure. The paper also demonstrated that RL snubbers were composed of commercial discrete circuit elements that meet the thermal constraints for automotive use. These results indicate that this procedure of optimal method is practical and efficiently for the optimal design of RL snubbers for damping LC resonances. This means that for any circuit, as long as the loop of LC resonance can be determined to be an equivalent circuit characterized by a third-order characteristic equation, contour plots by Q factor can be drawn, confirming that the optimal design of the RL snubber circuit is practically possible.

This procedure is based on the optimal design method [32–35] proposed based on circuit simulation and extended for practical use in brush motors motor system as an example. In this evaluation, the effective EMI suppression by the RL snubber LC resonance generated in brush motor is experimentally verified, assuming its application to the actual product design process. The organization of this thesis is as follows. Section 6.2 first explains the mechanism of noise generation in brush motor drive systems and the principle of LC resonance suppression by RL snubbers as a preliminary knowledge for the optimal design of RL snubbers. Section 6.3 describes the implementaion procedure of RL snubber and the extraction of third-order equivalent circuits for the application of RL snubbers in brush motor drive systems. Section 6.4 introduces the method of optimally designing RLs using the Q factor of resonance as a design criterion. Section 6.5 describes the verification of the LC resonance suppression effect of RL snubbers. Section 6.6 concludes the thesis with a summary of key points.

6.2 LC Resonance due to Switching Noise

6.2.1 brush motor drive system with PWM Control

As a preliminary step in applying the optimal design of RL snubber circuits, this section presents an example of a brush motor drive system to confirm that LC resonance occured by using the PWM controlled in the ECU. PWM control is a method of controlling average power by repeatedly turning power on and off. This control method is used in diverse applications such as motor drives, LED brightness adjustment, and power conversion. In this brush motor drive system, controlling the rotation of the motor improves the operational stability and the smooth of the mechanism in which it is installed.For this reason, vehicle manufacturers will consider applying PWM control depending on the type of vehicle in which it is installed. However, since the PWM control signal includes rapid switching (ON to OFF and OFF to ON), high frequency components are amplified and may appear as noise. In addition, the adoption of PWM control is sometimes decided late in the development process due to customer requirements, at which time measures are required to address EMI problems associated with switching noise. Thus, in brush

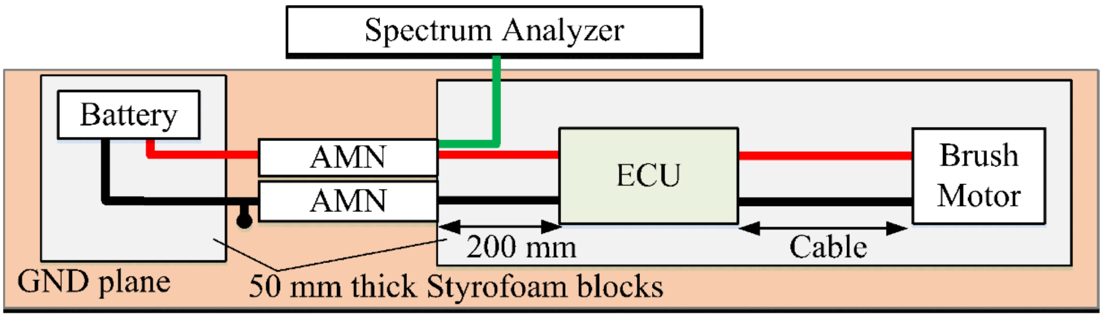

Figure 6.2 Configuration of conducted EMI testing of the brush motor drive system.

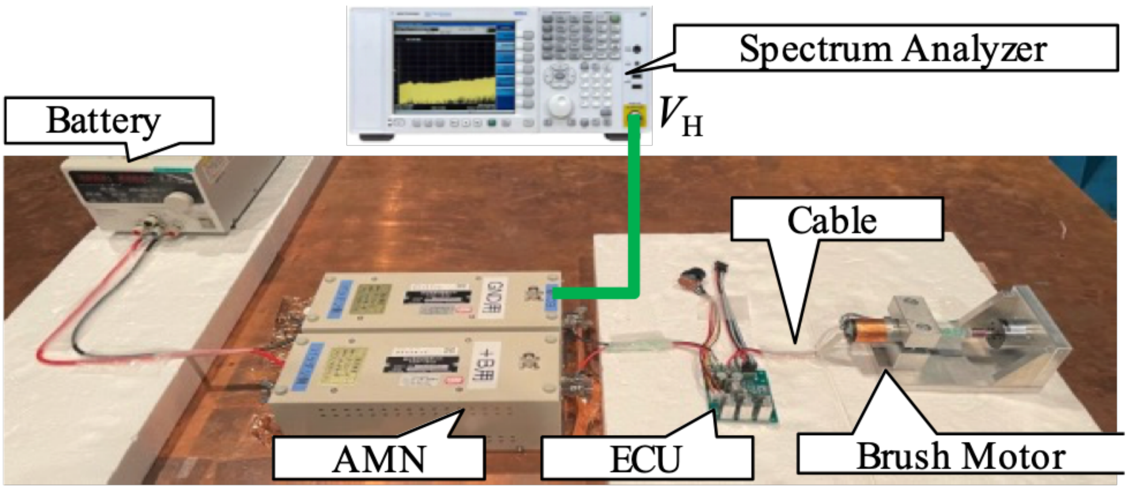

Figure 6.3 Evaluation system in brush motor drive system (CISPR25).

Figure 6.4 ECU(ONKTSQ-009A1, ONKYO) that controls the brush motor.

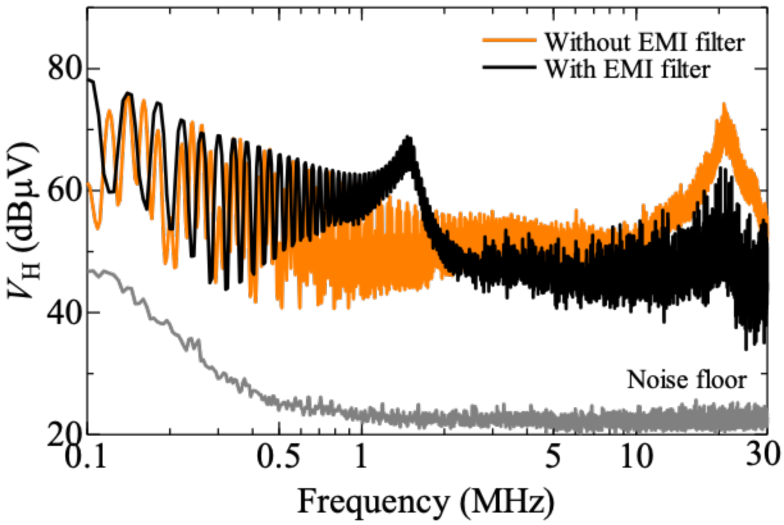

Figure 6.5 Conducted disturbances measured with and without EMI filter.

motor drive systems, there are two types of noise that cause EMI problems: brush noise from the brush motor and switching noise from the ECU. In this system, both brush noise generated at the brush motor and switching noise generated at PWM controlled power semiconductors mounted in the ECU cause EMI. Thus, consider the case where EMI countermeasures associated with switching noise are required after prototyping.

The mechanism of LC resonance generation when filters are actually installed with brush filters inside brush motors is described. Firstly, to evaluate the measurement with EMI filter and without the EMI filter, Fig. 6.2, Fig. 6.3 shows block diagram and a photo of the testing system following CISPR 25 [43], which specifies EMC tests, including the EMI test for ECUs. A 12V DC power supply was connected to the control ECU (ONKTSQ-009A1, ONKYO) in Fig. 6.4 via Artificial Mains Networks (AMNs), and a parallel two-wire cable of 200 mm in length. The ECU was connected to the brush motor (SX-17665-01, Igarashi Electric Works) via another parallel two-wire cable, 150 mm in length. The brush motor drive system was placed 50 mm above the system ground. The control ECU installed a low-side switch circuit to drive the motor, using PWM at 30 kHz and a duty ratio of 50%. In this study, the motor current was fixed at 3 A, and the rise time (T_{rise}) and fall time (T_{fall}) were set to 1 μs. Fig. 6.5 shows conducted EMI spectra measured with and without the EMI filter inside the brush motor. Without EMI filters inside brush motors, the switching noise has a spectrum of 20 dB/dec in the frequency range of 0.1 MHz to 2 MHz. Brush noise is also generated in the frequency range of 2 MHz to 30 MHz. On the other hand, the EMI filter suppressed the brush noise by 5 dB or more above 2 MHz, but it increased by more than 10 dB around 1.6 MHz, where the X capacitor, C_{x}, in the EMI filter resonated with the ESL of the cable. This indicates that the switching noise is increased by the EMI filter inside the brush motors to reduce brush noise.

Nextly, the equivalent circuit model of the brush motor drive system, including the measurement system, is shown in Fig. 6.6, indicating the resonant loop in the red dashed line a closed circuit in which resonance occurs. The parameters of the cable were identified using a 2-D electrostatic field solver and obtained as $R_{\mathrm{H}} = 9.73$ mΩ/m, $L_1 = L_2 = 1.005$ mH/m, and $k = 0.354$. AMN (TNW-1502) parameters were referred to in the datasheet. Z_{m} represents the impedance of the brush motor. The EMI filter is composed of two coils of $L = 0.6$ μH and the X capacitor of $C_{\mathrm{x}} = 0.047$ μF. The low-side switch circuit had the high-side FET, M1, kept off, and the low-side FET, M2, switched in a PWM mode. The X capacitor, the cable, the low-side switch, and the input capacitor C_{bp} form the resonant loop in the circuit, and the ESLs of the cable, L_1, and L_2, along with C_{bp}, significantly contribute to the resonance at the resonant frequency. This estimation is verified with the equivalent circuit of the resonant loop shown in Fig. 6.7, which includes parasitic impedances of C_{bp}, M2, the cable, C_{x}, and the motor. The parasitic impedances of the capacitors and the switch were referred to in their datasheets. The motor impedance was identified through measurements.

The impedance of the resonant loop, Z_{loop}, was calculated by circuit simulation and plotted in Fig. 6.8a and Fig. 6.8b. The calculated impedance resonates at 1.64 MHz, which agrees with that in the measured EMI spectrum in Fig. 6.6. The capacitance of C_{x} and the effective cable inductance are evidently seen in the impedance profile in Fig. 6.8a and Fig. 6.8b. This resonant frequency of 1.6 MHz is also equal to the frequency calculated by $f_0 = \frac{1}{2\pi\sqrt{LC}}$. where L_{loop} and C_{loop} are the ESL and capacitance of the entire resonant loop shown in Fig. 6.5. Lloop is calculated by $L_{\mathrm{loop}} = L_1 + L_2 + 2\mathrm{M} + L_{\mathrm{x}} + \mathrm{LMOS}$ where LMOS is the total ESL of the MOSFETs shown in M2. The ESL of M2 is 0.32 nH. Therefore, L_{loop} is 194 nH. C_{loop} is calculated by $C_{\mathrm{loop}} = C_{\mathrm{x}}$. Since C_{x} is much smaller than C_{bp}, C_{loop} is approximately equal to C_{x}. Therefore, f_0 is 1.64 MHz,

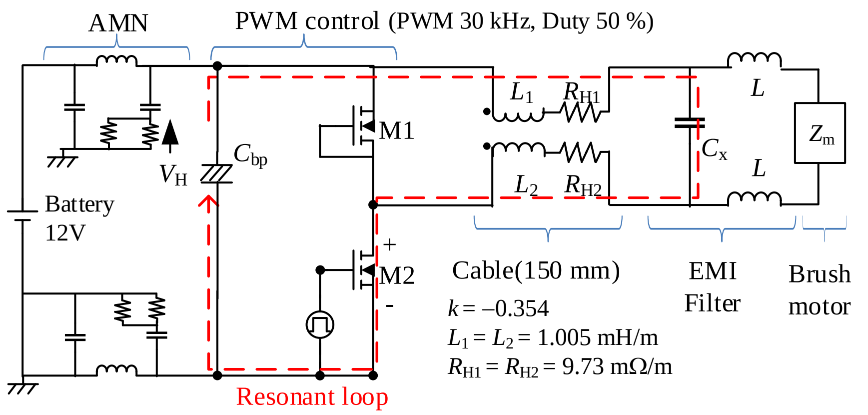

Figure 6.6 Equivalent circuit of circuit for brush motor drive systems.

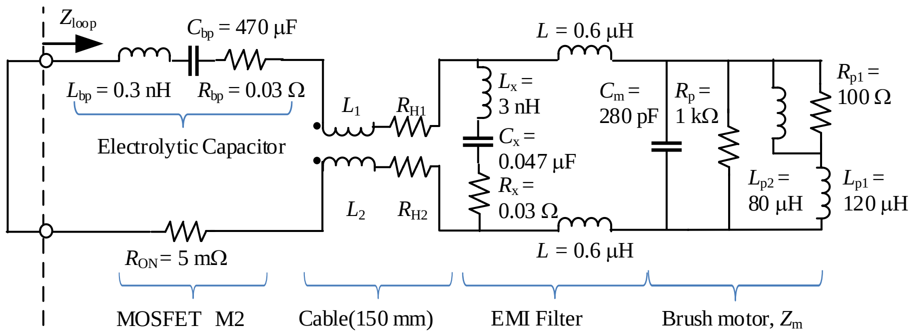

Figure 6.7 Equivalent circuit of analysis of resonant loop for significant elements.

which is consistent with the resonance frequency in Fig. 6.5.

6.2.2 LC Resonance Mitigating Solutions

In order to avoid or reduce such LC resonance from the target standard, generally, there are 5 types of mitigating solutions that can be considered. Five potential solutions to suppress EMI induced by the LC resonance are indicated, along with their implementation locations in Fig. 6.9. In addition, the Table.6.10 shows the issues for each solution, including the applicable effects, cost, and design difficulty.

Solutions 2–5 are implemented in the cable and motor parts, and they are applied during the design stages of those parts in Fig. 6.9. In particular, solutions 3 and 4 are considered ideal design solutions that can eliminate the resonance [26, 27]. Solutions 2 and 5 do not eliminate the resonance but instead shift the resonant frequency out of the

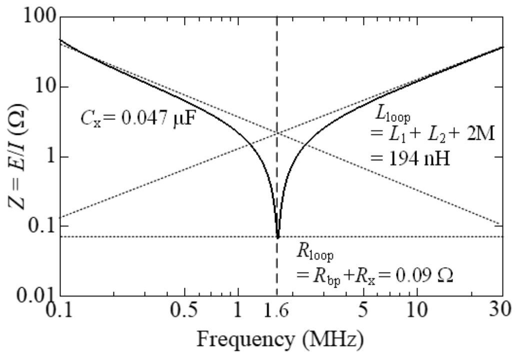

(a) Magnitude of impedance

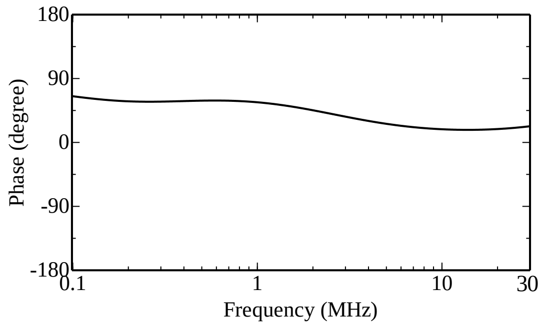

(b) Phase of impedance

Figure 6.8 Calculated impedance of resonant loop of analysis of resonant loop for significant elements.

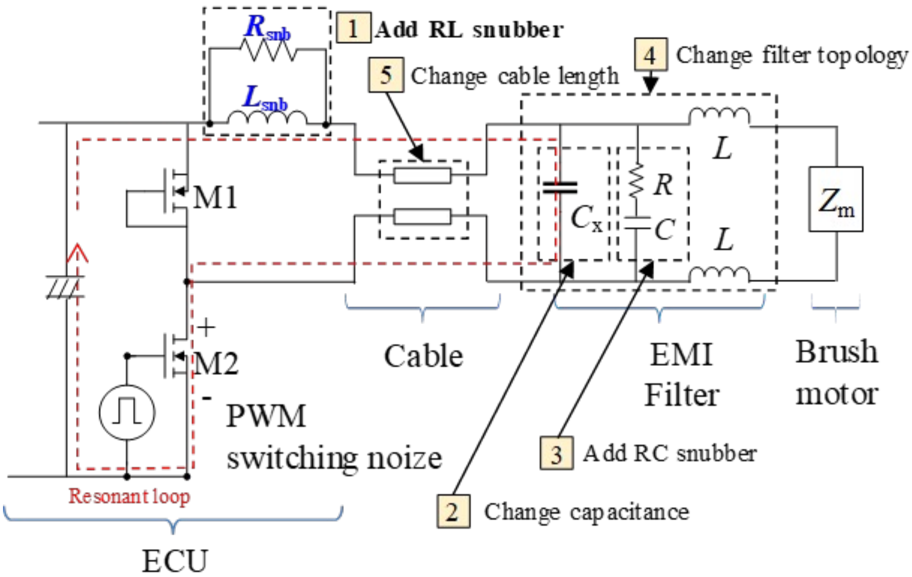

Figure 6.9 Resonance mitigating solutions in brush motor drive system.

carrier frequency bands by modifying the EMI filter design and the cable specifications. However, these solutions require redesigning several steps back in the design process and are challenging to implement in practice. In contrast, solution 1 requires only a step back to the previous design stage, the ECU design. An RL snubber comprises a pair of resistor R_{snb} and inductor L_{snb}, and it can be installed in series with the resonant loop in the ECU, as shown in Fig. 6.9. Therefore, it aligns well with the automotive design process and is used in this study.

There are also several approaches to optimally determine the parameters of the RL snubber. Two types of methods are generally used to damp LC resonance [26]. Solution 1-1 is that a simple and common way to select optimum parameters from many SPICE simulation results [26, 30, 32, 33, 37, 38]. Solution 1-2 is a ground truth trajectory analysis method using a simplified resonant circuit [32, 33]. This method determines the inductance by an a rule-of-thumb basis and analytically calculates the optimal resistance based on the root locus method. However, in this case, the optimal inductance is not always obtained, and the optimization of parameters is also insufficient. The existing methods have a common potential issue: the snubbers may be overdesigned. In the case of solution 1-3, for any circuit, as long as the loop of LC resonance can be determined to be an equivalent circuit characterized by a third-order characteristic equation, contour plots by Q factor can be drawn, and can determine that the optimal design parameters of the RL snubber circuit. Thus, the optimal design method presented in the previous paper [32–35] is practical because it only requires only a step back to the previous design stage and allows for flexibility in design parameters.

Figure 6.10 Mitigating solutions to LC resonance from the target standard

Mitigating Solution	1-1.RL snubber [26, 30, 37]	1-2.RL snubber [32, 33]	1-3.RL snubber [34, 35]	2.Change capacitance	3.RC snubber [26] [27]	4.Filter topology	5.Change cable length
Application Method	Simulation-based fitting	Root locus analysis	Q factor analysis (previous proposed method)	Change parameters to avoid resonance frequencies	Q factor analysis (previous proposed method)	Change parameters to avoid resonance frequencies	Change parameters to avoid resonance frequencies
Applicable Effects	Damping of LC resonance itself possible	Damping of LC resonance itself possible	Damping of LC resonance itself possible	Shift the resonant frequency out of the carrier frequency band	Damping of LC resonance itself possible	Eliminate the resonance	Shift the resonant frequency out of the carrier frequency band
Cost	Not always the lowest cost	Not always the lowest cost	Optimized for lowest cost	Cost of changing elements	Optimized for lowest cost	Cost of changing elements	Cost of changing cable length
Design Difficulty and Issue	The inductance or resistance is determined on a rule-of-thumb basis. These methods optimize only one parameter insufficient and not the other.	The inductance or resistance is determined on a rule-of-thumb basis. These methods optimize only one parameter insufficient and not the other.	Parameters are optimized analytically and uniquely by a contour plot drawn by a formula for the Q factor.	Not applicable after prototyping	Not applicable after prototyping	Not applicable after prototyping	Not applicable after prototyping

6.3 Procedure of the Optimal Design Method

In the previous section, the mechanism of brush motor LC resonance noise generation was explained. Then, the role of RL snubber in this study is described. This section presents a procedure to integrate an RL snubber into the ECU of an automotive brush motor drive system, addressing excessive EMI issues observed during prototype testing due to LC resonance shown in the previous section.

Initially, to optimize the RL snubber parameters, the RL snubber is embedded within the resonant loop that includes the ECU. The loop is then simplified to an equivalent circuit characterized by a third-order characteristic equation. This streamlined representation enables the application of our established optimal design approach for RL snubbers [34, 35]. The Q factor expresses the sharpness of the resonance peak of the resonant circuit, and this thesis utilizes contour plots to show the relationship between the Q factor, R_{snb} and L_{snb}, and their suppression effects. The concluding step is to determine the RL snubber's parameters using the Q factor calculated from the equivalent circuit model in this work, the optimal snubber parameters are determined as follows.

1. The RL snubber is embedded within the resonant loop circuit.
2. Simplifying to an equivalent circuit characterized by a third-order characteristic equation.
3. Drawing a contour plot of the Q factor at the resonance frequency.
4. Adding constraints in practical design (in this case on discrete elements and on thermal constraints).
5. Determining the optimal snubber parameters.
6. Verification of effectiveness by actual measurement.

6.3.1 Equivalent Circuit of Resonant Loop Characterized by a Third-order Characteristic Equation

In this chapter, the LC resonance loop in brush motor drive system is shown and simplified into an equivalent circuit, which is characterized by the third-order characteristic equation. The chapter then describes a method for determining the RL snubber constants for the brush motor drive system under study, using a contour diagram indicated by the calculated Q factor.

To optimize the RL snubber parameters, the resonant loop with an RL snubber installed in the ECU, as shown in Fig. 6.9, is simplified into an equivalent circuit dedicated to the resonance frequency band. The components of the LC resonance in a brush motor drive system are the ESL and coupling coefficient of the cable, the capacitance of the EMI filter's X capacitor, and the capacitance of the electrolytic capacitor in the ECU.

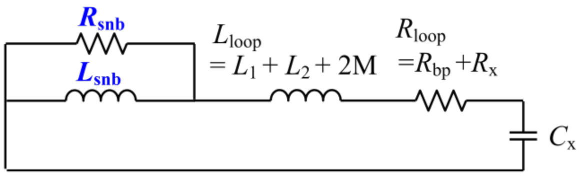

Figure 6.11 Simplified equivalent circuit of resonant loop.

The value used for the motor internal filter X capacitor is 0.047 μF. When actually inserting RL snubbers, it is difficult to insert them into motors and cables due to the design process. Therefore, it is examined by installing it inside the ECU. The simplified circuit represents the equivalent circuit when the low-side MOSFET is on. Furthermore, we focus on the resonance induced by the turn-on.

The simplified equivalent circuit, shown in Fig. 6.11, comprises the snubber parameters, the cable inductances, C_x, and the parasitic resistances R_{bp} and R_x. Other elements present in Fig. 6.9 are omitted here due to their significantly smaller impedances compared with the elements in Fig. 6.11. The impedances of C_{bp} and L_{bp}, as well as the on resistance of M2, were negligible compared with those of C_x and the cable's ESL around the resonant frequency. The motor circuit was also disregarded due to the decoupling effect of L of the EMI filter. Then, the resonant loop was simplified to the equivalent circuit, resulting in a third-order characteristic equation. L_{loop} approximates the entire ESL along the resonant loop, determined by L_1, L_2, and the coupling coefficient k. R_{loop} is the entire equivalent series resistance (ESR) of the resonant loop, determined by the ESRs of the electrolytic capacitor and the X capacitor C_x. L_{loop} and R_{loop} are respectively 194 nH and 0.09 Ω.

6.3.2 Determination of RL Snubber Parameters

The RL snubber parameters are determined to suppress the Q factor sufficiently by using the optimal design method [32–35]. This method derives the Q factor from the simplified equivalent circuit in Fig. 6.11.

Firstly, the relationship between the Q factor and the RL snubber parameters is derived from the simplified circuit. The Q factor at the resonance frequency is generally defined as

$$Q := \frac{X_L}{R} = \frac{X_C}{R} \tag{6.1}$$

where X_L is the inductive reactance, X_C is the capacitive reactance, and R is the resistance. The inductive part impedance of the simplified circuit Z_{RL} can be separated from the capacitance C_{oss}, giving the Q factor as

$$Q = \frac{|\mathrm{Im}\{Z_{RL}(\omega_0)\}|}{\mathrm{Re}\{Z_{RL}(\omega_0)\}} = \frac{\omega_0^3 L_{snb}^2 L_{loop} + R_{snb}^2(\omega_0(L_{loop} + L_{snb}))}{\omega_0^2 L_{snb}^2(R_{loop} + R_{snb}) + R_{snb}^2 R_{loop}} \tag{6.2}$$

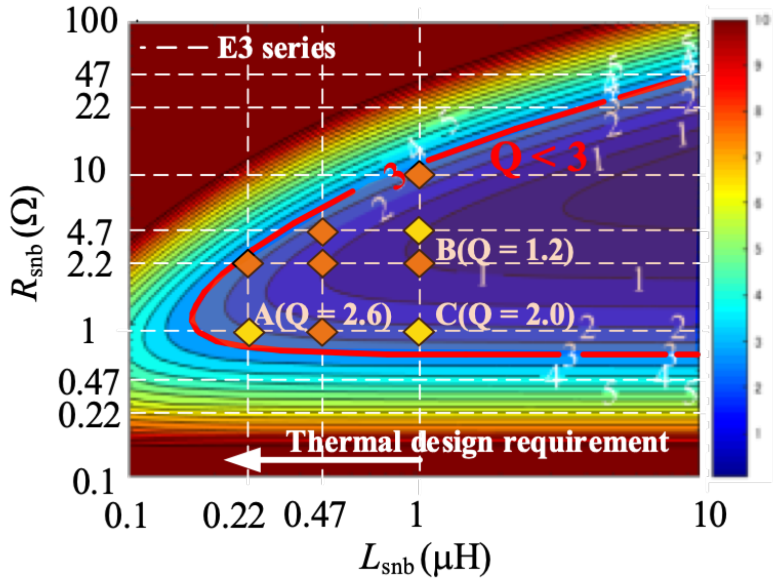

Figure 6.12 Contour map of Q factor for RL snubber parameters.

where Z_{RL} is the composite impedance of the closed loop circuit in Fig. 6.11. ω_0 is the angular resonant frequency at which the imaginary part of the impedance becomes zero as,

$$\omega_0 = \sqrt{\frac{-b \pm \sqrt{b^2 - 4ac}}{2a}} \tag{6.3}$$

The above equations a, b, and c are obtained as follows.

$$a = L_{\mathrm{snb}}^2 L_{\mathrm{loop}} C_x \tag{6.4}$$

$$b = R_{\mathrm{snb}}^2 C_x (L_{\mathrm{loop}} + L_{\mathrm{snb}}) - L_{\mathrm{snb}}^2 \tag{6.5}$$

$$c = -R_{\mathrm{snb}}^2 \tag{6.6}$$

The Q factor is plotted as a function of L_{snb} and R_{snb} in Fig. 6.12. The optimal parameters can be easily determined using Fig. 6.12. For example, if the design target for the Q factor is 3, the pair of L_{snb} and R_{snb} plotted as a diamond in Fig. 6.12 can be identified as the optimal pair of parameters. The Q factor is plotted as a function of L_{snb} and R_{snb} in Fig. 6.12.

Nextly, Adding constraints in this case on discrete elements and on thermal constrain as practical design. Also, in actual product design, not only resonance damping but also failure risks such as thermal breakdown of the element must be considered. For example, the target brush motor drive system requires a continuous current flow of approximately

3 A. The equivalent circuit in Fig. 6.9 shows that DC current flows through the coil in the RL snubber. Furthermore, in automotive applications, the brush motor drive system must be able to withstand operating in a high temperature environment of about $80°C$. Therefore, in this case, the coils in the RL snubber must be designed with thermal constraints with care.Thus, as a thermal constraint for the inductor, the maximum L_{snb} is usually set to 1 μH, following a rule of thumb. Furthermore, the parameters of each element in the RL snubber circuit should use commercially available and commonly used elements. Therefore, the design range based on the optimal design method should be a interval solution that includes discrete elements.E3 series values for resistances and inductances are indicated by white dashed lines in Fig. 6.12. Thus, when effectively suppressing LC resonance in consideration of actual applications, the optimal design of RL snubbers are the adequacy of the thermal design and the application to discrete elements as prerequisites. Finally, nine pairs of L_{snb} and R_{snb} were found to mitigate the Q factor below a specified threshold, e.g., Q $<$ 3, plotted with diamond shapes within the red line in Fig. 6.12.

6.4 Verification that the Proposed Implementation Procedure

6.4.1 Measurement Environment for RL Snubber Validation

In previous section, the third-order equivalent circuit of automotive brush motor drive system is shown and the method for determining the RL snubber constants is described. In this section, we verify the effect of the RL snubber determined in the previous section by actual measurement results. The measurement system of the automotive brush motor drive system is shown Fig. 6.3, and the points considered in the construction of the system and the measurement method are summarized. Then, we verify the suppression effect of the RL snubber using the actual measurement results.

The method of installing RL snubbers in brush motors is shown. Although the RL snubber should be inserted inside the ECU, in this study, the RL snubber is inserted between the ECU and the motor. Fig. 6.13 shows an actual image of an RL snubber. First, use a glue gun to fix the resistor and impedance elements of the RL snubber.Next, solder the RL snubber part to the male and female connectors. When inserting the RL

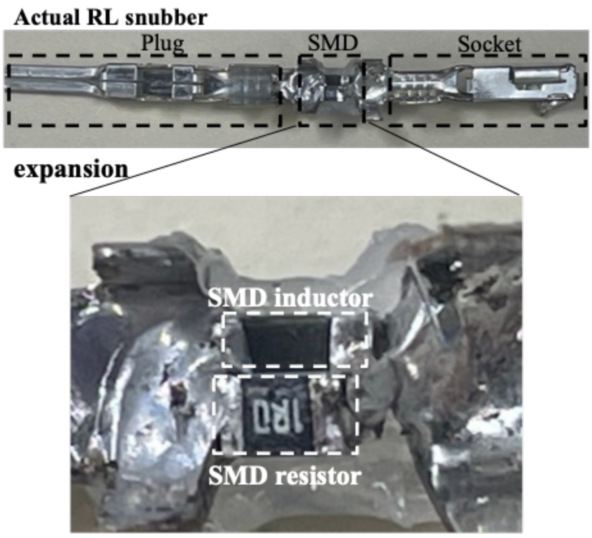

Figure 6.13 Fabricated RL snubber component.

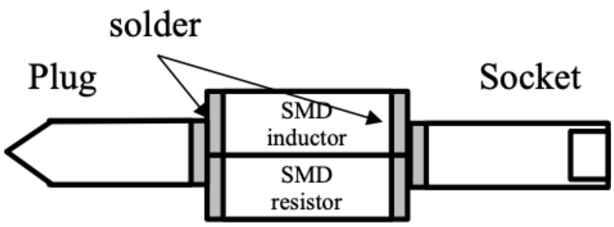

Figure 6.14 Schematic diagram of the RL snubber component.

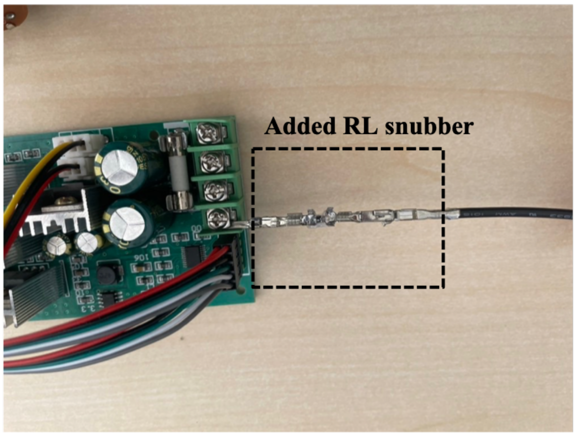

Figure 6.15 Actual device with the RL snubber component installed on the ECU.

snubber into the circuit, the male connector should be connected to the ECU and the female connector should be connected to the cable. Fig. 6.14 shows a photograph of an actual RL snubber. And Fig. 6.15 shows a photograph of the actual RL snubber connecting the cable to the ECU and the RL snubber.

Next, the evaluation environment for the conducted disturbance test is described. Conducted disturbance tests are conducted by laying a metal plate of a specified size on the floor. Therefore, a measurement system was constructed with reference to the CISPR25 standard, which defines the evaluation method for disturbance generated by electrical equipment in automobiles. Fig. 6.3 shows a diagram of the measurement system. First, a 900 mm high piece of Styrofoam was placed in the anechoic chamber. A copper plate of 1000 mm in length and 2000 mm in width was placed on top of the Styrofoam to serve as the system GND. The copper plate is connected to the floor of the anechoic chamber and is at the same potential. A DC power supply was used to drive the brush motors in brush motors, and the applied voltage was set to 12 V. The LISN was installed directly to the system GND, and the DC power supply and the GND terminal of the LISN were connected to a copper plate. 150 mm copper wire was used to connect the ECU to the brush motors. As shown in Fig. 6.17, the brush motors were clamped in brush motors with a jig to prevent the housing from rotating when driven. All devices except for the LISN were installed so that their bottom surfaces were 50 mm above the copper plate. The noise terminal voltage of the LISN was measured. The following Table 6.1 shows the settings of the spectrum analyzer used in this study.

6.4.2 Verification of Procedure with Simulation and Measurement Results

In this subsection, by simulation and measurement, the proposed implementation procedure for the RL snubber circuit is confirmed to be practically applicable. Three pairs of L_{snb} and R_{snb} were selected from the nine RL snubbers in previous section to

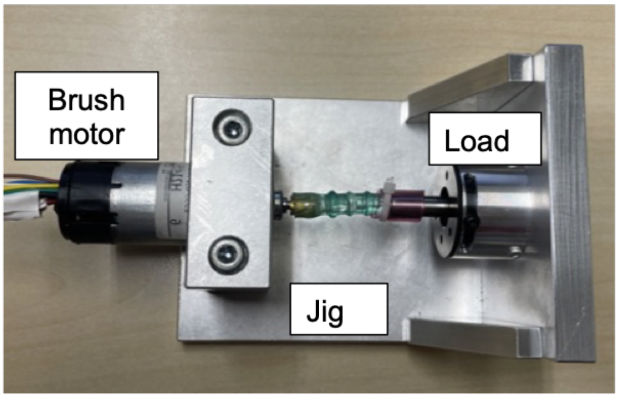

Figure 6.16 Jig used for controlling the torque of the brush motor.

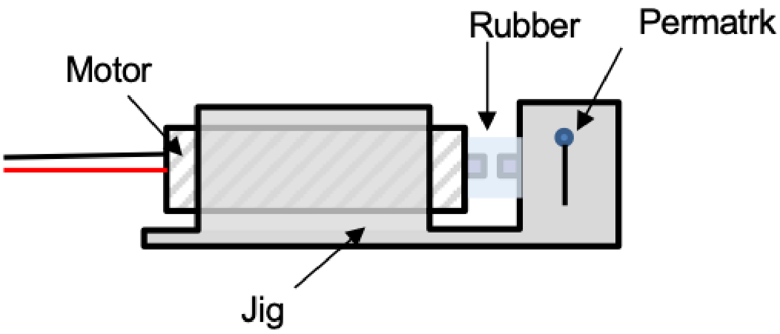

Figure 6.17 Jig used for controlling the torque of the brush motor.

Setting	**Value/Description**
Spectrum Analyzer	Agilent Technologies, N9020A
Bandwidth	10 Hz – 26.5GHz
Reference level	10 dBm
Attenuation	20 dB
RBW	9.1 kHz
VBW	30 kHz
Sweep time	26 s
Points	4001
Detector	Peak
Trace type	Max hold
Coupling	DC

Table 6.1 Spectrum Analyzer Settings

verify the resonance mitigation effect . They were expected to mitigate the Q factor to (A) 2.6, (B) 1.2, and (C) 2.0. These snubber parameters use inductors of 0.22, 0.47, and 1 μH, combined with resistors of 1 and 4.7 Ω, which are practically available E3 series discrete circuit components.

Table 6.2 Combination of elements that constitute the RL snubber circuit

	R_{snb}	L_{snb}	Q
A	1 Ω	220 nH	2.6
B	4.7 Ω	1 μH	1.2
C	1 Ω	1 μH	2.0

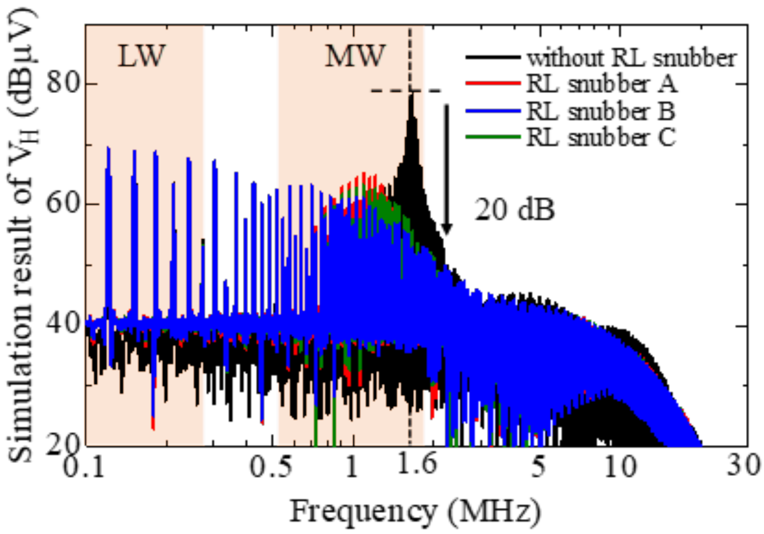

Figure 6.18 Simulation results of resonance-suppressing effects of RL snubbers.

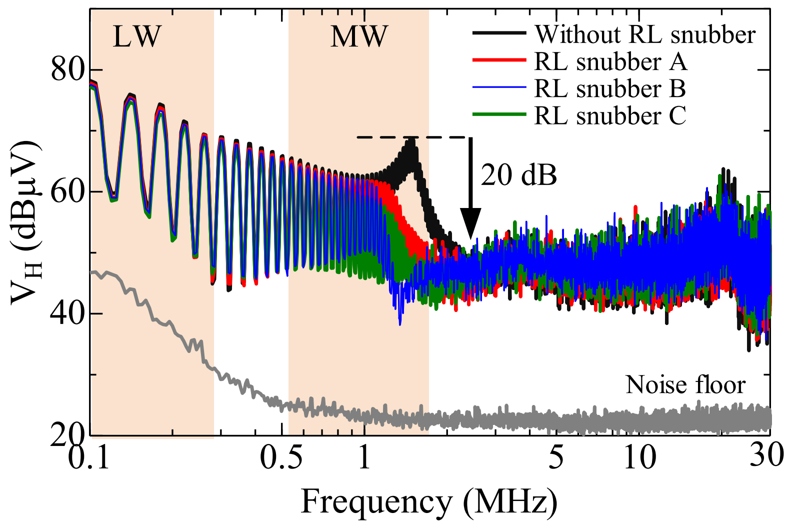

Figure 6.19 Measurement results of resonance-suppressing effects of RL snubbers.

Firstly, the suppression effect of RL snubber was calculated by circuit simulation as a relative rather than an absolute prediction. The noise source was a trapezoidal waveform given to the gate of the low-side FET in Fig. with the rise and fall times of 1 μs and the duty ratio of 50 % at 30 kHz. Simulation results of V_{H} in the case of RL snubbers (A), (B), and (C) are shown in Fig. 6.18. The circuit simulation shows that the conducted EMI was significantly suppressed for all three RL snubbers.

Next, the three RL snubbers, (A), (B), and (C), were installed in the ECU. The conducted EMI, V_{H} in Fig. 6.19 was measured to verify their resonance suppression effects experimentally. Fig. 6.19 shows the measured spectra of V_{H} for the three RL snubbers. The conducted EMI was suppressed by 10 dB or more at the resonant frequency for all three RL snubbers. Snubber (B) suppressed the maximum 20 dB. The EMI was suppressed adequately, even when the Q factor was 2.6. This means that all nine RL snubbers obtained by the proposed procedure suppress the resonance adequately. The procedure provides multiple effective snubbers with redundancy. It is confirmed that an RL snubber can be implemented in practical automotive brush motor drive systems to mitigate LC resonance and suppress EMI using the proposed procedure. Therefore, the proposed implementation procedure for the RL snubber circuit is confirmed to be practically applicable. The thesis also demonstrated that RL snubbers were composed of commercial discrete circuit elements that meet the thermal constraints for automotive use.

6.5 Conclusion

Optimal design of RL and RC snubber circuits has been described to reduce the EMI increase by LC resonance. In our previous work, we simplified the circuit of interest to a third-order equivalent circuit and derived an equation from the equivalent circuit that gives the Q factor as a function of the snubber parameters. It is then computationally shown that the snubber parameters are determined by reading the inductance or capacitance of the snubber along the contour lines of the target Q factor. To verify the procedure and the practicality of the proposed method, an application example is applied in brush motor drive system. In brush motor drive systems, it is difficult to change cables and filters inside brush motors that affect LC resonance due to constraints imposed by the design process. Therefore, the RL snubber circuit can be mounted inside the ECU, which is useful because it requires only a single step back in the development process. Therefore, we will verify whether the proposed method can be applied to the target circuit. The target circuit was simplified to a third-order equivalent circuit, and the equation giving the Q factor as a function of the snubber parameter was obtained from the equivalent circuit.

Nine RL snubbers obtained by the proposed procedure were simulated and mounted in the ECU, and all LC resonances were found to be adequately suppressed. It was shown that the LC resonances were suppressed according to the simulated Q factor of the circuit with the optimized snubbers added. Therefore, it was confirmed that the RL snubber can be implemented in a practical automotive brush motor drive system using the proposed procedure to mitigate LC resonance and suppress EMI. For a practical design, not only must the resonance be damped, but also the RL snubber must be determined by commercially available discrete circuit elements that meet the thermal constraints of the automotive application. By applying a previous optimal design method to satisfy these requirements, this thesis shows that multiple effective snubbers with redundant RL snubber parameters can be obtained by using a Q factor design method, which is useful for practical design.

Chapter 7

General Conclusion

In this thesis, the focus is on conducted emissions in brush motor drive systems as one of the multi-component systems, and the objective was to design efficiently. Overall, the research presented in this thesis demonstrated the broad applicability of efficient EMI design methods using equivalent circuit modeling in multi-component systems. Firstly, in order to perform (A) and (B), the accurate equivalent circuit was modeling of a brush motor drive system, which is one of the multi-component systems. In (A), the set-based design method and ANN-based optimal design method using the equivalent circuit model made it possible to obtain a multi-objective design method that satisfies multiple performance requirements quickly, accurately, and over a wide range of design parameters before prototyping. In (B), an implementation procedure that enabled solution method to be taken even when requirements are not satisfied in reliability tests after prototyping has been completed has been made possible. Thus, this was shown that the method proposed in this thesis contributes to improve the efficiency of EMC design methods by enabling (A) and (B) in the design process of multi-component systems.

In Chapter 2, EMI problem of brush motor drive system used as an example in this thesis is described. It was shown that the internal EMI filters inside brush motors system need to suppress not only brush noise but also resonance simultaneously, because resonance occurs between the filter capacitor and the parasitic inductance of the cable. The differential mode noise attenuation and common mode noise attenuation were investigated as filter characteristics, and the results showed that the filter was effective in reducing brush noise by 10 dB above 10 MHz, while the filter characteristics degraded by 10 dB below 1 MHz. As a result, in order to apply the multi-objective design, the required performance and design parameters in brush motors system targeted in this thesis are defined, and the target values of the multiple required performance and the design ranges of the multiple design parameters are explained.

In Chapter 3, the equivalent circuit model of the conducted EMI test environment for brush motor drive systems was identified in order to apply the multi-objective optimal design method before prototyping and the solution method after prototyping. In particular, a new measurement method using AMN was developed to evaluate the impedance of brush motors under dynamic conditions. The results showed the identification of a conducted EMI test system following CISPR25, the identification of the impedance at rest and under dynamic conditions of a brush motor, and the validity of its equivalent circuit model.

In Chapter 4, the procedure of the set-based design method and application were presented. To apply the design method, three levels of design range were prepared as initial data using the equivalent circuit model. Then, using the worst value of the frequency range required by the performance requirements, the response surface method was used to obtain a meta-modeling equation that can be expressed as a second order function. The results show that the proposed design method and procedure can obtain an interval solution range for multiple design parameters that satisfy multiple performance requirements.

In Chapter 5, multiple interval solutions were obtained by the optimal design method using ANN to obtain a wider interval solution range. We improved the modeling accuracy by training the ANN model with the frequency spectrum as training data, which could not be used in the set-based design method due to the limitations of the solver. As a result, by using the newly developed algorithm in obtaining interval solution ranges, including the interval solutions obtained by the set-based design method, is verified. In addition, the ANN was trained with both real and imaginary training data and with a design parameter of five levels. As a result, the latter increased the recall rate by about 40 % and reduced the precision of fit by about 15 %. Despite the reduction in the precision of fit, the algorithm was able to investigate a wide range of interval solutions, and the size within that range was widely, indicating that the latter was more effective.

In Chapter 6, the RL snubber implementation procedure was proposed and verified in the ECU of a brush motor drive system using the equivalent circuit model. For the application of the previously proposed optimal design, it was shown that the brush motor drive system with RL snubber can be represented by a simple equivalent circuit characterized by a third-order characteristic equation and satisfies the requirements of the optimal design method. Experimental results show that the implemented RL snubber effectively suppresses EMI using discrete circuit components while satisfying thermal constraints suitable for automotive applications. Therefore, it is confirmed that the proposed RL snubber implementation procedure is effective for practical EMI suppression.

Bibliography

[1] Y. Nahm and H. Ishikawa, "A new 3d-cad system for set-based parametric design," *The International Journal of Advanced Manufacturing Technology*, vol. 29, pp. 137–150, May 2006.

[2] H. Ishikawa, *Multi-objective optimum design : multi-objective satisfactory design by preference set-based design approach.* Korona-sha, 2010.

[3] Acumen Research And Consulting. (2022) Brushed dc motor market size - global industry, share, analysis, trends and forecast 2022 - 2030. [Online]. Available: https://www.acumenresearchandconsulting.com/brushed-dc-motor-market

[4] Maximize Market Research Pvt. Ltd. (2023) Brush dc motors market-global industry analysis and forecast (2023- 2029). [Online]. Available: https://www.maximizemarketresearch.com/market-report/global-brush-dc-motors-market/71704/

[5] M. K. Kazimierczuk *et al.*, "Accurate design of output filter for dc–dc pwm buck converter and derived topologies," *IEEE Transactions on Circuits and Systems I: Regular Papers*, vol. 70, no. 4, pp. 1786–1794, Apr. 2023.

[6] L. Zhai, "Comparison of two design methods of emi filter for high voltage power supply in dc-dc converter of electric vehicle," *IEEE Access*, vol. 8, pp. 66 564–66 577, Apr. 2020.

[7] J. Wang *et al.*, "Review of bidirectional dc–dc converter topologies for hybrid energy storage system of new energy vehicles," *Green Energy and Intelligent Transportation*, vol. 1, no. 2, pp. 100–110, Sep. 2022.

[8] Y. Fukumoto, Y. Takahata, O. Wada, Y. Toyota, T. Miyashita, and R. Koga, "Power current model of lsi/ic containing equivalent internal impedance for emi analysis of digital circuits," *IEICE Transactions on Communications*, vol. E84-B, no. 11, pp. 3041–3049, Nov. 2001.

[9] K. Iokibe, R. Higashi, T. Tsuda, K. Ichikawa, K. Nakamura, Y. Toyota, and R. Koga, "Validation of multiple power-supply-pin leccs-core model for conducted rf power

current simulation," *IEICE Transactions on Electronics (Japanese Edition)*, vol. J93-C, no. 11, pp. 516–520, Nov. 2010.

[10] K. Iokibe, T. Amano, K. Okamoto, and Y. Toyota, "Equivalent circuit modeling of cryptographic integrated circuit for information security design," *IEEE Transactions on Electromagnetic Compatibility*, vol. 55, no. 3, pp. 581–588, Jun. 2013.

[11] P. Hillenbrand, M. Böttcher, S. Tenbohlen, and J. Hansen, "Frequency domain emi-simulation and resonance analysis of a dcdc-converter," in *2016 International Symposium on Electromagnetic Compatibility - EMC EUROPE*, Wroclaw, Poland, Sep. 2016, pp. 176–181.

[12] S. Inoue, M. Ishigaki, A. Takahashi, and T. Sugiyama, "Design of an isolated bidirectional dc–dc converter with built-in filters for high power density," *IEEE Transactions on Power Electronics*, vol. 36, no. 1, pp. 739–750, Jan. 2021.

[13] L. Guibert, J.-P. Parmantier, I. Junqua, and M. Ridel, "Determination of conducted em emissions on dc–ac power converters based on linear equivalent thevenin block circuit models," *IEEE Transactions on Electromagnetic Compatibility*, vol. 64, no. 1, pp. 241–250, Feb. 2022.

[14] R. Kahoul, Y. Azzouz, P. Marchal, and B. Mazari, "New behavioral modeling for dc motor armatures applied to automotive emc characterization," *IEEE Transactions on Electromagnetic Compatibility*, vol. 52, no. 4, pp. 888–901, Nov. 2010.

[15] R. Kahoul, Y. Azzouz, B. Ravelo, and B. Mazari, "New behavioral modeling of emi for dc motors applied to emc characterization," *IEEE Transactions on Industrial Electronics*, vol. 60, no. 12, pp. 5482–5496, Dec. 2013.

[16] J. Benecke, S. Dickmann, and A. Linde, "Automatic hf model generation and impedance optimization for low voltage dc motors," in *Proc. Int. Conf. Elect. Mach.*, Vilamoura, Portugal, Oct. 2008, pp. 1–6.

[17] J. Benecke and S. Dickmann, "Inductive and capacitive couplings in dc motors with built-in damping chokes," in *EMC Zurich in Singapore 2006, 17th International Zurich Symposium on Electromagnetic Compatibility*, Singapur, Mar. 2006, pp. 69–72.

[18] J. Benecke and S. Dickmann, "Analytical hf model for multipole dc motors," in *EMC Zurich Munich 2007, 18th International Zurich Symposium on Electromagnetic Compatibility*, München, Sept. 2007, pp. 201–204, best Student Paper Award, First Prize.

[19] M. Kawakami, K. Nagao, H. Ishikawa, Y. Kami, and F. Xiao, "Study on application of the preference set-based design method to layout of microstrip lines with required performances," *in IEICE Tech. Rep.*, vol. EMCJ2015-19, Jun. 2015, in Japanese.

[20] Y. Kayano, Y. Kami, H. Ishikawa, F. Xiao, and H. Inoue, "A study on design of bent differential-paired lines by preference set-based design method," *in IEICE Tech. Rep.*, vol. EMCJ2017-16, May 2017, in Japanese.

[21] Y. Kayano, Y. Kami, H. Ishikawa, F. Xiao, and H. Inoue, "A study on design methodology of transmission line type filter by preference set-based design method part 2 design of experiments for metamodeling," *in IEICE Tech. Rep.*, vol. EMCJ2017-106, Mar. 2018, in Japanese.

[22] Y. Kayano, Y. Kami, H. Ishikawa, F. Xiao, and H. Inoue, "A study on design methodology of transmission line type filter by preference set-based design method part 3 comparison with design based on filter theory," *in IEICE Tech. Rep.*, vol. EMD2018-12, Jun. 2018, in Japanese.

[23] H. Okumura, H. Sekiguchi, and T. Funaki, "A study on reduction of common mode noise in non-isolated dcdc converter - effect on common mode noise reduction by symmetrical circuit," *IEICE Tech. Rep.*, vol. 111, no. 492, pp. 43–48, Mar. 2012, eMCJ2011-137.

[24] K. A., Y. Kami, H. Ishikawa, and F. Xiao, "Application of the preference set-based design method to fitler design," *Trans. of IEEE Japan A*, vol. 136, no. 10, pp. 621–628, 2016.

[25] Y. Kayano, Y. Kami, H. Ishikawa, F. Xiao, and H. Inoue, "A study on design methodology of transmission line type filter by preference set-based design method," *in IEICE Tech. Rep.*, vol. EMCJ2017-60, Nov. 2017, in Japanese.

[26] R. Blecic, R. Gillon, B. Nauwelaers, and A. Baric, "Spice analysis of rl and rc snubber circuits for synchronous buck dc-dc converters," in *Proc. 38th Int. Conv. Inf. Commun. Technol., Electron. Microelectron.*, Opatija, Croatia, May 2015, pp. 91–97.

[27] K. Harada and T. Ninomiya, "Optimum design of rc snubbers for switching regulators," *IEEE Trans. Aerosp. Electron. Syst.*, vol. AES-15, no. 2, pp. 209–218, Mar. 1979.

[28] Y. Yano, N. Kawata, K. Iokibe, and Y. Toyota, "A method for optimally designing snubber circuits for buck converter circuits to damp lc resonance," *IEEE Trans. Electromagn. Compat.*, vol. 61, no. 4, pp. 1217–1225, Aug. 2019.

[29] Y. Yano, H. Geshi, K. Iokibe, T. Watanabe, and Y. Toyota, "Linear equivalent circuit modeling of power converter circuit for conducted disturbance estimation — impact of trigger timing on the modeling —," in *IEICE Tech. Rep.*, vol. 116, no. 26, May 2016, pp. 41–45, in Japanese.

[30] K. Kam, D. Pommerenke, F. Centola, C. Lam, and R. Steinfeld, “Emc guideline for synchronous buck converter design,” in *Proc. IEEE Int. Symp. Electromagn. Compat.*, Austin, TX, USA, Aug. 2009, pp. 47–52.

[31] K. Iokibe, R. Higashi, T. Tsuda, K. Ichikawa, K. Nakamura, Y. Toyota, and R. Koga, “Validation of multiple power-supply-pin leccs-core model for conducted rf power current simulation,” *IEICE Transactions on Electronics (Japanese edition)*, vol. J93-C, no. 11, pp. 516–520, Nov. 2010, in Japanese.

[32] K. Iokibe, Y. Yano, and Y. Toyota, “Insertion of parallel rl circuits into power distribution network for simultaneous switching current reduction and power integrity,” in *2012 Asia-Pacific Symposium on Electromagnetic Compatibility (APEMC)*, May 2012, pp. 417–420.

[33] K. Iokibe, R. Yamagata, and Y. Toyota, “Rl snubbers on power distribution network of integrated circuits for conducted electromagnetic interference reduction and power integrity,” *IEICE Transactions on Communications (Japanese edition)*, vol. J97-B, pp. 497–506, July 2014, in Japanese.

[34] Y. Yano, N. Kawata, K. Iokibe, and Y. Toyota, “A method for optimally designing snubber circuits for buck converter circuits to damp lc resonance,” *IEEE Transactions on Electromagnetic Compatibility*, Jun. 2018, early access.

[35] N. Kawata, Y. Yano, K. Iokibe, and Y. Toyota, “Optimization method of on-board rl snubber parameters in common power distribution networks,” in *The 2016 IEICE General Conference*, Hukuoka, Japan, Mar. 2016, pp. B–4–41, in Japanese.

[36] N. Kawata, S. Yoshino, Y. Yano, K. Iokibe, and Y. Toyota, “Analysis formula to determine optimal resistance of on-board rl snubber mounted in power distribution network for digital ics,” in *the 67th Chugoku-section Joint Convention of Institutes of Electrical Engineering and Institutes of Electronics Information and Communication Engineers*, Hiroshima, Japan, Oct. 2016, pp. R16–09–03, in Japanese.

[37] K. Kam, D. Pommerenke, F. Centola, C. W. Lam, and R. Steinfeld, “Method to suppress the parasitic resonance using parallel resistor and inductor combination to reduce broadband noise from dc/dc converter,” in *2009 International Symposium on Electromagnetic Compatibility*, Kyoto, Japan, July 2009, pp. 353–356.

[38] H. S. Shin, H. A. Huynh, and S. Kim, “Design and optimization of inductive snubber for dc-dc converter,” in *2017 Asia-Pacific International Symposium on Electromagnetic Compatibility (APEMC)*, Seoul, South Korea, Jun. 2017, pp. 148–150.

[39] J. Benecke, “Impedance and emission optimization of low-voltage dc motors for emc compliance,” *IEEE Transactions on Industrial Electronics*, vol. 58, no. 9, pp. 3833–3839, sept. 2011.

[40] A. Veluswami, M. Nakhla, and Q.-J. Zhang, "The application of neural networks to em-based simulation and optimization of interconnects in high-speed vlsi circuits," *IEEE Transactions on Microwave Theory and Techniques*, vol. 45, no. 5, pp. 712–723, May 1997, iNSPEC Accession Number: 5587776.

[41] *Electromagnetic compatibility-Requirements for household appliances, electric tools and similar apparatus - Part 1: Emission*, Std., 2016.

[42] *Specification for radio disturbance and immunity measuring apparatus and methods — Part 2-1, Methods of measurement of disturbances and immunity — Conducted disturbance measurements*, Std., 2008.

[43] *Vehicles, boats and internal combustion engines - Radio disturbance characteristics - Limits and methods of measurement for the protection of on-board receivers*, Std., 2021.

[44] M. Inoue, Y.-E. Nahm, S. Okawa, and H. Ishikawa, "Design support system by combination of 3d-cad and cae with preference set-based design method," *Concurrent Engineering : Research and Applications*, vol. 18, no. 1, pp. 41–53, Mar. 2010.

[45] Y. Kami, Y. Kayano, H. Ishikawa, and F. Xiao, "On technique of preference set-based design," *in IEICE Tech. Rep.*, vol. EMCJ2017-59, Nov. 2017, in Japanese.

[46] M. Kawakami, Y. Kami, H. Ishikawa, and F. Xiao, "Application of the preference set-based design method to emi filter design," *in IEICE Tech. Rep.*, vol. EMCJ2015-105, pp. 13–18, Jan. 2016, in Japanese.

[47] M. Kawakami, H. Ishikawa, Y. Kami, and F. Xiao, "Application of the psd method to emi filter design considering the parasitic effect of the rel choke coil," in *Proceedings of the IEICE General Conference*, vol. 2016, no. 1, Mar. 2016, pp. 367–367.

[48] V. Tarateeraseth, B. Hu, K. Y. See, and F. G. Canavero, "Accurate extraction of noise source impedance of an smps under operating condition," *IEEE Transactions on Power Electronics*, vol. 25, no. 1, pp. 111–117, Jan. 2010.

[49] T. Yoshikawa, J. Wang, Y. Oguri, M. Tanaka, and M. Iida, "Noncontact measurement method for high-frequency impedance of load at the end of wire," *IEEE Transactions on Electromagnetic Compatibility*, vol. 61, no. 1, pp. 271–278, Feb. 2019, date of Publication: 10 May 2018.

[50] A. Ward, J. Liker, J. Cristiano, and D. Sobek, "The second toyota paradox: how delaying decisions can make better cars faster," *Sloan management review*, pp. 43–61, 1995.

[51] H. Inoue, Y. Kayano, and K. Miyanaga, "Novel multi-objective design approach for cantilever of relay contact using preference set-based design method," in *ICREPEC2019*, Nov. 2019, pp. 1–6.

[52] Y. Kayano, Y. Kami, H. Ishikawa, F. Xiao, and H. Inoue, "Application of the preference set-based design method to bent differential-paired lines," *C - Abstracts of IEICE TRANSACTIONS on Electronics (Japanese Edition)*, vol. J101-C, no. 5, pp. 233–244, May 2018.

[53] D. Montgomery, *Design and Analysis of Experiments.* Wiley, 2012.

[54] V. Devabhaktuni, C. F. Bunting, D. Green, D. Kvale, L. Mareddy, and V. Rajamani, "A new ann-based modeling approach for rapid emi/emc analysis of pcb and shielding enclosures," *IEEE Trans. Electromagn. Compat.*, vol. 55, no. 2, pp. 385–394, Apr. 2013.

[55] H. Jin, H. Ma, and E.-P. Li, "Emi prediction of packages by deep neural network," in *2018 IEEE International Symposium on Electromagnetic Compatibility and 2018 IEEE Asia-Pacific Symposium on Electromagnetic Compatibility (EMC/APEMC).* IEEE, May 2018, p. 72, conference Location: Suntec City, Singapore; Date Added to IEEE Xplore: 25 Jun. 2018.

[56] S. Piersanti and A. Orlandi, "Genetic algorithm optimization for the total radiated power of a meandered line by using an artificial neural network," *IEEE Trans. Electromagn. Compat.*, vol. 60, no. 4, pp. 1014–1017, Aug. 2018.

[57] J. Xu, M. Yagoub, R. Ding, and Q. J. Zhang, "Neural-based dynamic modeling of nonlinear microwave circuits," *IEEE Trans. Microw. Theory Techn.*, vol. 50, no. 12, pp. 2769–2780, Dec. 2002.

[58] A. Zaabab, Q.-J. Zhang, and M. Nakhla, "A neural network modeling approach to circuit optimization and statistical design," *IEEE Transactions on Microwave Theory and Techniques*, vol. 43, no. 6, pp. 1349–1358, Jun. 1995, iNSPEC Accession Number: 4994601.

[59] H. Chen and S. Ye, "Modeling and optimization of emi filter by using artificial neural network," *IEEE Trans. Electromagn. Compat.*, vol. 61, no. 6, pp. 1979–1987, Dec. 2019.

[60] J. Gao, D. Lu, S. Ye, and H. Chen, "Modeling of emi filter by means of recurrent neural network with encoding layer," in *Asia-Pacific Symposium on Electromagn. Compat. (APEMC)*, Dec. 2019, pp. 285–288.

[61] S. An, C. Fowler, B. Zheng, M. Y. Shalaginov, H. Tang, H. Li, L. Zhou, J. Ding, A. M. Agarwal, C. Rivero-Baleine, K. A. Richardson, T. Gu, J. Hu, and H. Zhang, "A

deep learning approach for objective-driven all-dielectric metasurface design," *ACS Photonics*, vol. 6, no. 12, pp. 3196–3207, 2019, publication Date: November 18, 2019.

Research Activities

Paper

1. **Shohei Kan**, Zhenhong Xu, Akito Mashino, Kengo Iokibe, Yoshitaka Toyota " Effective EMI Suppression Procedure Using RL Snubbers for Automotive Brush Motor Systems," *IEEE Letters on Electromagnetic Compatibility Practice and Applications*, Accepted

International Conferences

1. **Shohei Kan**, Ryuta Nakanishi, Zhenhong Xu, Kengo Iokibe, and Yoshitaka Toyota, "Multi-Objective Design of Filter Installed in Brush Motor by Preference Set-based Design Accounting for Cable Length," *2022 IEEE International Symposium on Electromagnetic Compatibility, Signal and Power Integrity (EMC+SIPI 2022)*, pp. 595, Spokane, WA, Aug. 1-5, 2022.

2. **Shohei Kan**, Norikazu Takahashi, Masaki Himuro, Akito Mashino, Kengo Iokibe, and Yoshitaka Toyota, "Multi-Objective Design of Filter Installed in Brush Motor by Artificial Neural Network Accounting for Cable Length," *2023 IEEE International Symposium on Electromagnetic Compatibility, Signal and Power Integrity (EMC+SIPI)*, p. 591, Grand Rapids, MI, Jul. 31 - Aug. 4, 2023.

Technical Reports

1. **Shohei Kan**, Atsushi Uemoto, Zhenhong Xu, Kengo Iokibe, Yoshitaka Toyota, "Parameter Identification of Noise Source Equivalent Circuit Model of Brush Motor Considering Temperature Dependence and Conducted Emission Prediction," 2021 IEICE Society Conference, B-4-36, Online, 2021.9.14-17. *(in Japanese)*

2. Zhenhong Xu, **Shohei Kan**, Kengo Iokibe, Yoshitaka Toyota, "Parameter Identification of Noise-Source Equivalent-Circuit Model of Brush Motor Considering Temperature Dependence and Conducted-Emission Prediction," The Conferrence Program of the 2021(72st)Chugoku-branch Joint Convention of Institutes of Electrical and Information Engineers, R21-15-06, Online, 2021.10.23. *(in Japanese)*

3. **<u>Shohei Kan</u>**, Zhenhong Xu, Kengo Iokibe, Yoshitaka Toyota, "Determination of Circuit Element Constant Ranges by Set-based Design for EMI Filters in Brush Motor Circuits Containing Cables," IEICE technical report, EMCJ2022-31, pp. 17-22, Tokyo, 2022.7.14.*(in Japanese)*

4. Akito Mashino, **<u>Shohei Kan</u>**, Kengo Iokibe, Yoshitaka Toyota, "Validation of Filter Element Ranges Obtained by Set-based Design for EMI Filter Installed in Brush Motor Connected with a Cable" The Conferrence Program of the 2022(73st)Chugoku-branch Joint Convention of Institutes of Electrical and Information Engineers, R22-15-09, Online, 2022.10.22.

5. **<u>Shohei Kan</u>**, Zhenhong Xu, Akito Mashino, Kengo Iokibe, Yoshitaka Toyota, "Suppression of LC Resonance by Applying RL Snubber to Brush Motor Drive System Including Low-side Switch Circuit," 2023 IEICE Society Conference, B-4-2, Saitama, 2023.3.7-10.

6. **<u>Shohei Kan</u>**, Norikazu Takahashi, Masaki Himuro, Akito Mashino, Kengo Iokibe, Yoshitaka Toyota, "Determination of Circuit Element Constant Ranges by ANN for EMI Filters in Brush Motor Circuits Containing Cables," IEICE technical report, EMCJ2023-34, pp. 29-32, Tokyo, 2023.7.21.*(in Japanese)*

7. Akito Mashino, **<u>Shohei Kan</u>**, Kengo Iokibe, Yoshitaka Toyota, "Identification of Dynamic Internal Impedance in Noise Source Equivalent-Circuit Model of Brush Motor," 2023 IEICE Society Conference, B-4-11, Nagoya, 2023.9.12-15.*(in Japanese)*

8. Yoshiaki Tanimoto, Akito Mashino, **<u>Shohei Kan</u>**, Kengo Iokibe, Yoshitaka Toyota, "Parameter Identification of Noise Source Equivalent Circuit for Conducted EMI Prediction of Brush Motor Circuit," The Conferrence Program of the 2023(74st) Chugoku-branch Joint Convention of Institutes of Electrical and Information Engineers, R23-15-10, Online, 2023.10.28.*(in Japanese)*

9. Sojun Maeta, Masaki Himuro, **<u>Shohei Kan</u>**, Kengo Iokibe, Yoshitaka Toyota, "Statistical Machine Learning Application for Design-time Reduction of EMI Filters in Brush Motor Circuit," The Conferrence Program of the 2023(74st)Chugoku-branch Joint Convention of Institutes of Electrical and Information Engineers, R23-23-02, Online, 2023.10.28.*(in Japanese)*

10. Ryo Maekawa, Akito Mashino, **<u>Shohei Kan</u>**, Kengo Iokibe, Yoshitaka Toyota, "Investigation of Algorithms for Determining the Maximum Rectangular Region of Design Parameters Obtained by Machine Learning," The Conferrence Program of the 2023(74st)Chugoku-branch Joint Convention of Institutes of Electrical and Information Engineers, R23-23-07, Online, 2023.10.28.*(in Japanese)*

Awards and Recognitions

1. 2022:Young Researcher Presentation Excellence Award, IEICE Technical Committee on Electromagnetic Compatibility, “Determination of Circuit Element Constant Ranges by Set-based Design for EMI Filters in Brush Motor Circuits Containing Cables”

2. 2023:EMCJ Young Scientist Excellence Award, IEICE Technical Committee on Electromagnetic Compatibility, “Determination of Circuit Element Constant Ranges by ANN for EMI Filters in Brush Motor Circuits Containing Cables”

Biography

Shohei Kan was born in Ehime, Japan, on March 1, 1991, and graduated from Okayama University in 2012 in Department of Communication Network Engineering.In 2015, he received his M.S. degree in the Graduate School of Natural Science and Technology from the same Okayama University. In same year, he started working at Analytic Engineering Department, Aisin Corporation. He is currently attempting to obtain his Ph.D. degree in the Graduate School of Natural Science and Technology in Okayama University. His research interests include the study on design method using equivalent circuit model to improve EMC design efficiency such as automotive brush motor system.